Data-Driven and Machine Learning-Based Load Modeling

Final Project Report

S-84G

Power Systems Engineering Research Center
Empowering Minds to Engineer
the Future Electric Energy System

Data-Driven and Machine Learning-Based Load Modeling

Final Project Report

Project Team
Zhaoyu Wang, Project Leader
Iowa State University

Graduate Students
Fankun Bu
Zixiao Ma
Yingmeng Xiang
Iowa State University

PSERC Publication 21-06

June 2021

For information about this project, contact:

Dr. Zhaoyu Wang
ECpE Department
Iowa State University
Phone: 515-294-6305
Email: wzy@iastate.edu

Power Systems Engineering Research Center

The Power Systems Engineering Research Center (PSERC) is a multi-university Center conducting research on challenges facing the electric power industry and educating the next generation of power engineers. More information about PSERC can be found at the Center's website: http://www.pserc.org.

For additional information, contact:

Power Systems Engineering Research Center
Arizona State University
527 Engineering Research Center
Tempe, Arizona 85287-5706
Phone: 480-965-1643
Fax: 480-727-2052

Notice Concerning Copyright Material

Acknowledgements

We express our appreciation for the support provided by PSERC's industry members. In particular, we wish to think industry advisors Yishen Wang (GEIRINA), Di Shi (GEIRINA), Cho Wang (AEP), Larry E Anderson (AEP), Carol Liu (AEP), and Robert J O'Keefe (AEP).

Executive Summary

Load modeling is of great significance for various power grid studies, such as power system operation optimization, energy reservation, and stability analysis. The overall purpose of this project is to develop and apply cutting-edge data-driven and machine learning-based methods to accurately model power system loads using real utility data.

First, we conducted a comprehensive review of the load models, analyze their advantages and disadvantages, research trends, and industrial applications, which laid a valid foundation for the model selection, parameter reduction, and order reduction. There are a variety of load models available in the power system industry and academia. The commonly used models be classified into static load models, dynamic load models, and composite load models.

- Static load models: They include the constant impedance-current-power (ZIP) model, exponential model, and frequency dependent model. Static models express the active and reactive power at any instant of time as functions of bus voltage magnitudes and frequency, and the dynamics of load are neglected.
- Dynamic load models: They include induction motor (IM) and exponential recovery load model. Dynamic models express the active and reactive powers as a function of voltage and time, and they consider the dynamics of load variations.
- Composite load models: For providing more accurate responses, composite load models are developed by combining static and dynamic load models. Typical composite load models are ZIP+IM composite load model, and Western Electricity Coordinating Council (WECC) model. The WECC model contains a substation transformer, shunt reactance, feeder equivalent, induction motors, single-phase AC motor, ZIP load, electronic load, and distributed energy resources (DER). It can effectively capture the commonly-observed fault-induced delayed voltage recovery (FIDVR) events and has drawn great attention recently.

The WECC composite load model (WECC CMLD) produces accurate responses; nevertheless, the large number of parameters and high model complexity raises new challenges for power system studies. For the parameter identification problem, the large number of parameters brings great difficulties to search for global optimum when performing parameter identification. The reason is twofold: firstly, the large number of parameters results in a large search space that reduces the optimization efficiency; secondly, the insensitive parameters and parameter interdependencies usually result in a large number of local optima, which increases the difficulty of achieving global optimum. Although the parameters have physical meanings, some of them only have marginal impacts on the model response altogether or along certain parameter variation directions. Moreover, considering the full load model parameter set could significantly increase the complexity of power system studies. Therefore, it is imperative to develop a method to screen out the insensitive parameters. Then, only the sensitive parameters are to be determined in the parameter identification problem, while the others can be kept at their respective default values. In this way, the dimension of the search space of load model parameters can be significantly reduced. Thus, lower computational cost (less model runs) and higher accuracy (easier to find the optimum) can be achieved when conducting power system studies such as parameter identification without compromising the fidelity of the load model.

Second, we developed multiple data-driven and machine learning based methods for dimension reduction in parameter space to address the above-mentioned problems. Specifically, three major methods were proposed and validated, explained as follows.

- A cutting-edge parameter reduction (PR) approach for WECC CMLD based on the active subspace method (ASM) was proposed, briefly explained as follows. Firstly, the WECC CMLD is parameterized in a discrete-time manner for the application of the proposed method. Then, parameter sensitivities are calculated by discovering the active subspace, which is a lower-dimensional linear subspace of the parameter space of WECC CMLD in which the dynamic response is most sensitive. The interdependency among parameters can be taken into consideration by our approach. Finally, the numerical experiments validate the effectiveness and advantages of the proposed approach for the WECC CMLD model.
- A novel approach inspired by the evolutionary deep reinforcement learning (EDRL) with an intelligent exploration mechanism was obtained to perform parameter identification for the composite load model with distributed generation (CMPLDWG). First, to extract parameters' contributions to dynamic power, parameter sensitivity analysis is conducted using a data-driven feature-wise kernelized Lasso (FWKL). Then, the EDRL with intelligent exploration, which can handle the natural high nonlinearity and nonconvexity of CMPLDWG, is employed to perform parameter identification. In the parameter identification process, the extracted parameter sensitivity weights are innovatively integrated into the EDRL with intelligent exploration to improve discovery efficiency. Finally, the proposed approach is validated using numerical experiments.
- A Python-PSSE-combined autonomous parameter identification program was developed. It enables efficient information change between the optimization method sited in the Python environment and the WECC load module in PSSE software. As the WECC load module is the available most convincing representation of the WECC load module, this approach can eliminate the possible errors brought by the inaccurate representation of the WECC load modeling. As an example of the heuristic optimization methods, the SSA is adopted to optimize the WECC load parameters using real event data provided by AEP. The SSA sends the WECC parameters to the PSSE as its inputs. Based on these WECC parameters provided by SSA, a dynamic simulation is conducted in the PSSE using the PMU frequency measurements and voltage measurements. After the simulation is conducted, an active power curve and a reactive power curve are obtained, and they are provided to the SSA. The SSA then compares the simulated P, Q curves with the real P, Q measurement curves to update the WECC parameters. The obtained results are very promising, and they validate the efficiency and accuracy of our proposed Python-PSSE-combined autonomous parameter identification program.

Third, we developed a large-signal order reduction (LSOR) method using singular perturbation theory to reduce the order of the WECC composite load model. The WECC composite load model is a complex high-order nonlinear system with multi-time-scale property, which poses challenges on power system studies with a heavy computational burden. In order to reduce the model complexity, an order reduction method was derived based on the singular perturbation theory. In this method, the fast dynamics are integrated into the slow ones to preserve the transient characteristics of the former. Then, accuracy assessment conditions are proposed and embedded into the LSOR to improve and guarantee the accuracy of the reduced-order model. Finally, the reduced-order WECC composite load model is derived by using the proposed algorithm. Simulation results show that the reduced-order large-signal model significantly alleviates the computational burden while maintaining similar dynamic responses as the original composite load model. The derived reduced-order model has guaranteed high accuracy that can replace the original load model in high-order system simulation to perform power system studies. This replacement can significantly reduce the difficulty of stability analysis and computational burden.

The major research outcomes of this project are listed as follows.

- Provided an all-inclusive review of load modeling.
- Developed a general global sensitivity analysis method to reduce the dimension of input space of any nonlinear model with scalar output.
- Proposed a WECC composite load model parameter identification approach using evolutionary deep reinforcement learning.
- Developed an autonomous parameter identification approach by calling PSSE dynamic simulation in python-based optimization algorithms.
- Derived an order reduction technique based on the singular perturbation theory to obtain a reduced load model.

Some next steps to move the research toward applications are discussed as follows.

- Test and validate the proposed methods using more real event data from the industrial partners, and finally make some software packages available to the public.
- Develop novel models with reduced complexity and computational requirements to better represent active distribution networks, distributed generators, and microgrids.
- Research parameter estimation algorithms that are able to process data from existing and emerging measurement devices with different resolutions, such as smart meters, PMUs, and SCADA.

Project Publications:

[1] J. Xie, Z. Ma, K. Dehghanpour, Z. Wang, Y. Wang, R. Diao, and D. Shi, "Imitation and Transfer Q-learning-Based Parameter Identification for Composite Load Modeling," *IEEE Transactions on Smart Grid*, vol. 12, no. 2, pp. 1674-1684, March 2021.

[2] Z. Ma, Z. Wang, Y. Wang, R. Diao, and D. Shi, “Mathematical representation of the WECC composite load model,” *Journal of Modern Power System and Clean Energy*, vol. 8, no. 5, pp. 1015-1023, September 2020.

[3] Z. Ma, B. Cui, Z. Wang, and D. Zhao, “Parameter Reduction of Composite Load Model Using Active Subspace Method”, *IEEE Transactions on Power Systems*, Accepted.

[4] A. Arif, Z. Wang, J. Wang, B. Mather, H. Bashualdo, and D. Zhao, "Load Modeling - A Review," *IEEE Transactions on Smart Grid*, vol. 9, no. 6, pp. 5986-5999, November 2018.

[5] C. Wang, Z. Wang, J. Wang, and D. Zhao, "SVM-Based Parameter Identification for Composite ZIP and Electronic Load Modeling," *IEEE Transactions on Power Systems*, vol. 34, no. 1, pp. 182-193, 2018.

[6] C. Wang, Z. Wang, J. Wang and D. Zhao, "Robust Time-Varying Parameter Identification for Composite Load Modeling," *IEEE Transactions on Smart Grid*, vol. 9, no. 4, pp. 3304-3312, July 2018.

[7] J. Zhao, Z. Wang, and J. Wang, "Robust Time-Varying Load Modeling for Conservation Voltage Reduction Assessment," *IEEE Transactions on Smart Grid*, vol. 9, no. 4, pp. 3304-3312, July 2018.

[8] F. Bu, Z. Ma, Y. Yuan and Z. Wang, "WECC Composite Load Model Parameter Identification Using Evolutionary Deep Reinforcement Learning," *IEEE Transactions on Smart Grid*, vol. 11, no. 6, pp. 5407–541, July, 2020.

[9] Z. Ma, Z. Wang, D. Zhao, and B. Cui, “High-fidelity large-signal order reduction approach for composite load model,” *IET Generation, Transmission and Distribution*, vol. 14, no. 21, pp. 4888–4897, August, 2020.

[10] Z. Ma, Z. Wang, Y. Yuan, Y. Wang, R. Diao, and D. Shi. “Stability and Accuracy Assessment based Large-Signal Order Reduction of Microgrids”, arXiv preprint.

Table of Contents

List of Figures

List of Tables

1. Introduction

1.1 Background

Load modeling is essential to power system analysis, planning, and control [1]-[2]. Although the need for accurate load models is recognized by power system researchers and engineers, more research is imperative to update existing load models and understand characteristics of modern loads with emerging smart grid technologies such as distributed generators (DGs), electric vehicles (EVs), and demand side management (DSM). The uncertainty and difficulty of load modeling comes from a large number of diverse load components, time-varying and weather-dependent compositions, and the lack of measurements and detailed load information. The goal of load modeling is to develop simple mathematical models to approximate load behaviors.

Load modeling consists of two main steps: 1) selecting a load model structure, and 2) identifying the load model parameters using component or measurement-based approaches. Component-based or physically-based modeling has been extensively investigated in the literature, and this method is based on the knowledge of physical behaviors of loads and mathematical relations that describe the functioning of load devices. However, obtaining such information is not always possible, which motivates the research in measurement-based modeling. Measurement-based modeling collects measurements from data acquisition equipment to derive load characteristics. The main advantage is that this approach directly obtains the data from the actual network, and can be applied to any load. However, a developed model at one network location may not be applicable to other locations. The parameters of load models are estimated by fitting the acquired data to a load model structure using identification and estimation techniques. Other research suggested the use of artificial neural networks (ANNs) to model loads by mapping the input data set to the output. This approach is useful when the model structure is unknown or hard to be mathematically represented. However, data-driven techniques require a large number of datasets and considerable computational effort.

1.2 Overview of the Problem

The WECC composite load model is a highly nonlinear and complex load model, and it has a significant number of parameters, i.e.,133 parameters for the basic WECC composite load model in PSSE software and more parameters for the WECC model with DG. It is a challenging problem to using event data to identify the parameters of the WECC composite load model to fit the active and reactive power measurements.

1.2.1 Main Issues

It would be quite difficult if all the parameters of the WECC model are considered as control variables in the optimization problem formulation of the load modeling, since the searching space would be very prohibiting. Also, it is not necessary to identify all the parameters, as not all the parameters are very sensitive in the curve-fitting. Parameter reduction (PR) is needed to identify those most sensitive parameters and simplify the problem. PR methods can be classified into local and global ones. Local PR methods are suitable for known parameters with small uncertainties, in which partial derivatives of output with respect to the model parameters are computed to evaluate the relative variation of output with respect to each parameter. Nonetheless, the input parameters are subject to a range in typical load modeling problems. Therefore, a global sensitivity metric is necessary to measure the sensitivity of output with respect to parameters.

There are many existing global PR approaches. One of the most common and simplest techniques in engineering is the so-called “One-At-A-Time” (OAT) method that varies one parameter while fixing the others. However, this method can only provide a rough qualitative approximation of the parameter sensitivities and cannot fully reveal the nonlinearity and interdependency among the parameters due to its low exploration of the parameter space. To quantitatively study the comprehensive parameter sensitivity patterns and their interdependencies, variance-based approaches such as Sobel indices were proposed for nonlinear and non-monotonic models. However, to precisely estimate the sensitivity indices with arbitrary order interactions between parameters, these approaches require a formidably large number of experiments. Thus, it motivates the recent research on exploring efficient numerical algorithms, including the analysis of variance (ANOVA) decomposition, Fourier Amplitude Sensitivity Test (FAST), and least absolute shrinkage and selection operator (LASSO). Despite the relative reduction in computational cost by these methods, they can result in instability and inaccuracy when the number of parameters increases. Considering the above-mentioned limitations of existing methods, more advanced methods should be developed to reduce the dimension of the load modeling problem.

1.2.2 Secondary Issues

The above WECC composite load model is a complex high order nonlinear dynamical system with multi-time-scale property, which means the state vector is high-dimensional and the transient velocity of each state varies significantly. These characteristics result in two main challenges. Firstly, it increases the difficulty of dynamic stability analysis due to the numerous state variables. Secondly, it makes simulation studies of a high-order power system computationally demanding or even infeasible. There are two main reasons for this high computational burden. One reason is the shear dimensionality of the problem. The other comes from the two-time-scale property of the model. This makes solving the model a stiff ordinary differential equation (ODE) problem, which requires small time steps to calculate the fast dynamics, and consequently results in long computational time to capture slow dynamics. The fast dynamics are often introduced by the intentionally added inductance and capacitance, moment of inertia, and parasitic elements inherent in the system. However, simply neglecting the fast dynamics may lead to modeling inaccuracies in dynamic response and stability property. In order to accelerate computation while maintaining the accuracy and faithful stability property of the original load model, it is imperative to develop a high-fidelity reduced-order load model.

1.3 Report Organization

The rest of this report is organized as follows. Chapter 2 provides an all-inclusive review of load modeling. Chapter 3 develops a general global sensitivity analysis method to reduce the dimension of input space of any nonlinear model with scalar output. A WECC composite load model parameter identification approach is proposed using evolutionary deep reinforcement learning in Chapter 4. Chapter 5 presents an autonomous parameter identification approach by calling PSSE dynamic simulation in python-based optimization algorithms. Chapter 6 derives an order reduction technique based on the singular perturbation theory to obtain a reduced load model. Chapter 7 concludes this report and describes the future research topics.

2. Load Modeling Review

2.1 Introduction

Load modeling is essential to power system analysis, planning, and control. For example, studies have shown the importance of accurate load representations in voltage stability assessment [1]. Although the need for accurate load models is recognized by power system researchers and engineers [2], more research is imperative to update existing load models and understand characteristics of modern loads with emerging smart grid technologies such as distributed generators (DGs), electric vehicles (EVs), and demand side management (DSM). The uncertainty and difficulty of load modeling comes from the large number of diverse load components, time-varying and weather-dependent compositions, and the lack of measurements and detailed load information. The goal of load modeling is to develop simple mathematical models to approximate load behaviors.

Load modeling consists of two main steps: 1) selecting a load model structure, and 2) identifying the load model parameters using component or measurement-based approaches. Component-based or physically-based modeling has been extensively investigated in literature [3]-[9]. The method is based on the knowledge of physical behaviors of loads and mathematical relations that describe the functioning of load devices. However, obtaining such information is not always possible, which motivates the research in measurement-based modeling [10]-[19]. Measurement-based modeling collects measurements from data acquisition equipment to derive load characteristics. The main advantage is that this approach directly obtains the data from the actual network, and can be applied to any load. However, a developed model at one network location may not be applicable to other locations. The parameters of load models are estimated by fitting the acquired data to a load model structure using identification and estimation techniques. Other research suggested the use of Artificial Neural Networks (ANN) to model loads by mapping the input data set to the output [25]-[30]. This approach is useful when the model structure is unknown or hard to be mathematically represented. However, data-driven techniques require a large number of datasets and considerable computational effort. Moreover, ANN-based models can only be applied to systems for which they were developed.

A review on load modeling was performed in 1990s [31],[32], which included a bibliography [33] listing papers on load models and typical values of parameters. The International Council on Large Electric Systems (CIGRE) established a new working group to provide guidance with respect to load modeling. The working group C4.605: "Modelling and Aggregation of Loads in Flexible Power Networks" aims to provide an overview of existing load models with a critical analysis on parameter identification methods. Developing new load models and validation techniques are also part of the agenda for CIGRE C4.605. The working group conducted a survey on international industry practice on load modeling in [34]. The paper summarized the key findings from questionnaires collected from power system operators around the world, and identified the prevalent types of load models being used. In [35], CIGRE presented a general overview on load modeling and aggregation. The report included modeling of active distribution networks and a detailed description of the commercial and residential load sectors. In this paper, we present a concise and thorough review on load modeling, including DG models. We review the existing work on load modeling and present the outstanding issues and new research trends. The commonly used load models are summarized and discussed. The ever-increasing integration of demand-side controls and DGs, particularly distributed PVs, further complicates load characteristics and poses additional challenges to load modeling. In addition, we introduce the latest advancements in developing load models, such as the use of real-time data for online modeling [21], modeling residential loads by considering both electrical characteristics and consumers' behaviors [36], and modeling microgrids (MGs) using a combination of component- and measurement-based methods [37][38].

2.2 Types of Load Models

Load modeling refers to the mathematical representation of the relationship between the power and voltage in a load bus [2]. Load models can be classified into two main categories: static and dynamic models. Fig. 2-1 shows the currently used load models in industry for static and dynamic studies [34].

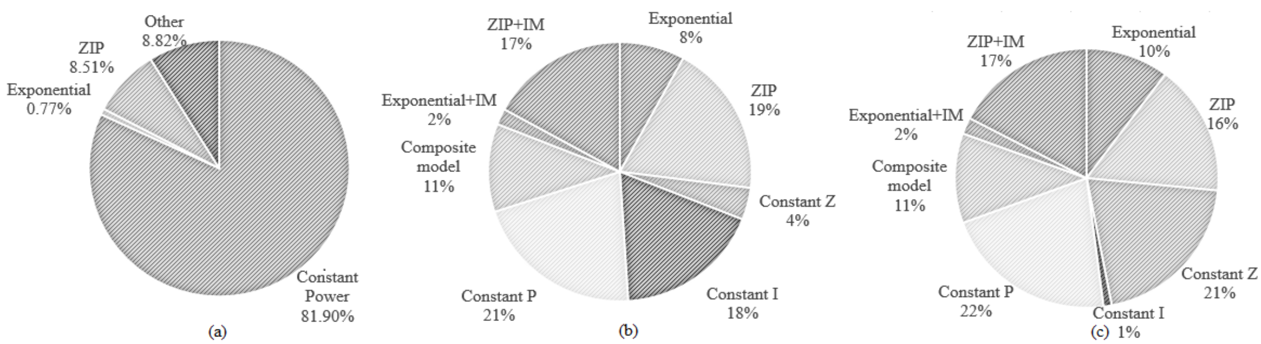

Fig. 2.1 Load models currently used in the industry for (a) steady-state analysis and dynamic studies (b) active power and (c) reactive power

2.2.1 Static Load Models

Static models express the active and reactive power at any instant of time as functions of bus voltage magnitudes and frequency. These models can be used to represent static loads e.g., resistive loads, and as an approximation for dynamic loads, e.g., induction motors.

1) ZIP Model

ZIP model is commonly used in both steady-state and dynamic studies [2]. This model represents the relationship between the voltage magnitude and power in a polynomial equation that combines constant impedance (Z), current (I), and power (P) components.

2) Exponential Model

The exponential model relates the power and the voltage at a load bus by exponential equations. This model has fewer parameters and is usually used to represent mixed loads [39]. More components with different exponents can be included in these equations. For example, by using three exponential components, the exponential model can be converted to a ZIP model.

3) Frequency Dependent Model

This model is derived by multiplying the exponential or ZIP model by a factor that depends on the bus frequency. The factor can be represented as follows.

$$Factor = \left[1 + a_f\left(f - f_0\right)\right] \tag{2.1}$$

where f is the frequency of the bus voltage, f_0 is the nominal frequency, and a, is the frequency sensitivity parameter. Adding the frequency term to the ZIP model has no physical meaning, since the component related to the constant impedance becomes dependent on the frequency [32].

4) Electric Power Research Institute (EPRI) LOADSYN Model

This model is used in the EPRI LOADSYN computational program and Extended Transient Midterm Stability Program (ETMSP) for dynamic studies [40][41]. The model combines ZIP, exponential, and frequency-dependent models.

$$P_L = P_0\left\{P_{a_1}\left(V/V_0\right)^{K_{pv1}}\left(1 + K_{pf_2}\Delta f\right) + \left(1 - P_{a_1}\right)\left(V/V_0\right)^{K_{pv2}}\right\} \tag{2.2}$$

$$Q_L = P_0 Q_{a_1}\left(V/V_0\right)^{K_{qv1}}\left(1 + K_{qf_1}\Delta f\right) + P_0\left(Q_0/P_0 - Q_{a_1}\right)\left(V/V_0\right)^{K_{qv2}}\left(1 + K_{qf_2}\Delta f\right) \tag{2.3}$$

where P_0 and Q_0 are the power consumed at the rated voltage V_0 of a device, if the model is used to represent a specific device. If it models the aggregate load at a bus, V_0 , P_0 and Q_0 are initial operating conditions. The active power is represented by frequency dependent and independent components. The reactive power is composed of two terms. The first represents the reactive power consumption of the load, and the second approximates the effect of the reactive consumption minus compensation, which finds the initial reactive power flow at a bus. P_{a1} is the frequency-dependent fraction of active power, Q_{a1} is the reactive load coefficient representing the ratio of uncompensated reactive load to active power, K_{pv1} and K_{pv2} are voltage exponents for frequency dependent and independent active power, respectively. Kq_{v1} and K_{qv2} are voltage exponents for the reactive power without and with compensation, respectively. K_{pf1} and K_{qf1} are the frequency sensitivity coefficients for active and uncompensated reactive power load, respectively. K_{qf2} is the frequency sensitivity coefficient for reactive power compensation.

2.2.2 Dynamic Load Models

Studies in voltage stability require the use of dynamic load models for accurate representation [2]. Dynamic models express the active and reactive powers as a function of voltage and time. Examples of the widely used dynamic models are presented as follows.

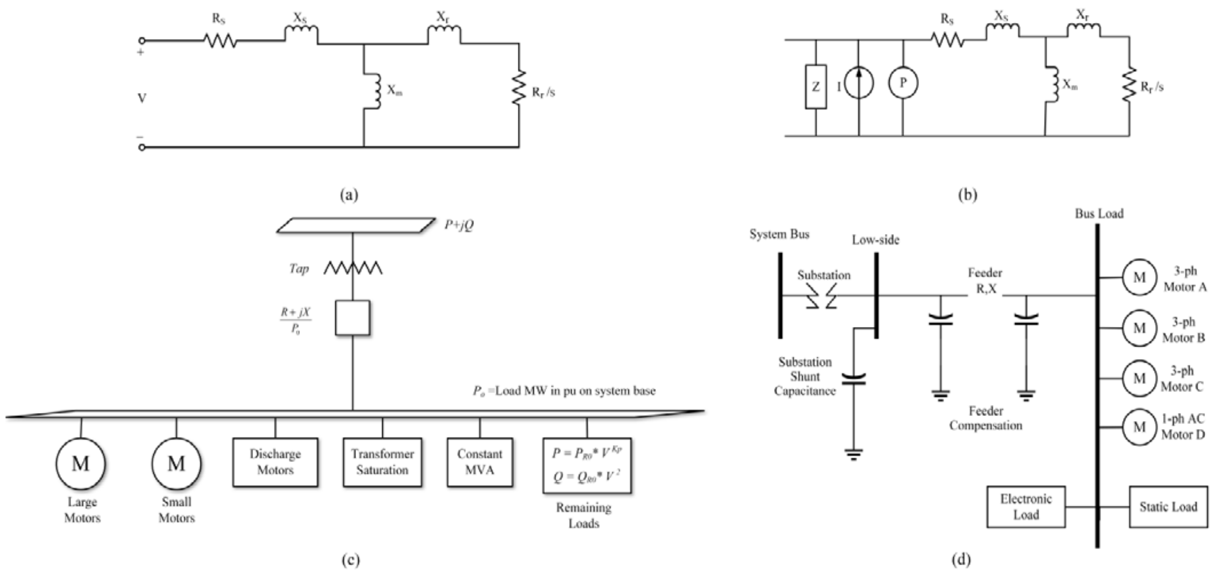

Fig. 2.2 Schematics of (a) induction motor, (b) ZIP+IM, (c) CLOD, (d) WECC CLM

1) Induction Motor (IM)

In dynamic models, the active and reactive power is represented as a function of the past and present voltage magnitude and frequency of the load bus. This type of model is commonly derived from the equivalent circuit of an induction motor [2], shown in Fig. 2.2 (a), where Rs and Rr are the static and rotor resistances respectively, Xs, Xr and Xm are the static, rotor and magnetizing reactance, respectively, and s is the rotor slip. The induction motor model is considered as a physically- based model.

2) Exponential Recovery Load Model (ERL)

The exponential recovery load model [43],[44] represents active and reactive power responses to step disturbances of the bus voltage. This model is commonly used for representing loads that slowly recover over a time period, which ranges from several seconds to tens of minutes. ERL is also used to model on-load tap changers (OLTCs) which restore the nominal supply voltage after a disturbance. The model is developed as a non-linear first-order equation to represent the load response, as shown in (4-7).

$$T_p \frac{dx_p}{dt} = -x_p + P_0 \left(V / V_0 \right)^{N_{ps}} - P_0 \left(V / V_0 \right)^{N_{pt}} \tag{2.4}$$

where x_p and x_q are state variables related to active and reactive power dynamics, T_p and T_q are time constants of the exponential recovery response, N_{ps} and N_{qs} are exponents related to the steady-state load response, N_{pt} and N_{qt} are exponents related to the transient load response.

The ERL is further extended in [45] as an adaptive dynamic model. The model has the same characteristics as the exponential recovery model, but with the power being a function of the voltage multiplied by the state variable.

$$T_p \frac{dx_p}{dt} = -x_p \left(V/V_0\right)^{N_{ps}} + P_0 \left(V/V_0\right)^{N_{pt}} \tag{2.5}$$

$$P_d = x_p \left(V/V_0\right)^{N_{pt}} \tag{2.6}$$

$$T_q \frac{dx_q}{dt} = -x_q \left(V/V_0\right)^{N_{qs}} + Q_0 \left(V/V_0\right)^{N_{qt}} \tag{2.7}$$

$$Q_d = x_p \left(V/V_0\right)^{N_{qt}} \tag{2.8}$$

2.2.3 Composite Load Models (CLM)

Recent studies focus on combining the dynamic and static load models [11],[13],[21],[46][47]. References [46] and [47] compared simulation results of different load models with transient disturbances, and concluded that composite models can provide more accurate responses. The widely used composite models are summarized in this subsection.

1) ZIP+IM

According to the study in [34], the composite load model consisting of ZIP and an induction motor is the most commonly used model in the US industry for dynamic studies. In [13], several composite load models were considered including ZIP+IM and Exponential+IM. The report concluded that the ZIP+IM structure is able to model loads with various conditions, locations, and compositions. The equivalent circuit of the ZIP+IM model is shown in Fig. 2.2 (b).

2) Complex Load Model (CLOD)

This model is adopted by the Siemens PTI PSS/E stability program [31]. CLOD is an aggregate dynamic model of large and small motors, non-linear models of discharge lighting, transformer saturation effects, constant MVA, shunt capacitors, and a series impedance and tap ratio to represent the effect of intervening sub-transmission and distribution elements. Fig. 2.2(c) shows the schematic of this model.

3) Western Electricity Coordinating Council (WECC) CLM

After the 1996 blackout of the Western Systems Coordinating Council (WSCC) [48], an interim composite load model containing a static part and a dynamic part was implemented by WSCC [49]. The model is assumed to have 80% static loads and 20% dynamic ones. The static part is represented by existing data from WSCC members, and the dynamic part is an induction motor model. The model was designed to capture the effects of dynamic induction motor loads for highly stressed conditions in summer peaks. The interim load model was unable to represent delayed voltage recovery events from transmission faults [5][50],[51]. WECC improved the interim model [6] by adding the electrical distance between the transmission system and the electrical end-uses, as well as adding special models for residential air- conditioners. By 2012, the WECC CLM was tested and implemented in major industry-level simulation software including PowerWorld Simulator and Siemens PTI PSSE [6]. Datasets were developed for four seasons in 12 climatic zones across the western region with different load sectors (residential, commercial, mixed and rural)[6]. The model structure is shown in Fig. 2.2 (d), which includes an electrical representation of a distribution system with a substation transformer, shunt reactance, and a feeder equivalent. At the consumer side, the load model includes a static load model, one power electronics model, and four types of motor models. Although CLM provides a detailed modeling, it is hard to implement as there are 131 parameters to be identified.

2.2.4 Artificial Neural Network-Based Modeling

ANN-based load modeling [25]-[30] matches observed system behaviors without using a physical form to obtain the output, i.e., it has no physical meaning and purely relies on measurement data. An ANN is composed by a set of processing units interconnected by weights. The ANNs are trained using a succession of input and output patterns, resulting in the final values of the connection weights that determine the load model. Reference [25] presented two ANN-based load modeling approaches. In [26], an ANN-based composite load model was proposed for stability studies. The authors used a two-step procedure with the first step to develop a recurrent neural network with simulation data and the second step to update it using measurement data. Although ANN is powerful in representing complex nonlinear systems., obtaining enough data over a wide range of operation conditions is challenging. In addition, ANN-based models must be updated periodically when new measurement datasets are available.

2.3 Load Model Parameter Identification

Load model identification methods can be classified into two categories: component-based and measurement-based. The component-based methods aggregate models of individual electrical components to form an aggregated load model. This approach requires knowledge on the load composition, i.e., the percentage of load consumed by each type of load components. Measurement-based approaches leverage data from devices such as PMUs, smart meters, etc. A model structure is selected and its parameters are derived using computation techniques such as statistics, artificial intelligence, and pattern recognition. Component-based methods start from the individual components, while measurement-based ones start from the measurement data as illustrated in Fig. 2.3. The two methods are summarized in Table I.

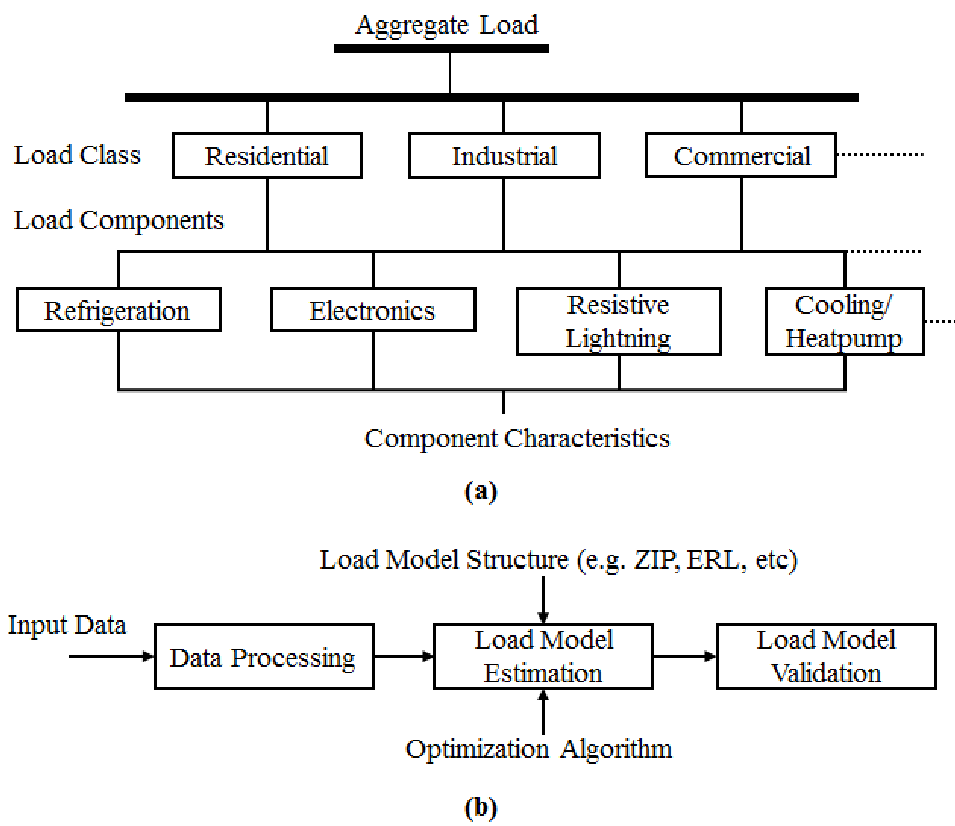

Fig. 2.3 (a) component-based modeling approach, (b) measurements-based method approach

2.3.1 Component-Based Approach

The component-based method is a bottom-up approach as illustrated in Fig. 8 (a). Load is commonly divided into industrial, commercial, and residential classes. The approach requires three datasets: 1) models of individual components, 2) component composition, i.e., the percentage of load consumed by each load component, and 3) class composition, i.e., the percentage contribution of each load class to the aggregate load. This approach has been used by WECC to develop their composite load models [6].

The individual load components can be represented using static or dynamic models. Resistive components such as electric cooking appliances and water heaters can be modelled as constant-impedance loads, while other loads such as SMPS are modeled as constant-power loads or the generic model in Fig. 2.3 [36]. The parameters for individual component models can be obtained through laboratory experiments [52]-[54].

Table 2.1 Comparison of measurement and component based approaches

	Advantages	Disadvantages
Measurement-based	- Based on data from actual systems - Provide accurate models for measured locations and time - A generic method that can be applied to various models - No need to have deep knowledge of loads	- Unable to account for different operation conditions - Models are developed using data measured in certain periods at specific locations, which lacks generalizability - Measurements with large disturbances are hard to obtain
Component-based	- Field measurement is not required - Physical representation of end-use devices - Can be applied to different operation conditions - Demand side management is considered	- Requires characteristics of individual load components. - Accurate and comprehensive load composition information is hard to obtain - Low adaptability to the integration of new loads

Determining the load composition is the most challenging task as it is impossible to obtain detailed consumption information of all electrical components in a power system. In addition, load composition is affected by geographical locations and weather conditions. For example, Fig. 2.4 show consumption profiles of different appliances in residential and commercial sectors during different seasons. Recently, the deployment of smart meters enables the two-way communication between customers and utilities, which provides a new and easy way to obtain accurate load compositions. To determine the load class composition, the metered demand at load buses can be used, which is typically available every 15 minutes.

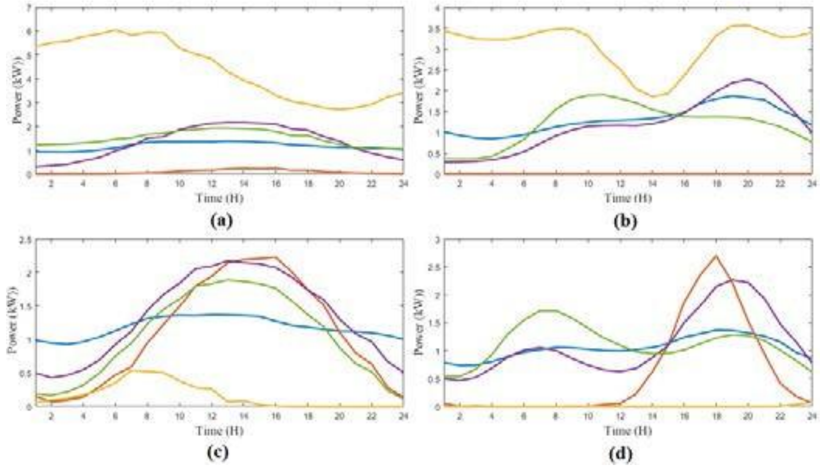

Fig. 2.4 Typical consumption profiles for (a) winter commercial class, (b) winter residential class, (c) summer commercial class, and (d) summer residential class

A different bottom-up approach was proposed in [55] for industrial facilities. Instead of obtaining the full load model of the system by using composition values of load classes, the paper proposed to create specific models for industrial loads, then obtain the system model using an aggregation algorithm developed in [56].

2.3.2 Measurement-Based Approach

Steps of the measurement-based approach are summarized in Fig. 2.3 (b): 1) obtain measurement data, 2) select a load model structure (e.g. ZIP, exponential, etc), 3) estimate model parameters, and 4) validate the load model. Measurement-based

load modeling leverages actual field data to capture load characteristics. The measurements should be obtained under different conditions and disturbances. The model parameters are estimated by minimizing the difference between the response of the load model and the field measurements. The problem can be formulated as a curve fitting problem using the following equation:

$$\min \frac{1}{n}\sum_{i=1}^{n}\left[\left(P_i^m - P_i^e\right)^2 + \left(Q_i^m - Q_i^e\right)^2\right] \tag{2.9}$$

where P_i^m and Q_i^m are the measured active and reactive power, respectively, and P_i^e and P_i^e are the modeled active and reactive power, respectively. The parameters are calculated using algorithms such as least-squares, genetic algorithm (GA), support vector machines (SVM), Kalman Filter (KF), Levenberg-Marquardt algorithm, and Simulated Annealing. Table II summarizes existing measurement-based techniques.

Table 2.2 Examples of measurement-based techniques

Ref.	Algorithms	Load Models	Data Sources
[17]	GA + Simplex search method	ZIP+IM	PMU: NE power grid in China
[20]	GA+LM	ZIP+IM	Simulation + Field measurements
[22]	Improved particle swarm optimization	Exponential + IM	Simulation + Laboratory experiments
[42]	LM	ERL	Simulation + Field measurements
[57]	Least Square	1st order IM model	Simulation
[58]	Gauss-Newton + Trajectory sensitivity	Differential- algebraic equations	Simulation
[59]	Instrumental Variable-based estimation	ZIP and Exponential and dynamic models	Simulation
[60]	Gradient-based parameter estimation	Fifth-order single rotor cage model	Laboratory experiments
[61]	Simulated Annealing	EPRI Loadsyn and IM	Simulation + Field measurements
[62]	Kalman Filter	ZIP	Korea Energy Management System
[63]	SVM	ZIP+IM	Simulation
[64]	Weighted recursive least squares	Exponential and ZIP	CPFL Energia, Brazil
[65]	Recursive least squares	Exponential	Field CVR test data

The measurement-based approach has been extensively studied in the literature. In [11], a multicurve identification technique was used to identify parameters of the ZIP+IM model. Multiple filed measurement datasets were collected and fitted to the model structure using a hybrid GA and simplex search algorithm. [21] presented an event-oriented method for online load modeling based on PMU data from the Illinois Institute of Technology MG. In [22], the authors used the sliding window technique to reflect the real-time dynamic behaviors of loads during disturbances such as voltage sags and interruptions. Least-square methods have been widely applied to identify parameters of various load models including ZIP+IM with frequency. The increasing installation of PMUs makes the online modeling an attractive approach. Reference [66] applied the unscented Kalman filter [67] to perform real- time estimation of the ERL model parameters. The developed approach was tested on both simulated and field measurements with a 3-second resolution. In [65], a time-varying exponential load model was used to represent the load, and a recursive least square algorithm was employed to identify the load model parameters. The paper used the load model to assess conservation voltage reduction (CVR) effects [68]. The authors in [69] used robust least squares approach to estimate time-varying parameters of a ZIP model at the substation level. The proposed method was used to identify the load-to-voltage dependence and analyze CVR.

There are studies using hybrid component- and measurement-based methods. [70] developed load models at high-voltage buses from load compositions of LV buses. SVM was used to classify the loads into various classes based on the load responses to large disturbances. The authors in [71] proposed a variable projection based optimization algorithm to identify the parameters of several different load models. For small disturbances, only the load component composition in each load class was identified, and the remaining parameters remained unchanged. The proposed method was tested on the 243-bus Indian Northern Regional Power Grid system. Reference [72] developed an approach to aggregate various load component models to obtain the system load model. Parameter estimation was used to determine the amount each component contributes to the total power consumption. A Gauss-Newton method based on trajectory sensitivities was used to determine the parameters of each load model structure. Trajectory sensitivities can quantify effects of small parameter changes on a dynamic system's trajectory, which can guide the parameter updates.

The authors in [14] used trajectory sensitivity for model simplification to reduce the number of parameters to be estimated. By applying the trajectory sensitivity analysis to measurement data, load model parameters were classified into two sets based on their sensitivities to the active and reactive power. Parameters with large sensitivities were grouped together and estimated using the measurement-based approach, while less sensitive parameters were set to be their default values. The parameters with low sensitivities are not necessarily unimportant, it means these parameters are hard to be identified from the current data. Reducing the number of parameters makes it possible to include more components in the load model. [23] presented an algorithm for estimating load model parameters based on the analytical similarity of model parameter sensitivities, and demonstrated its computational efficiency and accuracy. The authors in [73] analyzed model parameter sensitivities using eigenvalues of Hessian matrix. The paper used the LM algorithm to solve the optimization problem. The linear dependence between two load model parameters were then identified by examining the condition number of Jacobian matrix. This dependency analysis was used to ensure that low-sensitivity parameters were independent of high-sensitivity ones. Reference [74] presented a computationally efficient technique for estimating the composite load model (ZIP+IM) parameters based on analytical similarity of parameter sensitivity. The paper used the partial derivative of each parameter to identify parameters with similar sensitivities. LM algorithm was used to solve the optimization problem in (17). The presented technique was tested on real measurements collected from Cheongju and Suwon of South Korea. The computation time was reduced by three quarters after reducing the number of parameters from 12 to 9.

2.4 Summary

This section reviews the state-of-the-art of load models and parameter identification methods. New approaches for modeling LV networks and ADNs are also discussed. Load modeling is challenging due to the large number of diverse load components, the lack of precise load composition information, and the stochastic, time-varying and weather-dependent load behaviors. Currently, the ZIP+IM composite model is one of the most widely used models in US power industry [34].

WECC and EPRI have been actively investigating load modeling techniques. WECC focused on the component-based approach while EPRI is developing hybrid approaches that integrate component- and measurement-based methods. The WECC composite load model is comprehensive and flexible, however, it is complicated and hard to apply. There are also concerns about the numerical stability and consistency of the WECC model. ZIP+IM is less complicated, but it is unable to capture the full system characteristics. Furthermore, ZIP+IM cannot represent DGs' behaviors. CIGRE provided several overviews and recommendations on load modeling which were combined in [75][77].

For parameter identification, measurement-based techniques are prevalent as new devices such as PMUs and smart meters are installed. However, it is still challenging to identify a large number of unknown parameters. Sensitivity analysis has been proposed to reduce the number of parameters and identify the significant ones. Extreme sensitivities could lead to the failure of the load model with small changes in operating conditions. Further research on sensitivity analysis is needed. The deployment of smart measurement devices provides an opportunity to design hybrid approaches that integrate the measurement- and component-based methods. The introduction of new loads and controls will reshape the load composition. The deployment of smart meters provides an opportunity to improve the load composition estimation for component-based load modeling [78]. The amount of data collected from the measurement devices is massive, and processing a large number of data is challenging. Data collection and processing techniques such as data mining and clustering should be improved. Future research on parameter estimation algorithms should be able to process data from existing and emerging measurement devices with different resolutions, such as smart meters, PMUs, and SCADA. Meanwhile, the algorithms should be robust to bad data, missing measurements, changes in the voltage regulation scheme, and noises [79]-[80].

3. Parameter Reduction of Composite Load Model using Active Subspace

3.1 Introduction

Load modeling is significant for power system studies such as parameter identification, optimization and stability analysis, which has been widely studied [81]. It can be classified into static and dynamic load models. Constant impedance-current-power (ZIP) model, exponential model and frequency dependent model are typical static loads models, and traditional dynamic load models include induction motor (IM) and exponential recovery load model [82]. To provide more accurate responses, composite load models are developed by combining static and dynamic load models. Motivated by the 1996 blackout reported by the Western Systems Coordinating Council (WSCC), the classic ZIP+IM composite load model was developed to model highly stressed loading conditions in summer peak hours [83]. However, this interim load model was unable to capture the fault-induced delayed voltage recovery (FIDVR) events [84]. Therefore, a more comprehensive composite load model was proposed by Western Electricity Coordinating Council (WECC) that contains substation trans-former, shunt reactance, feeder equivalent, induction motors, single-phase AC motor, ZIP load, electronic load, and DER [85]. WECC composite load model (WECC CMLD) produces accurate responses, nevertheless, the large number of parameters and high model complexity raise new challenges for power system studies. Name parameter identification as one significant example, where the large number of parameters brings great difficulties to search for global optimum when performing parameter identification. The reason is twofold: firstly, the large number of parameters result in a large search space that reduces the optimization efficiency; secondly, the insensitive parameters and parameter interdependencies usually result in a large number of local optima, which increases the difficulty of achieving global optimum [86]. Although the parameters have physical meanings, some of them only have marginal impacts on the model response altogether or along certain parameter variation directions [87]. Moreover, considering full load model parameter set could significantly increase the complexity of power system studies. Therefore, it is imperative to develop a method to screen out the insensitive parameters. Then, only the sensitive parameters are to be determined in the parameter identification problem while the others can be kept at their respective default values. In this way, the dimension of search space of load model parameters can be significantly reduced. Thus, lower computational cost (less model runs) and higher accuracy (easier to find the optimum) can be achieved when conducting power system studies such as parameter identification without compromising fidelity of the load model.

The above problem can be resolved by dimension reduction in parameter space based on sensitivity analysis of a parameterized model whose inputs are system parameters. As discussed in [88], parameter reduction (PR) methods can be classified into local and global ones. Local PR methods are suitable for known parameters with small uncertainties, in which partial derivatives of output with respect to the model parameters are computed to evaluate the relative variation of output with respect to each parameter. Nonetheless, the input parameters are subject to a range in typical load modeling problems. Therefore, a global sensitivity metric is necessary to measure the sensitivity of output with respect to parameters.

There are many existing global PR approaches. One of the most common and simplest techniques in engineering is the so-called “One-At-A-Time” (OAT) method that varies one parameter while fixing the others. However, this method can only provide a rough qualitative approximation of the parameter sensitivities and cannot fully reveal the nonlinearity and interdependency among the parameters due to its low exploration of the parameter space. In [89], the OAT method was improved by proposing two sensitivity measures, mean μ and standard deviation σ based on the elementary effects methods. This method has higher exploration rate of the parameter space and can qualitatively analyze which parameter may have influence on nonlinear and/or interaction effects. This method is further extended by supersaturated design [90], screening by groups [91], sequential bifurcation method [92] and factorial fractional design [93] based on the number of parameters and experiments in a particular scenario [94].

To quantitatively study the comprehensive parameter sensitivity patterns and their interdependencies, variance-based approaches such as Sobel indices [95] were proposed for nonlinear and non-monotonic models. However, to precisely estimate the sensitivity indices with arbitrary order interactions between parameters, these approaches require a formidably large number of experiments [96]. In [97], a total-effect index was introduced, which can measure the contribution to the out-put variance of parameters, including all variance caused by its interactions of any order with any other parameters, as well as reducing the requirement of the number of experiments. These indices are usually estimated by Monte Carlo methods [98]. Such methods are accurate but suffer from high computational cost when large sample size is required. Thus, it motivates the recent research on exploring efficient numerical algorithms including the analysis of variance (ANOVA) decomposition [99], Fourier Amplitude Sensitivity Test (FAST) [100] and least ab-solute shrinkage and selection operator (LASSO) [101]. Despite the relative reduction in computational cost by these methods, they can result in instability and inaccuracy when the number of parameters increases (larger than 10) [94], [102]. Some researches delve into the trajectory sensitivity analysis, e.g., in [103], the time-varying parameter sensitivities of ZIP+IM model are derived based on perturbation and Taylor expansion method. However, such methods need explicit mathematical model and require the model output to be differentiable with respect to the parameters for the Jacobian matrices to exist, which makes it inapplicable for WECC CMLD. Different from OAT and and variance-based approaches, the active subspace method (ASM) is based on gradient evaluations for detecting and exploiting the most influential direction in the parameter space of a given model to construct an approximation on a low-dimensional subspace of the model's parameters as well as quantify the interdependencies among parameters [104]. As a Monte Carlo sampling based method, ASM also requires multiple experiments, but it has better accuracy and requires relatively lower sample size.

There are limited studies on the PR problem of WECC CMLD. In [81], the parameter sensitivity and interdependencies among parameters are analyzed using OAT method and clustering techniques, motivated by observing that different parameter combinations can give the same data fitting results in measurement-based load modeling. As discussed above, the OAT method suffers from low accuracy and low exploration rate of the parameter space. Moreover, the interdependency is simply determined by whether parameters have similar trajectory sensitivities in this work. In addition, the newly-approved aggregated distributed energy resources (DER A) model in WECC CMLD has not been considered. PR was conducted by means of data-driven feature-wise kernelized LASSO (FWKL) in [101], which uses multiple randomly-generated parameter vectors and corresponding output residuals to compute parameter sensitivities by solving a LASSO optimization problem. This approach avoids utilizing analytical gradient and can obtain the optimal sensitivity. In addition, the employment of LASSO ensures parameter interdependency is captured in a feature-wise manner. However, due to high non-convexity of WECC CMLD, the result is very sensitive to parameter setting of the algorithm and the distribution of the dataset. Also, the large number of experiments and optimization process greatly increase its computational cost.

In this chapter, a novel PR approach is proposed by leveraging the ASM. As an alternative PR technique, ASM is a relatively new dimension reduction tool that has shown its effectiveness in many fields such as bioengineering [105] and aerospace engineering [106]. The outstanding advantages of ASM include relatively low computational cost, high accuracy and the ability to quantify the parameter interdependency.

Motivated by the fact that the WECC CMLD is a differential-algebraic system and ASM can only deal with algebraic functions, we first cast the WECC CMLD as a discrete-time system for parameterization. Secondly, a comprehensive PR approach tailored for WECC CMLD based on ASM is proposed. Thirdly, factors influencing accuracy of PR results are rigorously analyzed. Finally, statistical and numerical experiments are conducted to validate the effectiveness of the proposed method. Comparative case studies with three classical PR methods are also conducted and discussed.

3.2 Problem Statement

In this section, the structure and function of WECC CMLD are introduced, then a parameterized model of the composite load is established for PR.

3.2.1 Introduction of WECC CMLD

As shown in Fig. 3.1, WECC CMLD consists of three 3-phase motors, one single-phase motor, one ZIP load, one electronic load and one DER A model. Three 3-phase motors represent three different types of dynamic components. Motor A represents three-phase induction motors with low inertia driving constant torque loads, e.g. air conditioning compressor motors and positive displacement pumps. Motor B represents three-phase induction motors with high inertia driving variable torque loads such as commercial ventilation fans and air handling systems. Motor C represents three-phase induction motors with low inertia driving variable torque loads such as the common centrifugal pumps. Single-phase motor D captures behaviors of single-phase air with reciprocating compressors. However, it is challenging to model the fault point-on-wave and voltage ramping effects [85]. Moreover, new A/C motors are mostly equipped with scroll compressors and/or power electronic drives, making their dynamic characteristics significantly different than conventional motors. Therefore, WECC uses a performance-based model to represent single-phase motors. As increasing percentage of end-uses become electronically connected [83], the WECC CMLD adopts a simplistic representation of power electronic loads as constant power loads with unity power factor. A ZIP load is used as static one in this model. The DER model is specified as the newly-approved DER A model presented in [107].

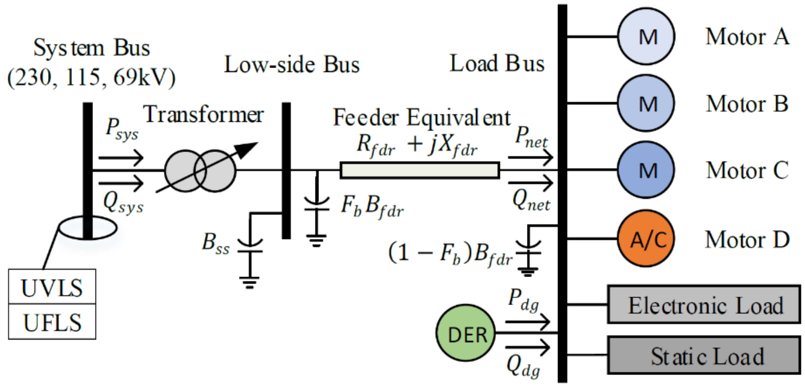

Fig. 3.1 A schematic diagram of the WECC CMLD[108]

3.2.2 Motivation for PR

The WECC CMLD contains 183 parameters, which pose significant challenges for power system studies such as parameter identification, optimization and control. By observing that part of the parameters can be determined by engineering judgment, we can filter out them according to the analysis in [101]. In particular, the parameters of transformer, feeder, and the stalling and restarting of induction motors can be excluded since they have small range of uncertainties and are usually pre-determined by their default values to meet practical engineering requirements. In this way, 64 parameters are screened out a priori. Nonetheless, the number of parameters that remains is still too large for power system studies. Therefore, in this chapter, we use ASM to further reduce the number of parameters. The WECC CMLD is a differential-algebraic system which is usually represented as a continuous-time state space model [84]. Considering that ASM requires a scalar function with domain as parameters and range as active or reactive power, in this section, we parameterize the WECC CMLD in a discretization manner. The parameterized model produces similar responses as the original one with high-fidelity as long as the Nyquist-Shannon sampling theorem is satisfied.

3.2.3 Parameterized WECC CMLD

The WECC CMLD is a hybrid model with dynamic and static components. The state vector $x \in \mathbb{R}^{n_d}$ of three-phase motors and DER is governed by the following differential equation

$$\dot{x}(t) = f\left(x(t),\ \theta(t),\ u(t)\right), \tag{3.1}$$

where $\theta(t) \in \mathbb{R}^{n_p}$ denotes the parameter vector; $u(t) = \left[\left|V(t)\right|,\ \varphi(t),\ \Delta f(t)\right]^T$ is the input vector consisting of volt-age magnitude, voltage angle and frequency deviation, respectively; $f : \mathbb{R}^{n_d} \times \mathbb{R}^{n_p} \times \mathbb{R}^{3} \to \mathbb{R}^{n_d}$ represents the dynamic model of three-phase motors, and DER; n_d and n_p are the total number of dynamic states and parameters. The active and reactive power output of the dynamic components, $y_d(t) = \left[P_d(t), Q_d(t)\right]^T$ is given by

$$y_d(t) = g_d\big(x(t),\ \theta(t),\ u(t)\big). \tag{3.2}$$

In PR using ASM, a mapping between parameters and active/reactive power is required for PR. Based on the fact that the input of load model u is usually sampled every T seconds, we can discretize (3.1) as

$$x(k) = \bar{f}\big(x(k-1),\ \theta(k-1),\ u(k-1)\big), \tag{3.3}$$

where $\bar{f}$ is the discretized function of f, $k = 1, 2, \ldots, N$, N is the total number of measurements. Note that the sampling rate should satisfy Nyquist-Shannon sampling theorem to guarantee that discrete sequence of samples can capture all the information from a continuous-time signal. Then, $x(k)$ can be calculated from the initial state $x(0)$ by iteratively evaluating $\bar{f}$ using past sequences of parameters and inputs, $\left[\theta(k-1), \ldots, \theta(0), u(k-1), \ldots, u(0)\right]$. Finally, by substituting (3.3) iteratively into (3.2), we can obtain the desired mapping using some algebraic function $\bar{g}_d$:

$$y_d(k) = \bar{g}_d\big(\theta(k), \ldots, \theta(0), u(k), \ldots, u(0), x(0)\big). \tag{3.4}$$

Regarding x and u as constants, Eq. (3.4) depicts the relation-ship between active/reactive power of dynamic components and parameters.

As for the static components such as single-phase motor, electronic load, and static ZIP load, the mapping from parameters to active and reactive power outputs can be represented as

$$y_s(k) = g_s\big(\theta(k), u(k)\big). \tag{3.5}$$

The total power output $y(k)$ of the WECC CMLD can be calculated by adding the dynamic and static parameterized model together. For ease of deriving PR approach for the composite load model, we define the parameterized model as g in the form of

$$y(k) = y_d(k) + y_s(k) = g\big(\theta(k),\ \mathrm{K},\ \theta(0),\ u(k),\ \mathrm{K},\ u(0),\ x(0)\big). \tag{3.6}$$

If the parameters are considered as time-invariant during a short time period, Eq. (3.6) can be simplified as

$$y(k) = g\big(\theta, u(k), \ldots, u(0), x(0)\big). \tag{3.7}$$

where $y(t) = \left[P(t), Q(t)\right]^T$, and $g = \left[g_P, g_Q\right]^T$.

3.3 PR Approach for WECC CMLD using ASM

In this section, we will use ASM to reduce the parameters of the WECC CMLD. Firstly, the preliminaries of ASM are introduced. Then, the application of ASM to WECC CMLD is elaborated in steps. Finally, the factors affecting the accuracy of PR is analyzed theoretically.

3.3.1 Preliminaries of ASM

An active subspace is a lower-dimensional linear subspace of the parameter space, along which input perturbations alter the model's predictions more than the perturbations along the directions which are orthogonal to the subspace on average. This subspace allows for a global measurement of sensitivity of output variables with respect to parameters, and is often used to decrease the dimension of the parameter space. Con-sider a parameterized function $g:\chi \to \mathbb{R}$ that maps the parameters of a system, $\bar{\theta} \in \chi := \left\{ x \in \mathbb{R}^m \mid -1 \le x_i \le 1, i = 1, \ldots, m \right\}$, to a scalar output of interest, e.g., active power *P* or reactive power *Q*, where χ indicates a normalized set of parameter values.

To discover the active subspace, we define the following *C* matrix,

$$C = \int_{\chi} \left(\nabla_{\bar{\theta}} g\left(\bar{\theta}\right) \right) \left(\nabla_{\bar{\theta}} g\left(\bar{\theta}\right) \right)^T \rho\left(\bar{\theta}\right) d\bar{\theta}. \tag{3.8}$$

where $\rho\left(\bar{\theta}\right):\chi \to \mathbb{R}_+$ is the joint probability function of parameters satisfying

$$\int_{\chi} \rho\left(\bar{\theta}\right) d\bar{\theta} = 1. \tag{3.9}$$

For any smooth function $g\left(\bar{\theta}\right)$, the matrix *C* is called average derivative functional in the context of dimension reduction, which weights input values according to the density $\rho\left(\bar{\theta}\right)$. Note that a single normalized parameter is a random variable taking values in [−1, 1], which when appropriately scaled represents a parameter in the original model (3.7). Since the dimension of the parameter space in this model is 64, we take $m = 64$ throughout. The matrix *C* is the average of the outer product of the gradient of $g\left(\bar{\theta}\right)$ with itself and has some useful properties that will allow us to deduce information about how $g\left(\bar{\theta}\right)$ is altered by perturbations in its arguments.

Remark 1: From (3.8), each element of *C* is the average of the product of partial derivatives (which can be regarded as parameter sensitivity)

$$C_{ij} = \int_{\chi} \left(\frac{\partial g}{\partial \bar{\theta}_i} \right) \left(\frac{\partial g}{\partial \bar{\theta}_j} \right) \rho d\bar{\theta}, \quad i, j = 1, \ldots, m, \tag{3.10}$$

where C_{ij} is the (*i*, *j*) element of *C*, and m is the number of parameters. If we consider $\nabla_{\bar{\theta}} g\left(\bar{\theta}\right)$ to be a random vector by virtue of $\bar{\theta}_i$'s density ρ, then *C* is the uncentered covariance matrix of the gradient of output with respect to the parameters [104]. This allows us to use the covariance matrix *C* to measure the correlation between each pair of parameter gradients. For simplicity, denote $\frac{\partial g}{\partial \theta_i}$ as s_i, denote the mean and standard

deviation of gradient of *i*th parameter as μ_{s_i} and σ_{s_i}, respectively. Then, the correlation between (*i, j*) parameter gradients is

$$\begin{aligned}
\rho_{s_i,s_j} &= \frac{\operatorname{cov}(s_i, s_j)}{\sigma_{s_i}\sigma_{s_j}} \\
&= \frac{\mathrm{E}\left[\left(s_i - \mu_{s_i}\right)\left(s_j - \mu_{s_j}\right)\right]}{\sigma_{s_i}\sigma_{s_j}} \\
&= \frac{C_{ij} - \mu_{s_i}\mu_{s_j}}{\sigma_{s_i}\sigma_{s_j}}
\end{aligned} \tag{3.11}$$

Eq. (3.11) shows that the *C* matrix encodes the correlation information between parameter gradients, which means the ASM takes into consideration the interdependency of parameters. This is one of the advantages compared to other PR methods.

The matrix *C* is symmetric, and thus permitting the spectral eigen-decomposition

$$C = W \Lambda W^T \tag{3.12}$$

where *W* is an orthogonal matrix whose columns $\omega_i, (i = 1, \ldots, m)$ are the orthonormal eigenvectors of *C*. $\Lambda = diag\left(\left[\lambda_1, \ldots, \lambda_m\right]\right)$, and $\lambda_1 \geq, \ldots, \geq \lambda_m$.

Since *W* is orthogonal, from the definition of eigenvectors and (3.8), the eigenvalues of *C* can be calculated as

$$\begin{aligned}
\lambda_i &= \omega_i^T C \omega_i \\
&= \omega_i^T \int_\chi \left(\nabla_{\bar{\theta}} g\left(\bar{\theta}\right)\right)\left(\nabla_{\bar{\theta}} g\left(\bar{\theta}\right)\right)^T \rho\left(\bar{\theta}\right) d\bar{\theta}\omega_i \\
&= \int_\chi \left(\left(\nabla_{\bar{\theta}} g\left(\bar{\theta}\right)\right)^T \omega_i\right)^2 \rho\left(\bar{\theta}\right) d\bar{\theta}, \quad i = 1, \ldots, m
\end{aligned} \tag{3.13}$$

From (3.13) we see that the eigenvalues of the C matrix are the mean squared directional derivatives of $g\left(\bar{\theta}\right)$ in the direction of the corresponding eigenvector. If an eigenvalue is small, then (3.13) shows that $g\left(\bar{\theta}\right)$ is insensitive in the direction of the corresponding eigenvector on average. On the contrary, a large eigenvalue indicates that $g\left(\bar{\theta}\right)$ changes significantly in the direction of the corresponding eigenvector.

After determining the eigen-decomposition (3.12), the eigen-values and eigenvectors can be separated according to the magnitudes of eigenvalues:

$$\Lambda = \begin{bmatrix} \Lambda_1 & 0 \\ 0 & \Lambda_2 \end{bmatrix}, \quad W = \begin{bmatrix} W_1 & 0 \\ 0 & W_2 \end{bmatrix} \tag{3.14}$$

where Λ_1 and W_1 contain the first n larger eigenvalues and corresponding eigenvectors, Λ_2 and W_2 contain the other $m - n$ smaller ones. To determine such separation, one can find the spectral gap between the nth and (*n+1*) th eigenvalues on a log plot in the order of magnitudes. It is worth noting that the existence of a significant spectral gap directly indicates the existence of active subspace [24].

Keeping in mind that *W* is orthogonal, from (3.14), any parameter vector θ can be represented as

$$\begin{aligned} \theta &= WW^T\theta \\ &= W_1W_1^T\theta + W_2W_2^T\theta \\ &= W_1\theta_1 + W_2\theta_2 \end{aligned} \tag{3.15}$$

Then, an output of interest with any parameter vector θ is

$$g(\theta) = g(W_1\theta_1 + W_2\theta_2) \tag{3.16}$$

From the definition of W_1 and W_2, we know that small perturbations on θ_2 have low impact on the value of *g*. Conversely, small perturbations on θ_1 will alter *g* significantly. According to this property, the range of W_1 is defined as the active subspace, and on the contrary, the range of W_2 as the corresponding inactive subspace of the model. These subspaces describe the sensitivity of the output of interest with respect to parameter variations.

It is worth noting that, though both ASM and principal components analysis (PCA) include the process of eigen-decomposition, they are intrinsically different. The PCA eigen-decomposed the covariance matrix of the parameter vector θ, whereas the matrix to be eigen-decomposed in the active subspace is defined as (3.8).

3.3.2 PR Algorithm Based on ASM

The overall algorithm for PR of WECC CMLD using ASM is summarized in Fig. 3.2. The key idea of the algorithm is elaborated in details as follows:

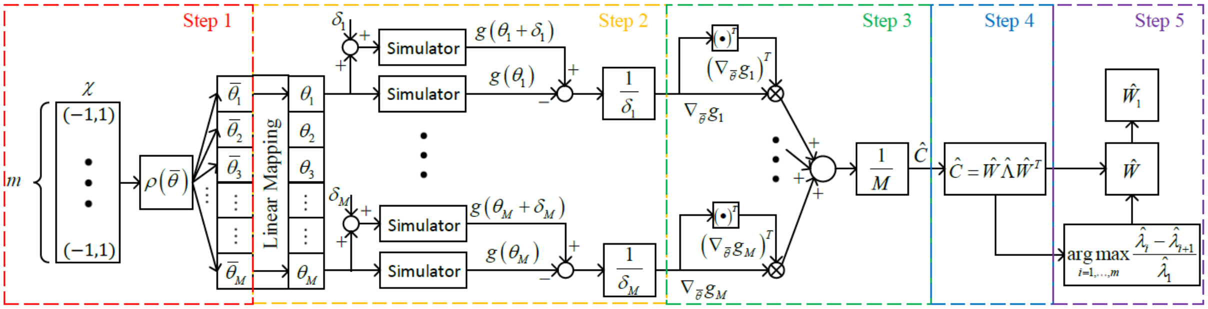

Fig. 3.2 The block diagram of the proposed PR algorithm based on ASM

Step 1: Construct the parameter set $\chi = [-1,1]^m$, m = 64 as the normalized parameter space for all the selected parameters of WECC CMLD, and draw M samples $\{\bar{\theta}_j\}, j = 1,\ldots,M$ from χ according to some probability density function satisfying (3.9). Usually, uniform distribution is chosen for simplicity.

Step 2: For each sampled parameter vector $\bar{\theta}_j$, approximate the gradient $\nabla_{\bar{\theta}} g_j = \nabla_{\bar{\theta}} g(\bar{\theta}_j)$ using first order forward finite differences method as follows:

$$\nabla_{\bar{\theta}} g(\bar{\theta}_j) = \begin{bmatrix} \dfrac{\partial g}{\partial \bar{\theta}_{j,1}} \\ \vdots \\ \dfrac{\partial g}{\partial \bar{\theta}_{j,m}} \end{bmatrix} \approx \begin{bmatrix} \dfrac{g(\theta_{j,1} + \delta_{j,1}) - g(\theta_{j,1})}{\delta_{j,1}} \\ \vdots \\ \dfrac{g(\theta_{j,m} + \delta_{j,m}) - g(\theta_{j,m})}{\delta_{j,m}} \end{bmatrix}, \quad j = 1,\ldots,M, \tag{3.17}$$

where δ_j is an arbitrarily small positive vector perturbation from the sampled parameter values. When g is a practical system, e.g., WECC CMLD, one needs to transform the normalized parameter vector $\bar{\theta}_j$ to θ_j that is in the standard range of parameters, using the following linear mapping,

$$\theta_j = \frac{1}{2} diag\left(\left(\theta_{upper} - \theta_{lower}\right)\bar{\theta}_j + \left(\theta_{upper} - \theta_{lower}\right)\right). \tag{3.18}$$

where θ_{upper} and θ_{lower} are upper and lower bounds of the parameter vectors, respectively. Thus, θ_j in (3.18) denotes the vector of real parameter values of the WECC CMLD.

Step 3: Approximate the average derivative functional C using Monte Carlo simulation as

$$C = \hat{C} \approx \frac{1}{M} \sum_{j=1}^{M} \left(\nabla_{\bar{\theta}} g_j \right) \left(\nabla_{\bar{\theta}} g_j \right)^T. \tag{3.19}$$

Step 4: Compute the eigen-decomposition of approximate matrix $\hat{C}$:

$$\hat{C} \approx \hat{W} \hat{\Lambda} \hat{W}^{'T}, \tag{3.20}$$

which is equivalent to calculating the singular value decom-position of the matrix

$$\frac{1}{\sqrt{M}} \left[\nabla_{\bar{\theta}} g_1, \mathrm{K}\ , \nabla_{\bar{\theta}} g_M \right] = \hat{W} \sqrt{\hat{\Lambda}} \hat{V}^T, \tag{3.21}$$

where the singular values are the square roots of the eigen-values of $\hat{C}$ and the left singular vectors are the eigenvectors of $\hat{C}$. The singular value decomposition perspective was first used in [109][29] to determine the active subspace that is related to the principal components of a collection of gradients.

Step 5: After the decomposition (3.21), one needs to search for the largest spectral gap among eigenvalues in $\hat{\Lambda}$ for subspace separation. The existence of a larger spectral gap indicates a more accurate determination of active subspace. To automatically find the optimal separation, we can use the following equation,

$$\Delta \hat{\lambda}_i = \frac{\hat{\lambda}_i - \hat{\lambda}_{i+1}}{\hat{\lambda}_1}, \quad i = 1, \mathrm{K}\ , m-1, \tag{3.22}$$

Then, the dimension of the active subspace is

$$\dim\left(range\left(W_1 \right) \right) = \underset{i=1,\mathrm{K}\ ,m-1}{\arg\max} \Delta \hat{\lambda}_i \tag{3.23}$$

From (3.23), we know that the index of the largest value of $\Delta \hat{\lambda}_i$ indicates the location of the largest spectral gap. In the dimension reduction context, often only the first value $\Delta \hat{\lambda}_1$ is considered such that the dimension of the active subspace is limited to one, which makes it more convenient for visualization of the output as a function of the active subspace [104][24]. Then, the magnitudes of elements in the first eigenvector describe the weights of parameters.

Remark 1: The active subspace describes the most sensitive direction in the parameter space along which the output of interest evolves fastest. Thus, from (16) the output of parameterized model can be approximated by only the active subspace of parameter space, i.e.,

$$g(\theta) \approx g(W_1 \theta_1), \qquad \theta_1 = W_1^T \theta. \tag{3.24}$$

Eq. (3.24) indicates that g is related to θ_1 which is a linear combination of original parameters θ. This linear combination reflects the weight of each parameter and their collective influence on the output of interest.

The accuracy of the approximation (3.24) depends mainly on two factors which will be further discussed in the next subsection.

3.3.3 Accuracy Analysis of PR Based on ASM

In this subsection, two main factors affecting the accuracy of PR using ASM introduced above will be discussed.

1)Sample size M: In the above algorithm, the most costly computation processes are eigen-decomposition and computing gradient for M times. In our case, the number of parameters is m = 64, so the computational cost of eigen-decomposition is negligible compared to the computation of gradient. Thus, the selection of M that is large enough for approximating Λ and W while minimizing the computational cost is of vital importance. To estimate the first n eigenvalues of matrix C, the sample size M can be chosen as

$$M = \beta n \log(m), \tag{3.25}$$

where β is an oversampling factor, which is usually selected between 70 and 120. In the next section, we will verify that this range of β is sufficient in the PR of WECC CMLD by experiment. The logarithm term log(m) follows from the bounds in the theorem proposed in [109].

2)Gradient approximation: The WECC CMLD suffers from high nonlinearity and complexity that render it difficult to derive a closed-form expression of gradient of output of interest with respect to the parameters. In view of the simulating g is not too expensive nor too noisy and m is not too large, we can utilize finite difference method to estimate the gradient. We know that, a smaller δ produces a more accurate approximation but with increased computational cost and vice versa. This relationship can be expressed as the following inequality by using (3.17),

$$\left\| \nabla_{\bar{\theta}} g(\bar{\theta}_j) - \frac{g\left(\theta_j + \delta_j\right) - g\left(\theta_j\right)}{\delta_j} \right\| \le \sqrt{m}\alpha\left(\delta_j\right), \quad j = 1, \ldots, M, \tag{3.26}$$

where $\lim_{\delta_j \to 0} \alpha\left(\delta_j\right) = 0$.

In the following, we will give a criterion for the selection of finite difference perturbation δ_j by restating Theorem 3.13 from [104].

Theorem 1 (Accuracy criterion of estimated active subspace [Thm. 3.13 in [104]]): Assume that $\left\| \nabla_{\bar{\theta}} g\left(\bar{\theta}_j\right) \right\| \le L$ for $j = 1, \ldots, M$, and choose small parameter ε and β in (25) satisfying

$$0 < \varepsilon \le \frac{\lambda_n - \lambda_{n+1}}{5\lambda_1}, \tag{3.27}$$

$$\beta \ge \max \frac{L^2}{n\varepsilon^2}\left\{\frac{\lambda_1}{\lambda_n^2}, \frac{1}{\lambda_1}\right\}. \tag{3.28}$$

If the finite difference perturbation is small enough such that

$$5m\alpha\left(\delta_j\right)^2 + 10L\sqrt{m}\alpha\left(\delta_j\right) \le \hat{\lambda}_n - \hat{\lambda}_{n+1}, \quad j = 1, \ldots, M, \tag{3.29}$$

then, the distance between real active subspace W_1 and the approximated one $\hat{W}_1$ using Monte Carlo and finite difference approximation method is bounded by

$$dist\left(range\left(\hat{W}_1\right), range\left(W_1\right)\right) \le \frac{4m\alpha\left(\delta_j\right)^2 + 8L\sqrt{m}\alpha\left(\delta_j\right)}{\left(1-\varepsilon\right)\lambda_n - \left(1+\varepsilon\right)\lambda_{n+1}} + \frac{4\varepsilon\lambda_1}{\lambda_n - \lambda_{n+1}} \tag{3.30}$$

for $j = 1, \ldots, M$, with high probability.

Proof: The proof follows the similar steps as in [104] by simply combining (3.25) and (3.28).

We choose $\delta_j = 1\times10^{-6}$, L = 1, m = 64, ε = 0.1, β = 100 and $\alpha\left(\delta_j\right) = \delta_j$ such that (3.27)-(3.29) hold. Then, based on Theorem 1, the error of active subspace estimate is bounded by 0.8 and the simulation result is not too far off.

Remark 2: When the two factors are appropriately set, another most influential factor is the normalized eigenvalue separation $\lambda_1 / \lambda_n - \lambda_{n+1}$ in (3.30), which depends on the system characteristics only. The existence of significant spectral gap indicates a clear active subspace and accurate estimation.

3.4 Case studies

In this section, the proposed ASM is applied to analyze the sensitivities of the parameters of WECC CMLD. Firstly, a basic case study is conducted to show the implementation process and how to interpret the result. Then, the proposed method is also applied to the FIVDR case to show its effectiveness on more complicated voltage profile. Finally, three classical PR techniques are applied to the WECC CMLD for comparison with the proposed method.

3.4.1 Case I: Apply ASM to WECC CMLD and Result Analyses

1)Simulation Setup: We first provide the simulation setup for the case studies. The range of parameters $\left[\theta_{upper}, \theta_{lower}\right]$ is set by adding plus and minus fifty percent of perturbations on the standard values given in the guideline of WECC CMLD [108] as shown in Table 3.1. Using (3.25) with m = 64, n = 1 and β = 120, the sample size is calculated as $M_{ASM} \approx 500$. In Section 3.4.3, we will show the convergence of parameter sensitivity with respect to increasing sample size, from which we can conclude that $M_{ASM} = 500$ is a good balance between accuracy and computational cost. Then, the samples are drawn uniformly from χ. When approximating the gradient using (3.17), the finite difference perturbation δ is chosen as 1×10^{-6}, which is small enough to satisfy (3.29). Since ASM assumes scalar function g, we conduct the simulation by selecting active and reactive power as output of interest separately. The voltage and power measurements for PR in this simulation is generated by the Power System Simulator for Engineering (PSS/E) and the ACTIVSg500 test case with a line-to-ground fault [101] as shown in Fig. 3.3. The case study is conducted on a standard PC with an Intel(R) Xeon(R) CPU running at 3.70 GHz and with 32.0 GB of RAM using MATLAB.

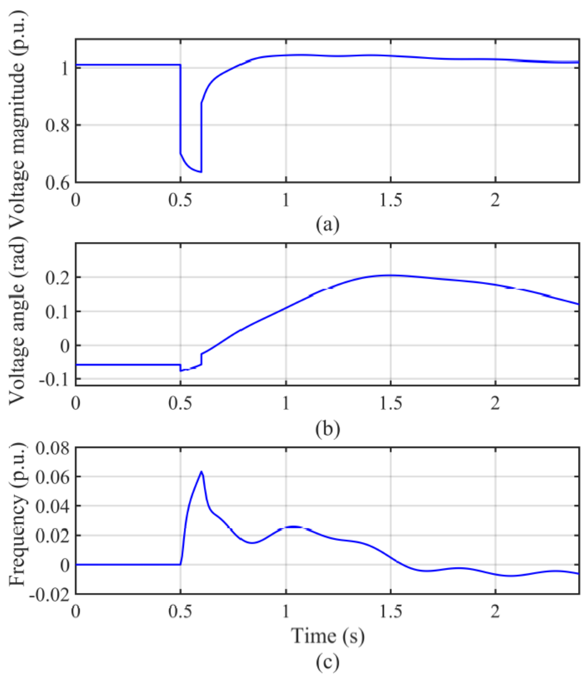

Fig. 3.3 The load bus inputs: (a) voltage magnitude; (b) voltage angle; (c) frequency

Table 3.1 Numerical range of load parameters of WECC CMLD

Parameter	LB	UB	Parameter	LB	UB	Parameter	LB	UB
Motor A			LppC	0.06	0.24	Electronic Load		
TpoA	0.046	0.184	LsC	0.9	3.6	Frcel	0	0.38
TppoA	0.001	0.004	RsC	0.015	0.06	Vd1	0.5	1.5
LpA	0.05	0.20	HC	0.1	0.4	Vd2	0.25	1
LppA	0.042	0.168	EtrqC	1.8	2.2	DER_A		
LsA	0.9	3.6	DC	0.5	2.0	Trv	0.01	0.04
RsA	0.02	0.08	Motor D			Trf	0.02	0.06
HA	0.05	0.20	Kp1	0	1	Kqv	0.5	2
EtrqA	0.5	2.0	Kp2	6	24	Tp	0.01	0.04
DA	0.5	2.0	Kq1	3	12	Tiq	0.01	0.04
Motor B			Kq2	5.5	22	Tpord	2.5	10
TpoB	0.05	0.20	Np1	0.5	2	Kpg	50	200
TppoB	0.001	0.005	Np2	1.6	4.8	Kig	5	20
LpB	0.08	0.32	Nq1	1	4	Tg	0.01	0.04
LppB	0.06	0.24	Nq2	1.25	5	Tv	0.01	0.04
LsB	0.9	3.6	CmpKpf	0	2	Xe	0.13	0.5
RsB	0.015	0.06	CmpKqf	-6.6	-1.6	Load Fraction		
HB	0.5	2.0	Static Load			Fma	0	0.5
EtrqB	1	3	P1c	0	0.4	Fmb	0	0.5
DB	0.5	2.0	P2c	0	0.6	Fmc	0	0.5
Motor C			Q1c	0	0.4	Fmd	0	0.5
TpoC	0.05	0.20	Q2c	0	0.6	Fel	0	0.5
TppoC	0.001	0.005	Pfreq	-0.2	0.2	Fzip	0	0.5
LpC	0.08	0.32	Qfreq	-2	-0.5	Fdg	-0.5	0

2) Discovering Active Subspace and Parameter Sensitivities: To discover the active subspace, we can follow the algorithm provided in Section 3.3.2. Given the simulation setup as above, we firstly approximate the matrix C by Monte Carlo simulation (3.19) for $M_{ASM} = 500$ with the gradient estimated by finite difference method (3.17). In this case study, the $g\left(\theta_j + \delta_j\right)$ and $g\left(\theta_j\right)$ before transient are obtained using the mathematical model of WECC composite load developed in [110] for faster calculation of the gradient. Instead, one can also use other commercial software such as PSS/E or PSLF with potentially longer simulation time. Once the approximate C is constructed, the singular value decomposition is applied to abstract the eigenvalues and corresponding eigenvectors. The eigenvalues of $\hat{C}$ are shown in Fig. 3.4 in descending order. Recall that a significant spectral gap indicates the existence of active subspace, so it is important to look into the gaps of eigenvalues in Fig. 4. Note that the largest spectral gap exists between the first and second ones even though it seems that the one between the 45th and 46th ones is larger since it is a semilog plot. To clearly show the largest spectral gap, we conduct the normalized eigenvalue separation (3.22) and the result in Fig. 3.5 clearly shows the dominance of the gap between the first and second eigenvalues.

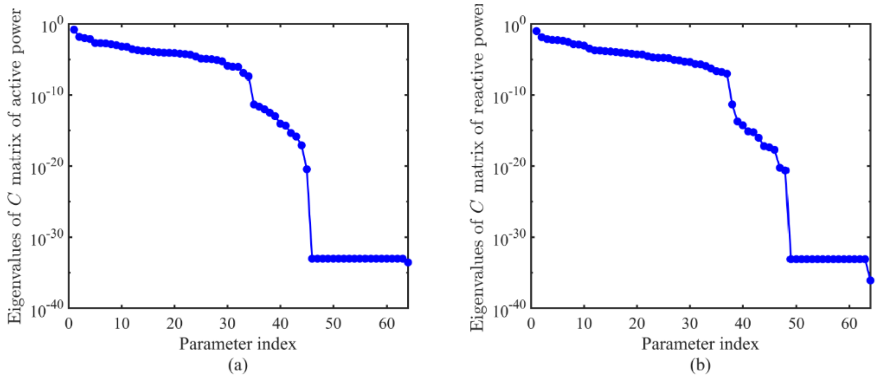

Fig. 3.4 The semilog plot of the magnitudes of eigenvalues of matrix $\hat{C}$ with respect to (a) real power and (b) reactive power

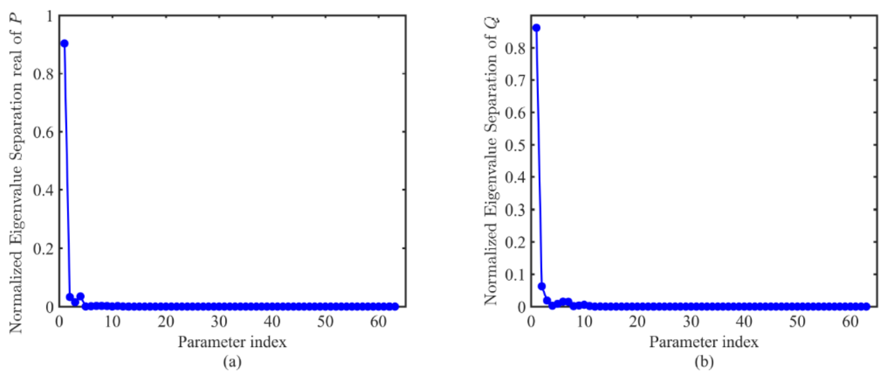

Fig. 3.5 The normalized eigenvalue separation of the magnitudes of eigenvalues of matrix $\hat{C}$ with respect to (a) real power and (b) reactive power

Then, the first eigenvector forms the active subspace of and the magnitude of each element of the eigenvector describes the sensitivity of each corresponding parameter and their interdependency. The weights of parameters with respect to the real and reactive power are shown in Fig. 3.6 and Fig. 3.7, respectively. The parameters in the red rectangles that have the largest weights imply the reduced parameter space. However, noting that the weights of parameters in the green rectangle though dominated by those in the red, are still larger than those that are almost zero. Thus, one may wonder whether these parameters also have significant impacts on the output of the interest as well. To verify the PR result, we will perform further studies in the following subsections.

3)Sufficient Summary Plot: In this subsection, we utilize sufficient summary plot to empirically validate the active subspace discovered in the last subsection. Sufficient summary plot was originally developed as a visualization tool for deter-mining low-dimensional combination of inputs in regression graphics. In the context of PR, it is often used to verify the active subspace, because it reveals the relationship between the output of interest P or Q, and the linear combination of input parameters $W_1^T \theta_j$. If the relationship presents evidently tight and univariate trend, then one can conclude that the discovered active subspace is validated.

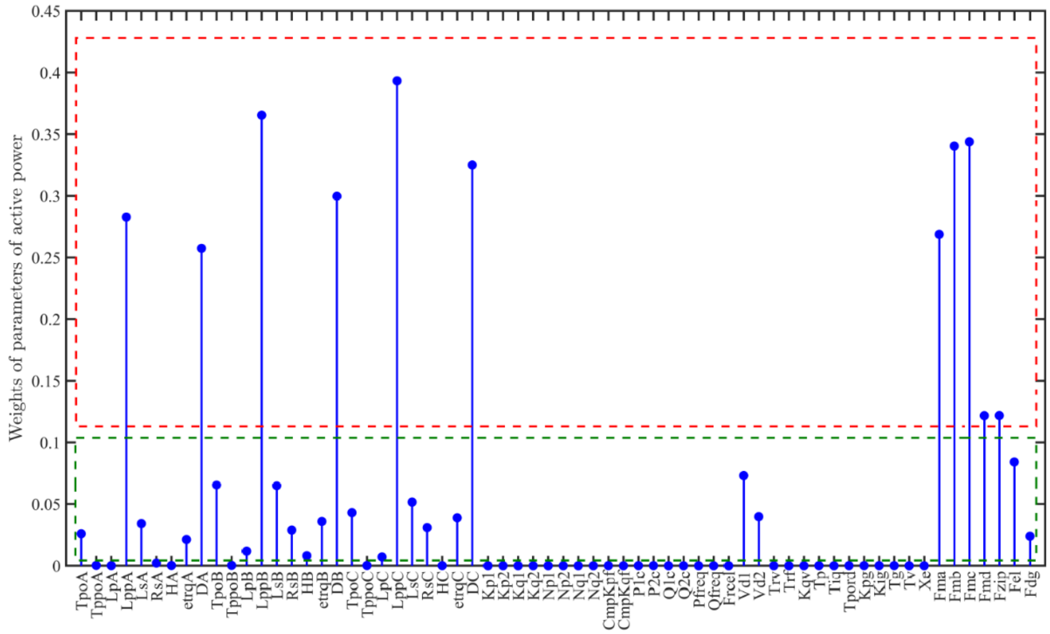

Fig. 3.6 The magnitudes of first eigenvector denoting the sensitivities of parameters of WECC CMLD with respect to real power

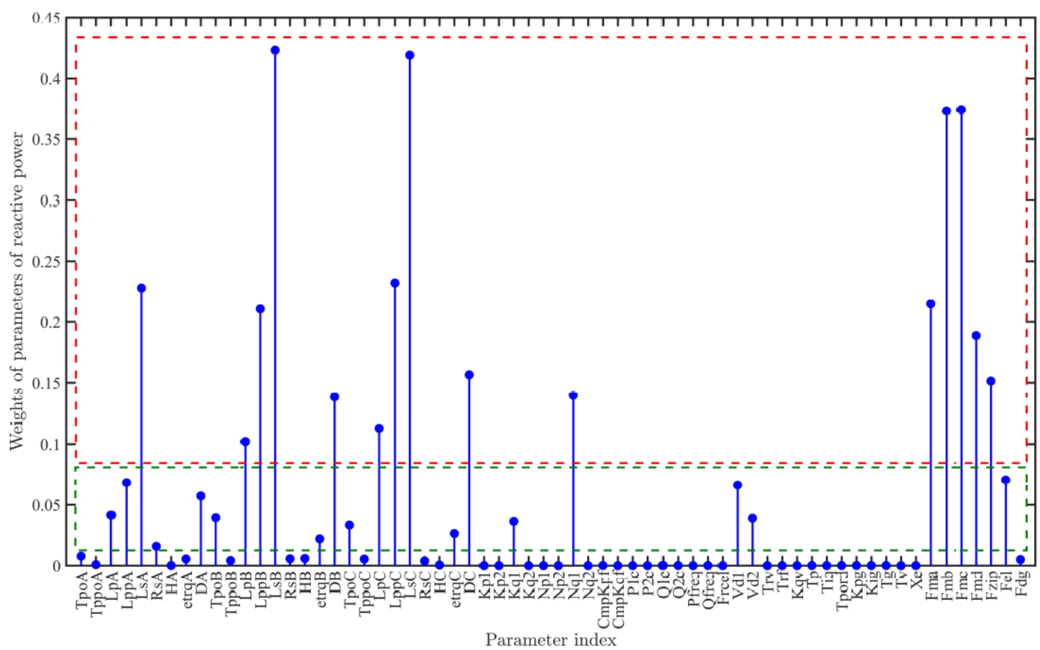

Fig. 3.7 The magnitudes of first eigenvector denoting the sensitivities of parameters of WECC CMLD with respect to reactive power

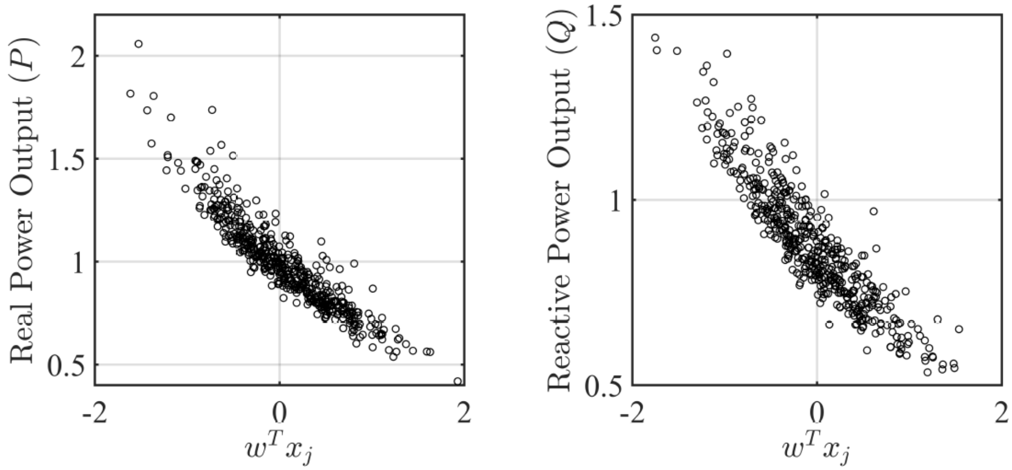

Fig. 3.8 Sufficient summary plots of (a) real and (b) reactive power using 500 samples

Fig. 3.8 shows the sufficient summary plots of real and reactive power with respect to $W_1^T \theta_j$. The obvious linear trends verify the effectiveness of active subspace.

4)PR Result Validation: To finally determine the dimension of reduced parameter space, we conduct the following simulations on the WECC CMLD. We first add 20% of positive perturbations to the insensitive parameters outside the red rectangles of Fig. 3.6 and Fig. 3.7. The results are shown as red lines in Fig. 3.9 and Fig. 3.10, respectively. Then, we add same perturbations to the parameters outside both rectangles to test whether restricting the PR result will lead to significant accuracy improvement. The results are shown in green dashed lines in Fig. 3.9 and Fig. 3.10. Finally, we add the same perturbations to the most sensitive parameters in the red rectangles, and the results are denoted in blue dotted lines.

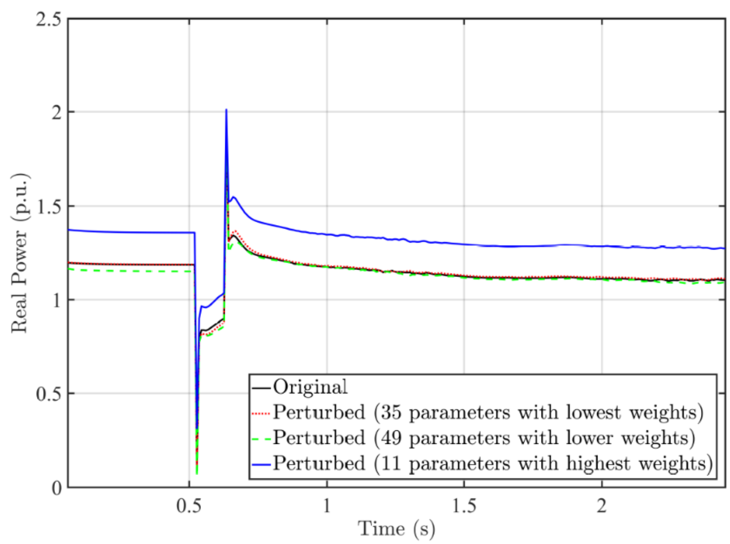

Fig. 3.9 Typical consumption profiles for (a) winter commercial class, (b) winter residential class, (c) summer commercial class, and (d) summer residential class

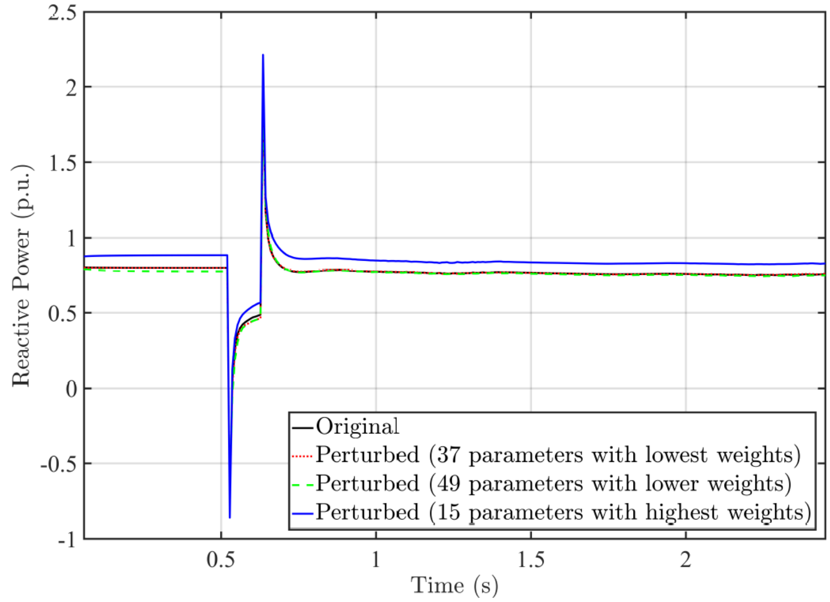

Fig. 3.10 Validation of PR result for reactive power of WECC CMLD, with different combinations of parameters perturbed by twenty percent

From Fig. 3.9 and Fig. 3.10, we find that the real and reactive power are sensitive to the parameters inside the red rectangles and insensitive to the others. Moreover, including the parameters inside the green rectangles as sensitive ones does not have a noticeable impact on accuracy. Therefore, we can conclude that the parameters of the WECC CMLD can be reduced to the ones in the red rectangles only with almost the same dynamic response, which verifies the effectiveness of ASM.

3.4.2 Case II: Influence of FIDVR on Reduction Result

In this subsection, we will test the performance of the proposed method on FIDVR case which is obtained from real utility data, as shown in Fig. 3.11. This case contains multi-phase faults, including phase-to-phase, phase-to-phase-to-ground and three-phase-to-ground faults. The other simulation setup is the same as that in Case I.

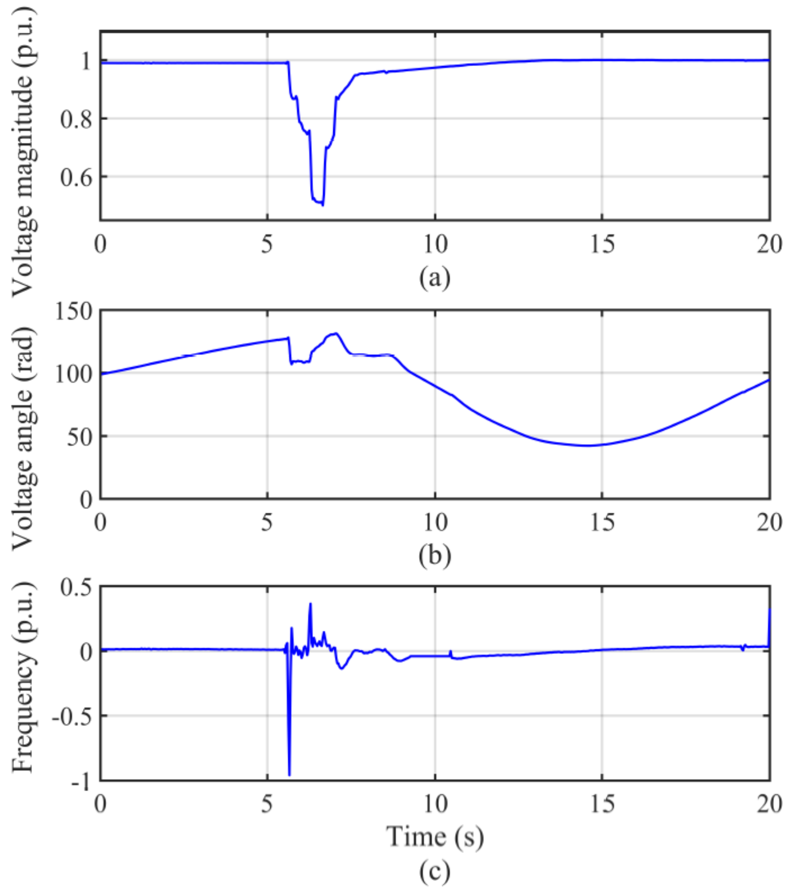

Fig. 3.11 The load bus input profile of FIDVR case: (a) voltage magnitude; (b) voltage angle; (c) frequency

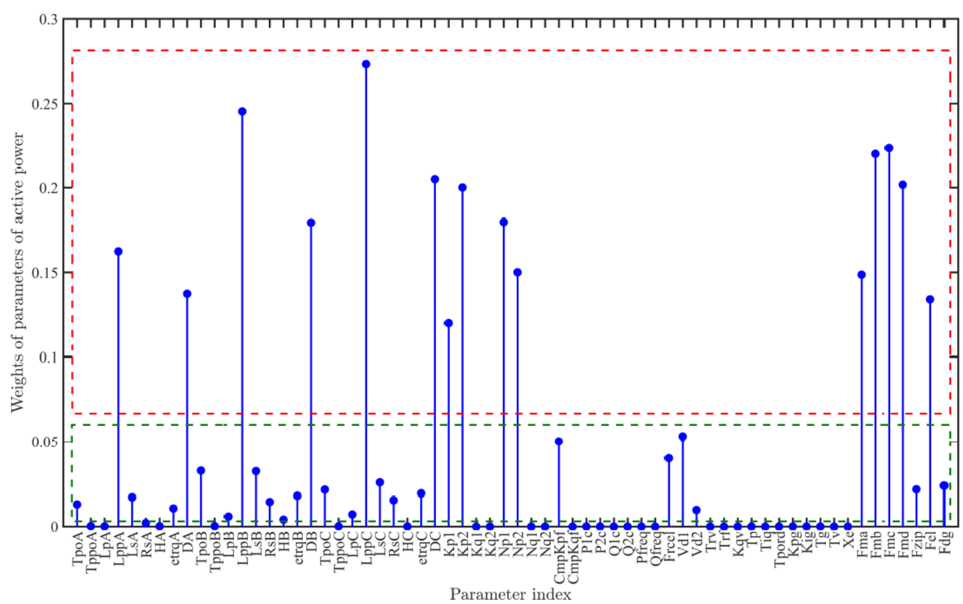

Fig. 3.12 Parameter sensitivities of WECC CMLD with respect to active power in FIDVR case

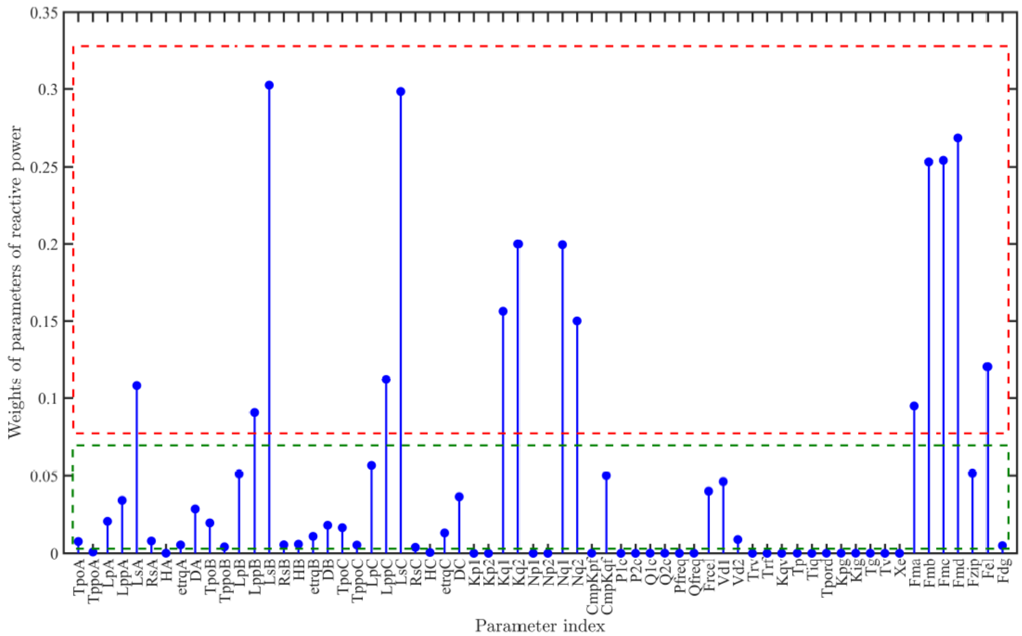

Fig. 3.13 The parameter sensitivities of WECC CMLD with respect to reactive power in FIDVR case

Comparing the parameter sensitivity results in Fig. 3.12 and Fig. 3.13 with Case I, we can find that the parameters of single-phase motor become sensitive. This can be attributed to that the single-phase motor plays an important role in capturing the dynamics during the delayed-recovery stage. Same as in Case I, 20% of perturbation is added to three parameter sets: parameters with lowest sensitivities (outside all the rectangles in Fig. 3.12 and Fig. 3.13), parameters with lower sensitivities (outside the red rectangles), and most sensitive parameters (inside the red rectangles). The comparison results in Fig. 3.14 and Fig. 3.15 show that the output of interest is altered significantly in the calculated sensitive direction but is almost not influenced when perturbing the insensitive parameters. This verifies the effectiveness of our method on FIDVR case.

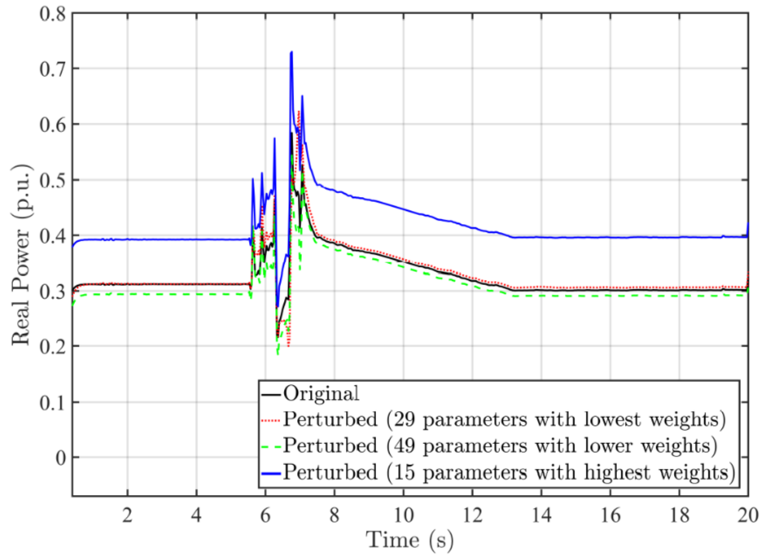

Fig. 3.14 Validation of PR result for real power of WECC CMLD, with different combinations of parameters perturbed by twenty percent

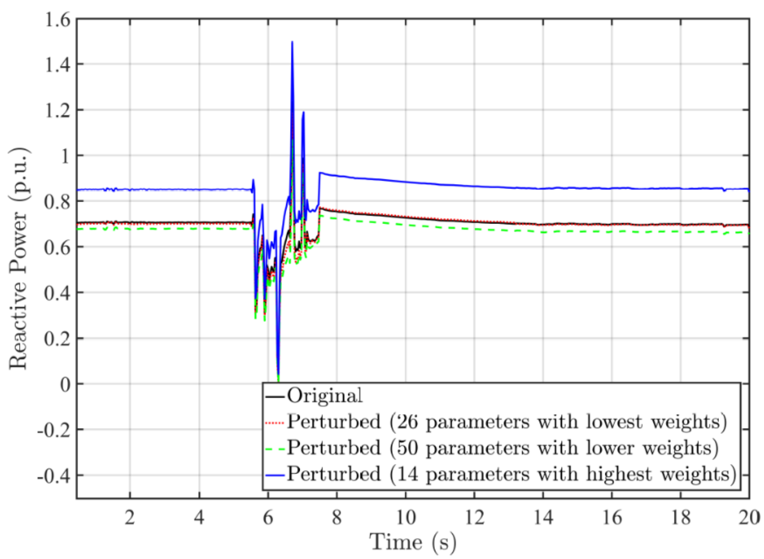

Fig. 3.15 Validation of PR result for reactive power of WECC CMLD, with different combinations of parameters perturbed by twenty percent

3.4.3 Case III: Comparison with Three Classical PR methods

In this subsection, the proposed ASM method is compared with three representative and widely-used methods: FWKL method [101], Sobel method [97] and Morris method in [89]. The regularization parameter λ of FWKL is chosen as 100. The sample size of Monte Carlo simulation for Sobel method is selected as $M_{Sobel} = 1500$. The times of repetition for Morris method is selected as $M_{Morris} = 15$. The other simulation setups are the same as in Case I. Since the results of active and reactive power are consistent, for simplicity, only the results of active power are shown here.

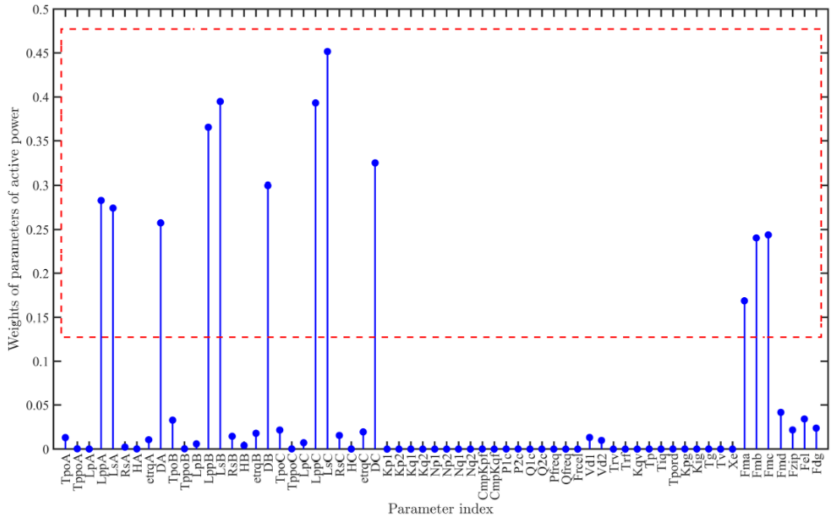

Fig. 3.16 Parameter sensitivities calculated by FWKL method. 12 parameters in the red rectangle are considered as sensitive ones

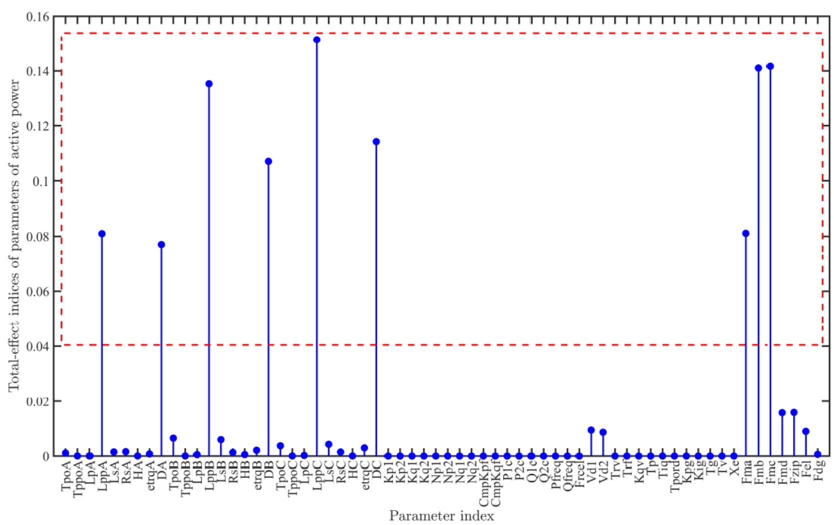

Fig. 3.17 Parameter sensitivities calculated by Sobel method. 9 parameters in the red rectangle are considered as sensitive ones

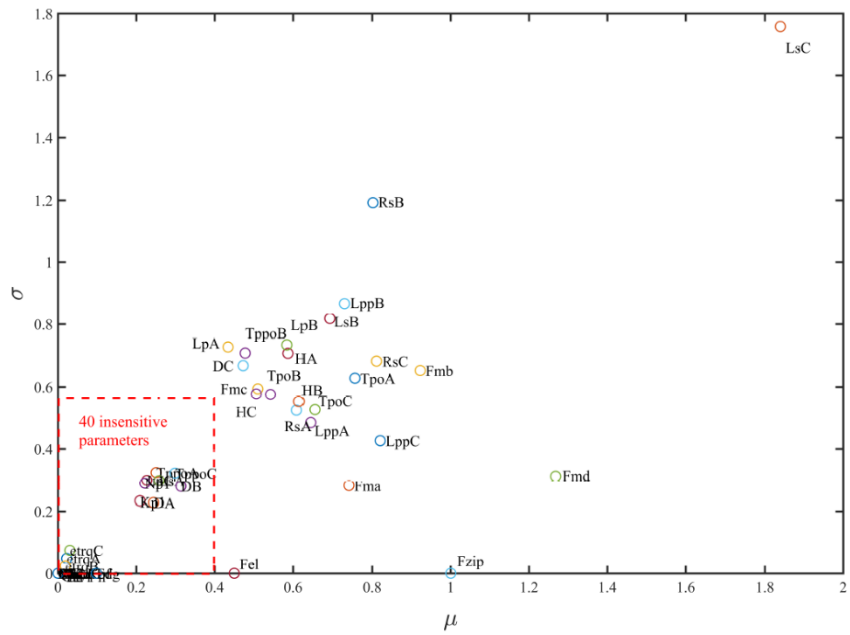

Fig. 3.18 Parameter sensitivities calculated by Morris method

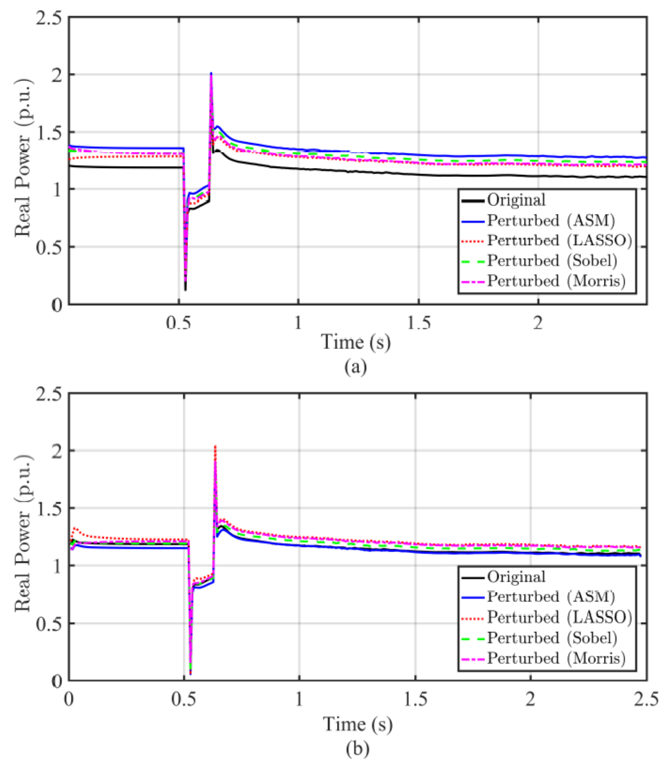

Fig. 3.19 Comparison of results validation of four methods by adding 20% perturbation on: (a) sensitive parameters; (b) insensitive parameters

The parameter sensitivities calculated by three methods are shown in Fig. 3.16~3.18, respectively. In Fig. 3.18, 24 parameters outside the red rectangle are considered as sensitive ones. μ and σ are the mean and standard deviation of the elementary effects, respectively. We can observe that, Morris method reduces least number of parameters, while Sobel method reduces the most. Moreover, the identified sensitive parameter indices by Sobel are the most similar to those by ASM. The result validation is conducted by adding 20% on all sensitive and insensitive parameters sets, respectively. From Fig. 3.19, we can observe that, the blue line (ASM) deviates farthest away from the black line (original) in the sensitive direction, and is closest to that in the insensitive one. This indicates that ASM is the most accurate among the four methods for this case.

Table 3.2 Comparison of key features of the four PR methods

	Category	Accuracy	Interaction	Computation
ASM	Gradient, Monte Carlo	Accurate	Quantitative	$2mM_{ASM}$
FWKL	Optimization	Rough	Qualitative	Depends
SOBEL	Variance, Monte Carlo	Accurate	Quantitative	$M_{Sobel}(m+2)$
Morris	OAT	Rough	Qualitative	$M_{Morris}(m+1)$

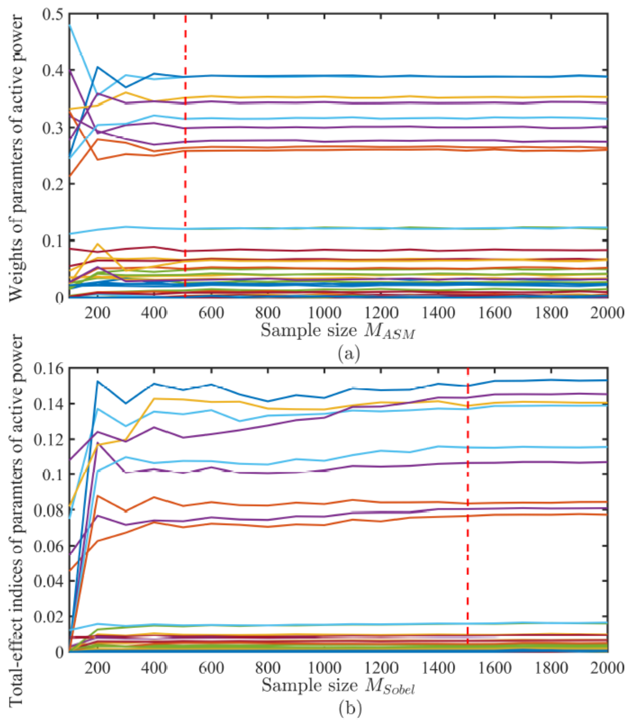

Fig. 3.20 Comparison of convergence rates of: (a) ASM; (b) Sobel

Some key features of the four methods can be concluded as Table. 3.2. Note that the computational cost of ASM, Sobel and Morris are considered in terms of the number of experiments. FWKL is optimization-based, thus its computational cost depends on the numbers of both iterations and experiments, which makes it take more time than the other three methods. To further compare the computational cost of ASM and Sobel methods, we sequentially increase the Monte Carlo sample sizes to observe the converge rate of parameter sensitivities. Fig. 3.20 shows that the sensitivities obtained by ASM converge after 500 samples, while Sobel needs about 1500 ones. As a conclusion, the ASM is the most accurate with relatively lower computational cost (than Sobel and FWKL methods).

3.5 Summary

A novel PR approach for the WECC CMLD is proposed based on ASM. With this approach, the sensitivities of parameters are computed while the interdependency among the parameters is taken into consideration. By applying the proposed algorithm to the WECC CMLD, the dimensions of parameter spaces can be significantly reduced. The PR result is validated by sufficient summary plot and perturbation tests with different voltage cases. The comparison with other classical methods has shown the advantages of the proposed method.

Note that the ASM requires scalar function which limits its application to vector-valued parameterized model whose output is $\left[P,Q\right]^T$. Therefore, it cannot be directly used to analyze the parameter sensitivity for both real and reactive power simultaneously. One may use a scalar to combine them, however such output of interest may lack the physical meaning. We would like trying to extend the scalar ASM to deal with vector-valued functions in the future work.

4. WECC Composite Load Model Parameter Identification using Evolutionary Deep Reinforcement Learning

4.1 Introduction

Parameter identification of load models is essential to power systems studies, such as planning, operation and control [81],[85],[103],[111]. Due to the increasing diversity of load types and the integration of distributed energy resources (DERs) [112],[113], parameter identification still remains a challenging problem to academic researchers and industrial practitioners. Measurement-based approaches are widely employed to perform parameter identification, where voltage and power measurements in fault-induced delayed-voltage-recovery (FIDVR) events are used to determine the parameters of given dynamic load models.

Previous works have mainly focused on identifying parameters of a composite load model which consists of a ZIP and an induction motor, where ZIP model is a combination of a constant-impedance load, a constant-current load and a constant-power load. In [103], based on trajectory sensitivities, the induction motor parameter number is reduced and only critical parameters are identified. The proposed approach is validated using real field measurements, and it is demonstrated that the approach can decrease identification time without losing the composite load model's dynamic characteristics. In [114], a robust time-varying parameter identification approach is proposed for synthesis load modeling. The synthetic load model includes time-varying ZIP, induction motor, and equivalent line impedance model. To achieve the goal of robustness enhancement, dynamic programming is used to detect voltage disturbances, and then a time-varying parameter identifier with a smaller iteration threshold is designed. In [115], a multi-modal long short-term memory deep learning method is employed to identify the time-varying parameters of the composite load model. In [116], a computationally efficient technique is utilized for identifying the composite load model parameters, by performing a similarity analysis of parameter sensitivity. The partial derivative of each parameter is employed to identify parameters with similar sensitivities, and Levenberg-Marquardt algorithm is used to solve the optimization problem. To improve computational efficiency, in [117], model parameter sensitivities are analyzed using eigenvalues of Hessian matrix, and the linear dependence between two parameters are then identified by examining the condition number of the Jacobian matrix. In [82], a robust time-varying parameter identification approach is developed for the composite load model. A batch-mode regression form is constructed to guarantee data redundancy, and the down-weighting coefficient for each measurement is calculated to reduce the impacts of outliers. To sum up, in previous works, both traditional optimization methods and modern learning-based approaches are employed to perform parameter identification of the composite load model which consists of a ZIP model and an induction motor model.

In recent years, as a large number of DERs are integrated into distribution systems, the composition of loads has changed significantly [118]-[120]. In order to accurately capture the characteristics of this new type of load in modern power grids, the Western Electricity Coordinating Council (WECC) has developed a composite load model with distributed generation (CMPLDWG) [121]. Also, researchers have dedicated great efforts into studying this newly-proposed advanced load model. In [8], an easy-to-use tool is developed to generate dynamic load data to enhance utilities' planning studies. This tool can be adjusted to accommodate different customer types, various load components and characteristics. In [85], a generic modeling and open-source implementation of the WECC composite load model are presented, which reduces the gap between the WECC model and its further implementation. In [81], an approach is proposed for dynamic composite load modeling, where parameter dependency of the complex dynamic load model is analyzed and visualized using matrix decomposition and data clustering techniques. Meanwhile, the parameter identification performance is improved by adding a regularization term to include apriori parameter information into the objective function. However, the apriori parameter information is not generally available. In addition, the newly-approved aggregated distributed energy resources (DER_A) model in CMPLDWG has not been considered in [81]. In [122], the parameter identification process is divided into two steps: determining load composition and selecting a best-fit parameter vector candidate from Monte-Carlo simulations. To sum up, the primary disadvantages of previous WECC model parameter identification approaches are that they rely on prior knowledge of parameters or a comprehensive library of parameter candidates.

The CMPLDWG model contains 183 parameters, and the order of differential equations reaches 25. Therefore, the traditional optimization methods might not be able to handle the high-dimensional parameter vector and the severe nonconvexity of model structure. Considering this, we seek to perform parameter identification for CMPLDWG using an advanced learning-based approach with an embedded intelligent exploration (IE) mechanism, which is inspired by the evolutionary deep reinforcement learning (EDRL) technique. The proposed approach can efficiently avoid deceptive local optima and can handle the high-dimensional parameter vector [123],[124]. Specifically, first, the parameter sensitivity analysis (PSA) is conducted to obtain sensitivity weights reflecting contributions of parameters to dynamics, using feature-wise kernelized Lasso (FWKL), where Lasso denotes the least absolute shrinkage and selection operator. Then, the extracted parameter sensitivity weights are integrated into EDRL with IE to perform intelligent CMPLDWG parameter exploration by avoiding purely randomized or ineffective search. Parallelly, the EDRL with IE performs parameter exploitation using evolutionary strategy. Finally, the EDRL with IE guides the identifier to balance exploitation and exploration by designing time-varying dynamic weights assigned to the approximated performance gradient and novelty gradient.

The main innovations and contributions of the work in this chapter are summarized as follows: (1) To address the challenges of parameter identification caused by the nonlinearity of CMPLDWG model, we have designed a mechanism of intelligent exploration for encouraging the parameter identifier to escape from deceptive local optima. The exploration mechanism is achieved through time-varying dynamic weights which intelligently balance the exploitation and exploration. Most importantly, once the parameter identifier is stuck in a local optimum, it is stimulated to aggressively explore undiscovered parameter space. (2) The extracted CMPLDWG parameter sensitivity weights are innovatively integrated into the intelligent exploration to achieve directed and efficient parameter space discovery. By doing this, the parameter identifier can avoid purely randomized or inefficient exploration.

4.2 CMPLDWG Model and Overall Parameter Identification

4.2.1 CMPLDWG Model

This chapter focuses on the comprehensive WECC composite load model, which consists of three sections: substation, feeder and load, as illustrated in Fig. 3.1. The substation section is com-posed of a transformer model and a shunt capacitor model. The feeder section is denoted using an equivalent feeder model. The load section includes three three-phase induction motor models with different dynamic characteristics, one single-phase A/C performance-based motor model, an electronic load model, a static load model and a distributed generator model. In this chapter, the distributed generator model is specified as the newly-approved DER_A model presented in [107][21]. Table I shows a list of WECC CMPLDWG model parameters of which detailed definitions can be found in [121],[107]. In addition, the mathematical state-space representations of CMPLDWG model are presented in [110].

4.2.2 Overall Framework of the Proposed Approach

The process of identifying unknown CMPLDWG parameters comes down to finding optimal parameters by reducing the following estimation residual [81]:

$$\min_{\theta} \ l\left(Y,\theta,V\right)=\min_{\theta}\frac{1}{2}\left(\left\|Y-f\left(\theta,V\right)\right\|_2^2\right). \tag{4.1}$$

where, Y denotes active/reactive power measurement vector, θ represents the vector of parameters to be identified, V denotes voltage measurement vector, l represents calculating the estimation residual, $\left\|\cdot\right\|_2$ is the l_2-norm, and $f\left(\cdot\right)$ denotes the mathematical representation of CMPLDWG model developed in [110]. More detailed variable definitions will be elaborated in Section 4.3. To determine the optimal parameters for CMPLDWG, the EDRL approach with IE is developed in this chapter.

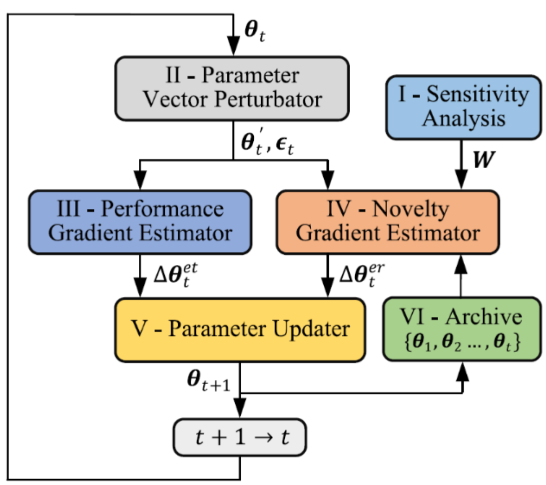

Fig. 0.1 Overall structure of the proposed parameter identification approach for CMPLDWG model

The components of parameter identification framework are illustrated in Fig. 4.1: Component I - Sensitivity Analysis: Sensitivity analysis evaluates the contributions of parameters to dynamic power measurements, and is based on the observation that the change of some parameters has an insignificant impact on power measurements. The high-order characteristic of induction motors and DER_A in CMPLDWG can significantly complicate PSA when using traditional methods. To address this challenge, an alternative data-driven PSA approach, FWKL, is proposed. The FWKL utilizes a set of randomly-generated CMPLDWG parameter vectors and corresponding calculated residuals to extract weights indicating parameter sensitivities. The PSA is formulated as a Lasso optimization problem given as

$$\min_{W \in \mathbb{R}^d} \frac{1}{2}\left\| e - \Theta^T W \right\|_2^2 + \lambda \left\| W \right\|_1 . \tag{4.2}$$

where, e is the estimation residual vector, Θ denotes the randomly-generated parameter vectors in a matrix form, $W = \left[W_1, \ldots, W_d\right]^T$ represents the parameter sensitivity weight vector, $\left\|\cdot\right\|_1$ is the l_1-norm and λ is the regularization parameter which is determined using grid search with cross-validation. Note that sensitivity analysis is a one-off work for each fault event. The extracted parameter sensitivity weight vector, *W*, is passed to the novelty gradient estimator in each iteration whose number is denoted by *t*. Component II - Parameter Vector Perturbator: In each iteration, to per-form evolution, a perturbator is designed to generate multiple mutated parameter vectors, $\theta_t^{'}$'s, using the identified parameter vector in the last iteration, θ_t, and random variance vector, ε_t. $\theta_t^{'}$'s and ε_t's are then sent to a performance gradient estimator and a novelty gradient estimator to approximate performance and novelty gradients, respectively. Component III - Performance Gradient Estimator: This estimator achieves the function of exploitation of EDRL. Specifically, using $\theta_t^{'}$'s and ε_t's generated by the parameter vector perturbator, the performance gradient estimator determines the direction in which θ_t should move to improve expected reward. The performance gradient, $\Delta\theta_t^{et}$, is then passed to a parameter updater. Component IV - Novelty Gradient Estimator: This component performs exploration by estimating the novelty gradient, $\Delta\theta_t^{er}$, using the generated $\theta_t^{'}$'s and ε_t's, and it also intelligently encourages the parameter identifier to explore unvisited parameter space. $\Delta\theta_t^{er}$ is then sent to the parameter updater. Component V - Parameter Updater: To balance exploitation and exploration, the parameter updater assigns time-varying dynamic weights to the approximated performance and novelty gradients:

$$\Delta\theta_t = \omega_t \Delta\theta_t^{et} + \left(1-\omega_t\right)\Delta\theta_t^{er}, \tag{4.3}$$

where, ω_t denotes a dynamic weight. Then, θ_{t+1} is calculated and added into the parameter vector archive to update the explored parameter space. Component VI - Archive: The archive collects the previously generated parameter vectors which are passed to the novelty gradient estimator for novelty evaluation. Component II to V compose the EDRL algorithm with IE. Since the construction of the parameter vector archive is straightforward, we will focus on elaborating the modules of sensitivity analysis and EDRL with IE in the next two sections.

4.3 Parameter Sensitivity Analysis

PSA examines the sensitivity of dynamic power measurements with respect to load model parameters. In previous works, partial derivative of dynamic power to each parameter is calculated to conduct sensitivity analysis of induction motor parameters [116]. However, it becomes challenging to directly apply analytical approaches to calculate partial derivatives because of the high order and the complicated structure of mathematical differential equations of the WECC composite load model. For example, the three-phase induction motor model in CMPLDWG is of 5th order and the DER_A model has ten state variables. Such a complex high-order nonlinear system can significantly complicate the calculation of partial derivatives. To address this challenge, we seek to employ a high-dimensional feature selection technique to evaluate the dependence of dynamic power on the CMPLDWG parameters [125]. Specifically, we use a data-driven FWKL instead of employing analytical derivatives [116].

Let $\theta_i \in \mathbb{R}^d$ be a randomly-generated parameter vector and d be the number of parameters, therefore, the power residual corresponding to θ_i can be calculated as

$$e_i = \left\| f\left(\theta_i, V\right) - Y \right\|_2, \tag{4.4}$$

where, $V \in \mathbb{R}^K$ is a vector of voltage measurements, K denotes the total number of measurement points, $Y = \left[P^T, Q^T\right]^T$, $P \in \mathbb{R}^K$ and $Q \in \mathbb{R}^K$ represent the vector of recorded active power and reactive measurements, respectively. Also, T denotes the transpose. With a large number of generated θ_i 's, we can obtain n independent and identically distributed (i.i.d.) sample and residual pairs:

$$\left\{\left(\theta_i, e_i\right), i = 1, \ldots, n\right\}. \tag{4.5}$$

To perform supervised feature selection, first, we represent the original parameter vectors and corresponding residuals in a matrix format as

$$\Theta = \left[\theta_1, \ldots, \theta_n\right] \in \mathbb{R}^{d \times n}, \tag{4.6a}$$

$$e = \left[e_1, \ldots, e_n\right]^T \in \mathbb{R}^n. \tag{4.6b}$$

Then, PSA is formulated as a Lasso optimization problem formulated in (4.2) which works well for linear regression. However, the nonlinear dependency in our specific problem hinders its application. Therefore, we employ the feature-wise nonlinear Lasso to solve our problem and the key idea is to apply a nonlinear transformation in a feature-wise manner. Specifically, the generated parameter matrix, Θ, is represented in a feature-wise manner:

$$\Theta = \left[\beta_1, \ldots, \beta_d\right]^T \in \mathbb{R}^{d \times n}, \tag{4.7}$$

where, $\beta_k = \left[\theta_{k,1}, \ldots, \theta_{k,n}\right]^T \in \mathbb{R}^n$ is a vector denoting the k-th feature for all samples. To capture the nonlinear dependency of e on θ, dynamic power residual and parameter vector are transformed by a nonlinear function $\varphi(\cdot):\mathbb{R}^n \to \mathbb{R}^p$. Then, the Lasso optimization problem given in the objective function (4.2) in the transformed space is reformulated as

$$\min_{W\in\mathbb{R}^d} \frac{1}{2}\left\|\varphi(e)-\sum_{k=1}^{d} W_k\varphi(\beta_k)\right\|_2^2 + \lambda\|W\|_1. \tag{4.8}$$

Although the objective function (4.8) can capture nonlinear dependency, there is no constraint for $W_k, k=1,\ldots,d$, and the same transformation function $\varphi(\cdot)$ for e and β_k limits the flexibility of capturing nonlinearity. To solve this, we seek to employ a revised FWKL to perform feature selection [125], and the revised objective function is formulated as

$$\min_{W\in\mathbb{R}^d} \frac{1}{2}\left\|\bar{U}-\sum_{k=1}^{d} W_k\bar{V}^{(k)}\right\|_{Frob}^2 + \lambda\|W\|_1, \tag{4.9a}$$

$$s.t. \quad W_1,\ldots,W_d \geq 0. \tag{4.9b}$$

where, $\|\cdot\|_{Frob}$ denotes the Frobenious norm, $\bar{U}=\Gamma U\Gamma$ and $\bar{V}^{(k)}=\Gamma V^{(k)}\Gamma$ are centered Gram matrices, $U_{i,j}=U(e_i,e_j)$ and $V_{i,j}^{(k)}=V(\theta_{k,i},\theta_{k,j})$ are Gram matrices, $U(e,e')$ and $V(e,e')$ are kernel functions, $\Gamma = I_n - \frac{1}{n}1_n 1_n^T$ denotes the centering matrix, I_n represents the *n*-dimensional identity matrix, and 1_n denotes the n-dimensional vector with all ones. For the two kernel functions $U(\cdot)$ and $V(\cdot)$, we employ the Gaussian kernel which is formulated as

$$K(x,x') = \exp\left(-\frac{(x-x')^2}{2\sigma_x^2}\right), \tag{4.10}$$

where, σ_x is the Gaussian kernel width.

In the objective function (4.9a), the decoupling between $U(\cdot)$ and $V(\cdot)$ provides more flexibility compared with the objective function (4.8). In addition, the non-negativity constraint in (4.9b) fits the specific application in our problem, since negative sensitivity parameter weights do not have practical interpretability. Intuitively, problem (4.9) tends to find non-redundant parameters with significant contributions to power residual, and equivalently, to dynamic power. Also, for two strongly dependent features, either of their sensitivity weights tends to be eliminated. The parameter sensitivity weight vector, *W*, is then integrated into the parameter identification algorithm to accelerates the learning process, which will be presented in Section 4.4.

4.4 Parameter Identification using the EDRL with IE

As stated in previous sections, the severe nonlinearity, high nonconvexity and the large number of parameters bring significant challenges to perform parameter identification for the CMPLDWG model when using existing approaches. This motivates us to tackle this challenge utilizing the EDRL with IE, which is recently demonstrated to be able to perform well on high-dimensional optimization tasks [123],[126]. The basic idea of performing optimization tasks using evolution strategy is: During each iteration, a population of parameter vectors is perturbed based on one selected parameter vector among a meta-population, and then, these mutated vectors are recombined to update the selected ancestor vector. In this chapter, the EDRL is also hybridized with IE to improve exploration. Compared with traditional random and blind search strategy, the IE module achieves efficient and directed exploration, which can efficiently assist EDRL to escape from local optima. The detailed steps are described as follows:

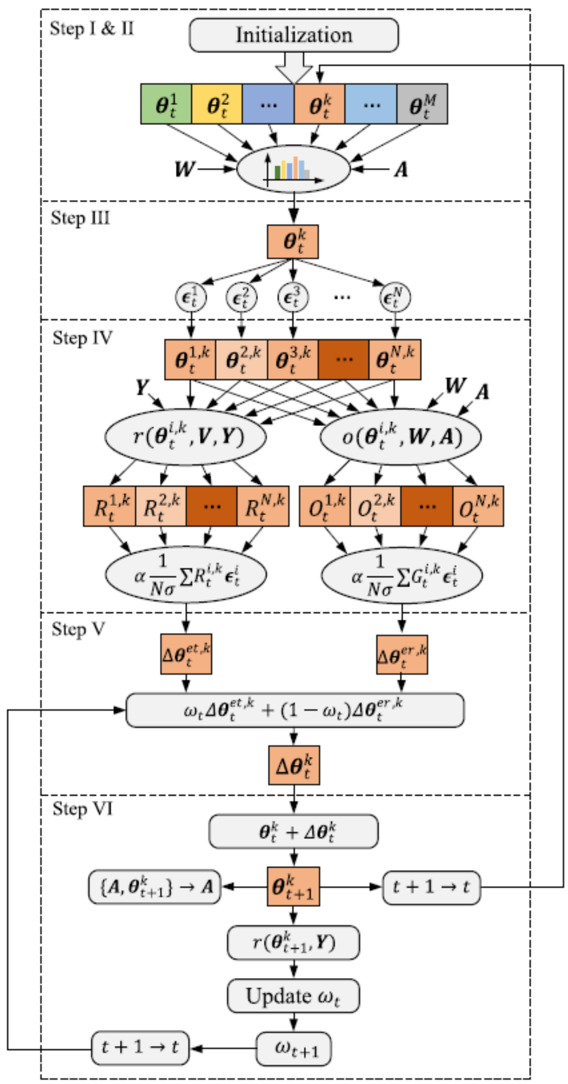

Fig. 0.2 Detailed structure of the EDRL with an intelligent exploration mechanism

Step I - Initialization: The first step is to initialize *M* random parameter vectors which will be updated in each iteration. Note that only one vector is probabilistically selected to update in each iteration. The initialized *M* vectors are denoted as $S=\left\{\theta_1^1,\ldots,\theta_1^M\right\}$, where *t* denotes the number of iteration. The objective of constructing a meta-population is to enhance additional diversity. *M* and the tuning parameters in the remaining sections are determined using grid search with cross-validation which is a general hyperparameter optimization technique.

Step II - Sampling: In each iteration *t*, we probabilistically determine which parameter vector among the *M* meta-population to be updated based on parameter vectors' novelties. The novelty is evaluated in terms of Euclidean distances from a vector to the vectors in the newest archive. Specifically, first, the originality of each parameter vector in *S*, θ_t^k, conditioned on current parameter vector archive, *A*, is evaluated as

$$O_t^k=o\left(\theta_t^k,W,A\right)=\frac{1}{|C|}\sum_{j\in C}\left\|W.*\left(\theta_t^k-\theta_j\right)\right\|_2, \tag{4.11}$$

where, $1 \leqslant k \leqslant M$, $C=kNN\left(\theta_t^k,A\right)=\left\{\theta_1,\ldots,\theta_{N'}\right\}$, *kNN* denotes *k*-nearest neighbors algorithm, and .* denotes the element-wise multiplication operation. The purpose of *kNN* is to select representative parameter vectors in *A* for evaluating the novelty of θ_t^k. Intuitively, a small *k* can introduce higher distance variance, while a large *k* means higher computational cost. We have conducted numerical experiments to determine the optimal *k* value which is sufficient for evaluating the novelty of a newly explored parameter vector while avoiding high computational time. The intro-duction of *W*, which is obtained from PSA, aims to revise Euclidean distances between vectors. This revision is based on the consideration that parameters with different sensitivity weights have different contributions to vector novelty. Then, for each parameter vector in *S*, the novelty score which determines the probability of being selected to be updated is calculated as

$$P_t^k=\frac{O_t^k}{\sum_{j=1}^{M}O_t^j}. \tag{4.12}$$

P_t^k tells us that selecting the parameter vectors with high novelty scores can achieve directed or guided exploration.

Step III - Variation: In this step, variation is performed on the selected parameter vector in Step II, θ_t^k, to generate multiple workers. The function of these workers is explained as follows: First, EDRL produces parameter vectors in the neighborhood of θ_t^k, and then θ_t^k is updated by following the direction determined by the population of the produced parameter vector workers. To obtain *N* workers, Gaussian noise is applied to θ_t^k as follows

$$\theta_t^{i,k}=\theta_t^k+\sigma\varepsilon_t^i \quad i=1,\ldots,N, \tag{4.13}$$

where, σ is a fixed noise standard deviation, $\varepsilon_t^i \sim N(0, I)$ and I is an N-dimensional identity matrix.

Step IV - Gradient Estimation: In this step, the performance and novelty gradients determined by the meta-population of generated vectors in Step III are approximated. For each mutated parameter vector, $\theta_t^{i,k}$, its fitness can be evaluated via calculating the difference between the estimated dynamic power and the real dynamic power. First, the power residual caused by the mismatch between estimated parameters and real parameters, $e_t^{i,k}$, is calculated by substituting $\theta_t^{i,k}$ into (4.4). Then, the reward is obtained by inversing $e_t^{i,k}$:

$$R_t^{i,k} = r\left(\theta_t^{i,k}, V, Y\right) = \frac{1}{e_t^{i,k}} \quad i = 1, \ldots, N, \tag{4.14}$$

Equation (4.14) indicates that as the residual decreases the reward increases. Thus, the performance gradient of e_t^k is approximated via taking a sum of the sampled parameter vector perturbations weighted by the reward:

$$\Delta\theta_t^{et,k} \approx \alpha \frac{1}{N\sigma} \sum_{i=1}^{N} R_t^{i,k} \varepsilon_t^i, \tag{4.15}$$

where, α is a learning rate. In (4.15), $\Delta\theta_t^{et,k}$ indicates a stochastic reward experienced over a full iteration of multiple worker interactions, which means the performance gradient relies on multiple workers and this can effectively avoid the high variance brought by a certain single mutated vector. Note that the calculated reward, $R_t^{i,k}$, is normalized through 1 to N before performing the gradient approximation in (4.15).

For the novelty gradient, first, the novelty with respect to each perturbed vector, $O_t^{i,k}$, is calculated using (4.11). Then, the novelty gradient of θ_t^k is approximated as

$$\Delta\theta_t^{er,k} \approx \alpha \frac{1}{N\sigma} \sum_{i=1}^{N} O_t^{i,k} \varepsilon_t^i, \tag{4.16}$$

Similar with $R_t^{i,k}$, $O_t^{i,k}$, is normalized before computing the novelty gradient. Intuitively, $\Delta\theta_t^{er,k}$ indicates the direction which the parameter identifier should follow to increase the average originality of parameter vector distribution.

Step V - Gradient Combination: Using the computed performance and novelty gradients with respect to θ_t^k, we can balance exploitation and exploration by introducing a time-varying dynamic weight, ω_t. Thus, the overall gradient based on which θ_t^k should be updated is computed as follows:

$$\Delta\theta_t^k = \omega_t \Delta\theta_t^{et,k} + \left(1 - \omega_t\right) \Delta\theta_t^{er,k}, \tag{4.17}$$

Intuitively, the algorithm follows the approximated gradient in parameter-space towards directions that both exhibit novel behaviors and achieve high rewards. A large ω_t tends to encourage θ_t^k to follow the performance gradient and restrain it to follow the novelty gradient. In comparison, a small ω_t tends to aggressively guide θ_t^k to mutate to unseen parameter space and hold back exploitation.

Step VI - Updating: After obtaining $\Delta\theta_t^k$, the updating of θ_t^k is expressed as follows:

$$\theta_{t+1}^k = \theta_t^k + \Delta\theta_t^k, \tag{4.18}$$

θ_{t+1}^k is then added into the archive A for updating the pre-existing vector landscape. As more learned parameter vectors are saved into A, the base for evaluating future parameter vectors' novelty changes and stimulates the algorithm to discover unexplored parameter space.

In addition to updating θ_t^k and A in each iteration, the dynamic weight, ω_t, should also be updated for avoiding local optima. To do this, first, the latest reward, R_{t+1}^k, which is brought by θ_{t+1}^k, is calculated. We also define a "drag hand", R_b^t, to record the best reward among historical rewards. Then, the dynamic weight in (4.17), ω_t, is updated using Algorithm 1, where, $\Delta\omega$ denotes the weight updating rate, and C_b^t counts the number of rewards that are less than R_b^t in succession. C_{set} is a threshold which determines the frequency of updating ω_t when the parameter vector is stuck in a local optimum. Also, C_b^t and R_b^t are updated in each iteration, as presented in Algorithm 1. Note that Step II to VI constitute the entire operation in each iteration *t*.

4.5 Case study

In this section, the proposed parameter sensitivity analysis and parameter identification algorithms are validated using numerical experiments. Before performing verification, we firstly screen out the CMPLDWG parameters that are necessary to be identified. This screening is based on the consideration that CMPLDWG contains multiple types of parameters, of which some parameters can be determined by field measurements and engineering judgement. Specifically, the transformer impedance, substation shunt capacitive susceptance, feeder impedance and capacitive susceptance can be accurately calculated using transformer, capacitor and feeder parameters [127],[128]. For the stalling and restarting of induction motors, engineering judgement can be lever-aged to estimate the settings [121],[129]. This is based on the observation that the stalling or restarting of a large number of induction motors can cause abrupt current, voltage and power changes [130],[131], which can be further corroborated in [81]. Also, the tripping of a large number of induction motors can cause sudden current decrease, power decrease and voltage increase. Excluding the parameters which can be accurately calculated using the electric power grid modeling technique can significantly reduce the complexity of parameter identification process. On the other hand, indistinguishably identifying all CMPLDWG parameters can pose an unnecessary computational burden on the proposed parameter identification algorithm. In our problem, 61 CMPLDWG parameters are screened out for parameter identification, as shown in Table III, and the remaining parameters are set with default values.

In this case study, the Power System Simulator for Engineering (PSS/E) and the ACTIVSg500 test case are employed to generate voltage and power measurements for parameter identification [132]. The fault-induced voltage-recovery curves are shown in Fig. 4.3. MATLAB is used to execute the processes of parameter sensitivity analysis and parameter identification. The case study is conducted on a standard PC with an Intel Xeon CPU running at 3.70 GHz and with 32.0 GB of RAM.

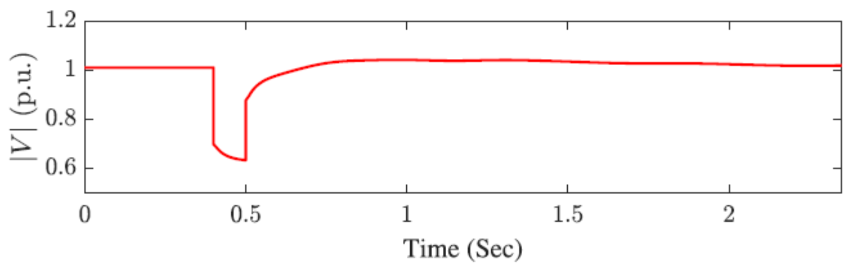

(a) Load bus voltage magnitude.

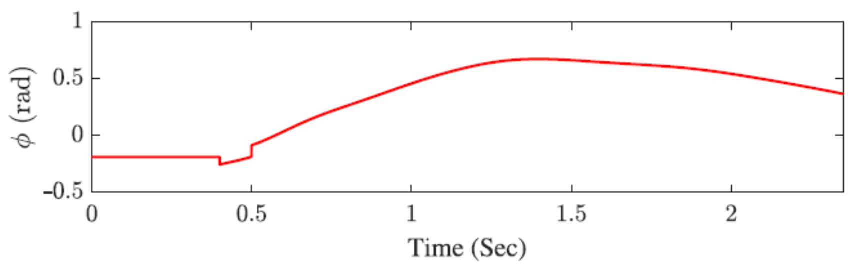

(b) Load bus voltage angle.

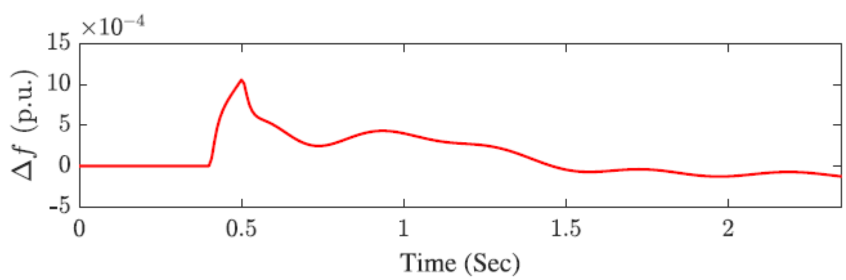

(c) Load bus frequency.

Fig. 0.3 Fault-induced voltage-recovery curves at the load bus

4.5.1 Parameter Sensitivity Identification

To fully extract the sensitivity weights hidden in the randomly-generated parameter samples and corresponding power residuals, first, we have created a comprehensive library containing 40,000 parameter vector and residual pairs which are divided into two sections, training dataset and test dataset, for cross-validation. Note that the dataset size is determined based on our numerical experiment result that once the dataset size exceeds 16,000, the FWKL gives us stable extracted parameter weights for different sets of the randomly selected parameter vector and residual pairs. Generating each pair of the parameter vector and the corresponding residual takes about 0.3

seconds. Then, the tuning parameters of FWKL are determined using grid search with cross-validation based on the training and test datasets [133]. Finally, the FWKL algorithm is applied to the entire dataset to conduct parameter sensitivity analysis. Based on our sensitivity analysis result, the load fraction parameters, the synchronous and sub-transient reactances of three-phase induction motors, and the exponential load torque coefficients of three-phase induction motors have a significant effect on the load dynamics in the fault event specified in Fig. 4.3, as shown in Fig. 4.4. The remaining parameters have small or no effect on the dynamic procedure. It should be noted that the values of parameter sensitivity weights change according to specific dynamic events since the weight vector in (4.9) partially depends on the voltage and power measurements, which are determined by specific fault cases. Therefore, PSA should be conducted on a case-by-case basis to obtain more accurate parameter sensitivity weights for specific fault events.

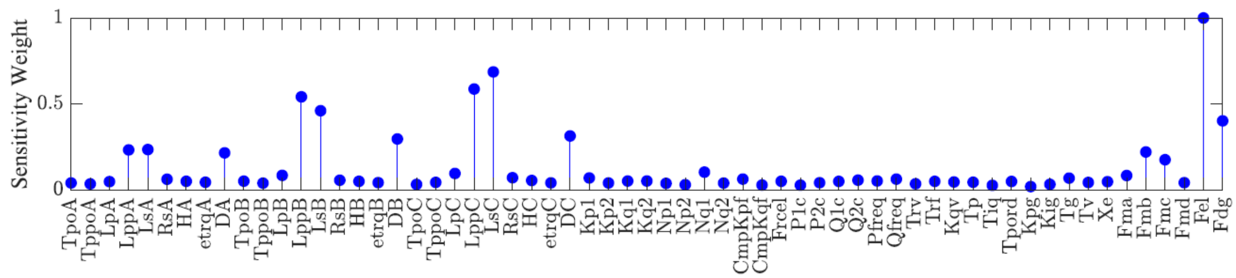

Fig. 0.4 Sensitivity weights of WECC composite load model parameters

4.5.2 Parameter Identification

The extracted parameter sensitivity weights are integrated into EDRL algorithm with IE to perform parameter identification using given voltage and power measurements. There are only a couple of published technical reports involved with WECC model parameter settings. In this case, the numerical intervals of parameters for randomly selecting initial values are determined based on [134],[135], along with our experience on deriving detailed mathematical representation of WECC composite load model [110]. The numerical intervals are presented in Table 4.1, where, LB denotes lower bound and UB denotes upper bound. Table 4.2 shows the real and corresponding identified parameter values of CMPLDWG. As can be observed, the EDRL with IE can give us satisfying identified parameters. The identification accuracy is further corroborated by Fig. 4.5, in which, the estimated active and reactive power curves can closely fit the actual curves. While our approach is not designed for online parameter identification, it is of importance to examine the computational time. In our case studies, each iteration takes about 2 seconds.

Table 0.1 Numerical interval of load parameters

Parameter	LB	UB	Parameter	LB	UB	Parameter	LB	UB
Motor A			LppC	0.06	0.24	Electronic Load		
TpoA	0.046	0.184	LsC	0.9	3.6	Frcel	0	0.38
TppoA	0.001	0.004	RsC	0.015	0.06	DER_A		
LpA	0.05	0.20	HC	0.1	0.4	Trv	0.01	0.04
LppA	0.042	0.168	EtrqC	1.8	2.2	Trf	0.02	0.06
LsA	0.9	3.6	DC	0.5	2.0	Kqv	0.5	2
RsA	0.02	0.08	Motor D			Tp	0.01	0.04
HA	0.05	0.20	Kp1	0	1	Tiq	0.01	0.04
EtrqA	0.5	2.0	Kp2	6	24	Tpord	2.5	10
DA	0.5	2.0	Kq1	3	12	Kpg	50	200
Motor B			Kq2	5.5	22	Kig	5	20
TpoB	0.05	0.20	Np1	0.5	2	Tg	0.01	0.04
TppoB	0.001	0.005	Np2	1.6	4.8	Tv	0.01	0.04
LpB	0.08	0.32	Nq1	1	4	Xe	0.13	0.5
LppB	0.06	0.24	Nq2	1.25	5	Load Fraction		
LsB	0.9	3.6	CmpKpf	0	2	Fma	0	0.5
RsB	0.015	0.06	CmpKqf	-6.6	-1.6	Fmb	0	0.5
HB	0.5	2.0	Static Load			Fmc	0	0.5
EtrqB	1	3	P1c	0	0.4	Fmd	0	0.5
DB	0.5	2.0	P2c	0	0.6	Fel	0	0.5
Motor C			Q1c	0	0.4	Fdg	-0.5	0
TpoC	0.05	0.20	Q2c	0	0.6	Fzip	0	0.5
TppoC	0.001	0.005	Pfreq	-0.2	0.2			
LpC	0.08	0.32	Qfreq	-2	-0.5			

Table 0.2 Real and identified CMPLDWG parameters

Parameter	Real	Identified	Parameter	Real	Identified	Parameter	Real	Identified
Motor A			LppC	0.12	0.1064	Electronic Load		
TpoA	0.092	0.0906	LsC	1.8	1.7535	Frcel	0.25	0.1551
TppoA	0.002	0.0024	RsC	0.03	0.0286	DER_A		
LpA	0.1	0.1037	HC	0.2	0.2839	Trv	0.02	0.0262
LppA	0.083	0.0495	EtrqC	2	2.3741	Trf	0.03	0.0221
LsA	1.8	1.8637	DC	1	1.0687	Kqv	1	1.4408
RsA	0.04	0.0275	Motor D			Tp	0.02	0.0207
HA	0.1	0.1188	Kp1	0	0.8636	Tiq	0.02	0.0153
EtrqA	1	0.8368	Kp2	12	11.675	Tpord	5	4.0030
DA	1	0.9661	Kq1	6	8.0773	Kpg	100	68.3279
Motor B			Kq2	11	10.950	Kig	10	9.9675
TpoB	0.1	0.0883	Np1	1	1.3602	Tg	0.02	0.0156
TppoB	0.0026	0.0034	Np2	3.2	4.4470	Tv	0.02	0.0163
LpB	0.16	0.1094	Nq1	2	1.6632	Xe	0.25	0.2239
LppB	0.12	0.1797	Nq2	2.5	2.5239	Load Fraction		
LsB	1.8	2.0663	CmpKpf	1	0.5	Fma	0.2	0.1969
RsB	0.03	0.0302	CmpKqf	-3.3	-4.2400	Fmb	0.3	0.4393
HB	1	1.4290	Static Load			Fmc	0.3	0.3113
EtrqB	2	2.4816	P1c	0.2	0.1953	Fmd	0.1	0.1300
DB	1	1.2146	P2c	0.3	0.2094	Fel	0.2	0.1804
Motor C			Q1c	0.2	0.1588	Fzip	0.1	0.1774
TpoC	0.1	0.0941	Q2c	0.3	0.1727	Fdg	-0.2	-0.2053
TppoC	0.0026	0.0034	Pfreq	0	-0.0942			
LpC	0.16	0.1268	Qfreq	-1	-0.8593			

It is also of significance to examine the collected best reward R_b^t and dynamic weight ω_t in each iteration, which are shown in Fig. 4.6 and 4.7, respectively. In Fig. 4.6, the loss corresponding to the collected best reward, e_b^t, is also shown for examining parameter identification performance. It can be seen that during Iteration 1 to 1226, the proposed parameter identification approach simultaneously performs exploitation and exploration, and the best reward increases continuously, as shown in Fig. 4.6.

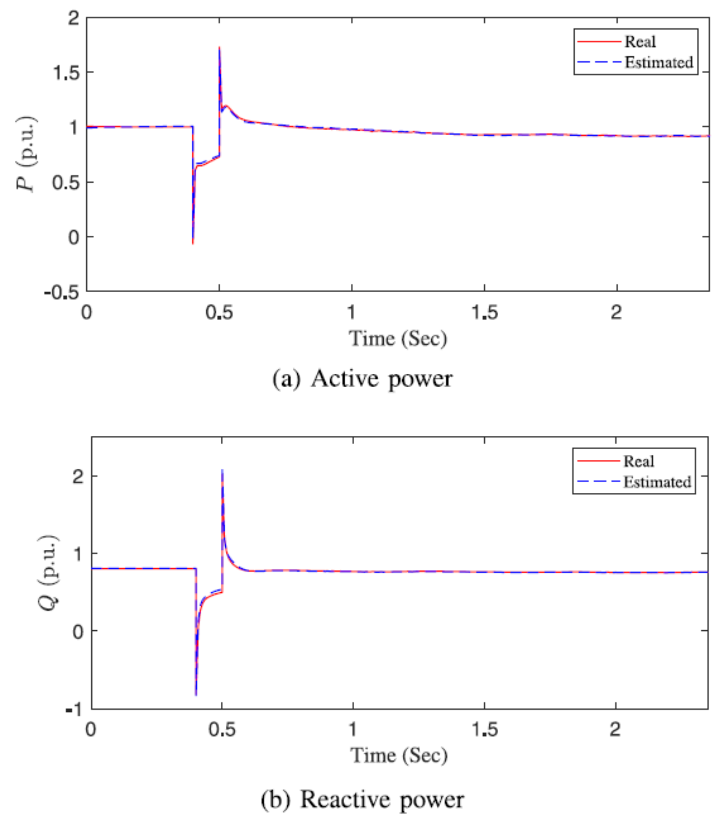

Fig. 0.5 The real power curves and the estimated power curves using the identified parameters

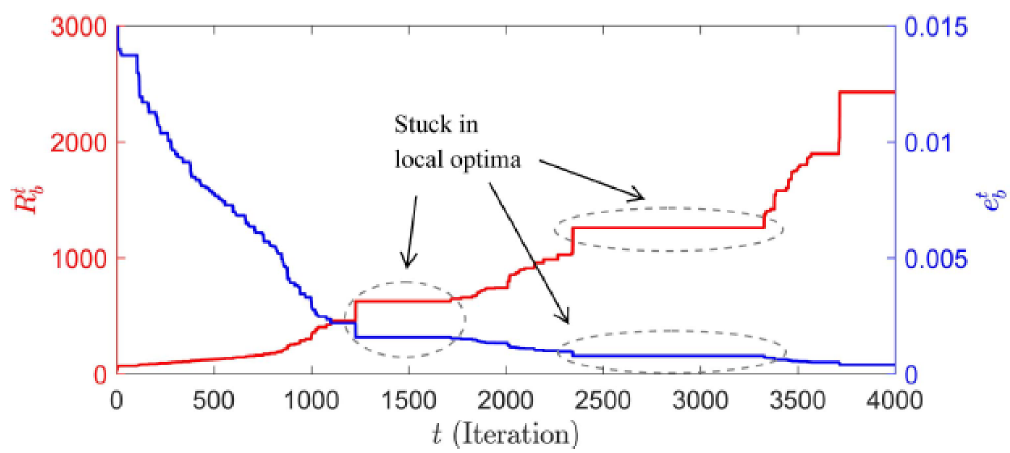

Fig. 0.6 The best reward and corresponding loss

The corresponding learning process in this iteration range can be confirmed in Fig. 4.7, in which ω_t is firstly initialized as 0, once it stays invariant for 10 continuous iterations (C_{set}), it is decreased in a step size of 0.05 ($\Delta\omega$) to force the parameter identifier to follow more closely with novelty gradient. Once an unseen better reward occurs, ω_t gradually increases to 1 to encourage the identifier to act following the approximated performance gradient. During Iteration 1 to 1226, although ω_t alternatively decreases and increases, it does not reach 0. From Iteration 1227 to

1717, the parameter identifier is stuck in a local optimum and the best reward stays invariant, as shown in Fig. 4.6. During this iteration range, first, ω_t is designed to gradually decrease to 0, which means the identifier is stimulated to explore more aggressively in the unseen parameter space, as presented in Section IV. This is verified by the variation of dynamic weight ω_t, as shown in Fig. 4.7, where, from Iteration 1227 to 1717, ω_t decreases to 0 and keep unchanged, which means the identifier completely inhibits the performance gradient. At Iteration 1718, the identifier discovers a parameter vector which can give higher reward than any of the previous best rewards. As expected, ω_t immediately jumps to 1 to avoid possible sliding out from the newly explored optimum with higher reward, due to novelty exploration inertia. From Iteration 1718 to 2342, the identifier simultaneously performs exploitation and exploration as shown in Fig. 4.6, accordingly, ω_t varies in the range of a non-zero value to 1, as shown in Fig. 4.7. This is simi-lar to the process which occurs in the range of Iteration 1 to 1226. Similar with the range of Iteration 1227 to 1717, in the range of Iteration 2343 to 3324, ω_t decreases to 0 and R_b^t stays invariant, as shown in Fig. 4.7 and 4.6, respectively. At Iteration 3325, ω_t jumps to 1 to force the identifier immediately per-form exploitation, which is similar at Iteration 1718, as shown in Fig. 4.7. Also, the best reward starts to increase at Iteration 3325, as shown in Fig. 4.6. The aforementioned cyclic process continues to pursue better rewards as the number of iterations increases, as shown in Fig. 4.6 and 4.7.

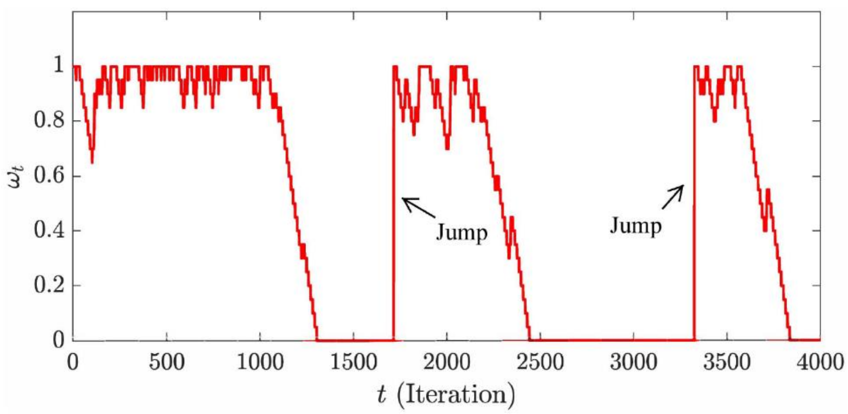

Fig. 0.7 Variation of the time-varying dynamic weight

It is interesting to examine the efficaciousness of integrating sensitivity weights into the IE module. To do this, we perform additional CMPLDWG parameter identification using EDRL with IE without revising parameter vector novelty scores. Fig. 4.8 shows two best reward collection curves corresponding to EDRL with IE by integrating *W* and without integrating *W*, respectively. As can be seen, the introduction of *W* accelerates the exploitation and exploration in reaching the same best reward.

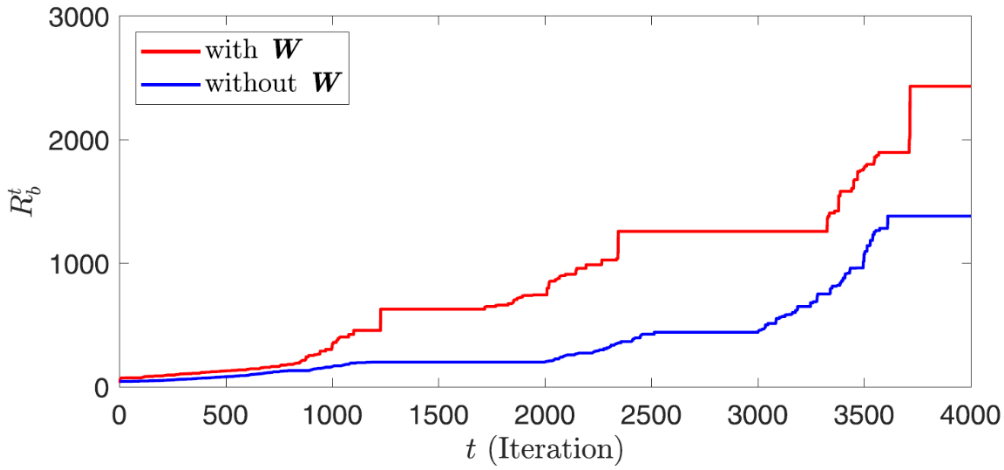

Fig. 0.8 The introduction of parameter sensitivity weights into EDRL with IE improves learning performance

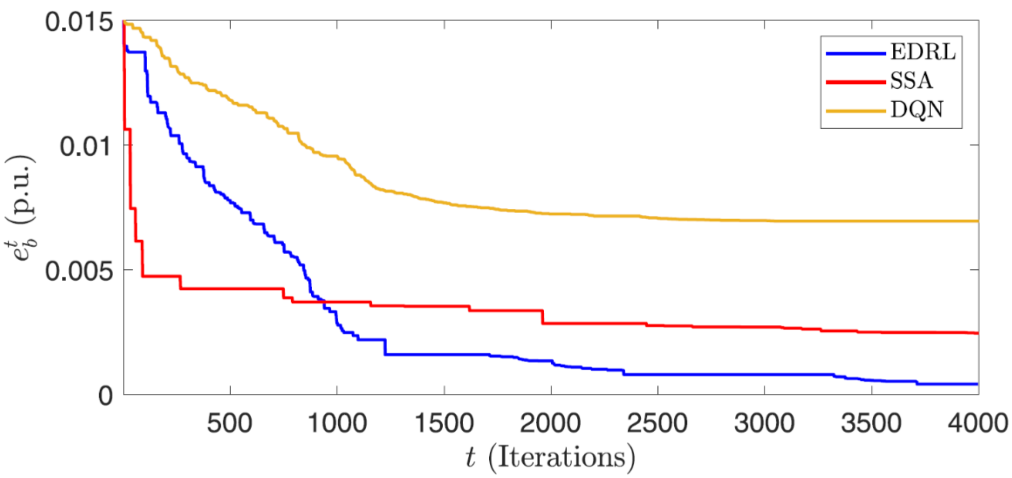

Fig. 0.9 Performance comparison of EDRL, SSA and DQN

It is also significant to compare the proposed parameter identification approach with the presented algorithms in previous works. First, we focus on comparing our algorithm with the proposed parameter identification approach in [81], which also aims to identify a large number of parameters. The comparison shows that our approach can achieve better parameter identification accuracy and does not rely on apriori knowledge. And also, our method is easier to implement due to the utilization of mathematical representation of CMPLDWG model. In addition, the parameter identification accuracy using the proposed approach in [81] significantly relies on apriori knowledge about parameter setting. We have also compared the performance of our proposed approach with that of two other state-of-the-art optimization algorithms, Salp Swarm algorithm (SSA) and deep Q-networks (DQN). SSA is a newly proposed metaheuristic optimizer inspired by the process of looking for a food source by salps. SSA has demonstrated satisfying performance compared with other metaheuristic algorithms [136]. DQN is a cutting-edge reinforcement learning technique designed for sequential decision-making tasks [137]. The performance of the three algorithms (EDRL, SSA and DQN) is shown in Fig. 4.9. It can be seen that our proposed approach outperforms the other two methods in terms of the average fitness error, e_b^t . In comparison, SSA shows the fastest convergence rate. DQN takes the longest time to converge and shows the largest average fitness error. It is also important to point out that DQN needs a significantly longer time to train a stable actor with satisfying identification performance.

4.6 Summary

This chapter presents a parameter identification approach for WECC composite load model. The proposed method employs a data-driven nonlinear feature selection technique to perform parameter sensitivity analysis, which avoids solving highly complex analytical derivatives caused by the high order and nonlinearity of differential equations of WECC composite load model. After that, the proposed method utilizes a cutting-edge approach inspired by evolutionary reinforcement learning technique, which is hybridized with an intelligent exploration mechanism to perform parameter identification. The parameter sensitivity weights are innovatively embedded in the reinforcement learning process to achieve efficient exploration. The numerical experiments demonstrate that the proposed approach can achieve promising accuracy. It is also shown that the proposed identifier can escape from local optima through the assistance of the intelligent exploration mechanism when stuck in local optima. Finally, it is verified that the integration of sensitivity weights into the reinforcement learning process accelerates the learning rate.

While our proposed approach can perform parameter identification of WECC composite load model with satisfying accuracy, the computational cost hinders its online application. Also, the model complexity stands in the way of widely applying WECC composite load model in the electric power industry. Considering this, one prospect for research on CMPLDWG is to simplify the model or develop a surrogate model to significantly reduce the computation cost and/or model complexity, while keeping the primary characteristics of WECC model.

5. Python-PSSE-Combined Autonomous Parameter Identification Program

5.1 Introduction

The WECC composite load model is widely used in power system stability analysis, energy conservation, and power system operation optimization, etc. A brief description of the WECC composite load model (CMPLDW) is shown in Fig. 5.1. The CMPLDW consists of a bus, a feeder, three three-phase motors, a single-phase motor, an electronic load, a static load. The transformer and feeder contain 18 parameters, the three-phase motors contain 65 parameters, the single-phase motor contains 34 parameters, the electronic load contains 5 parameters, and the static load contains 11 parameters. In total, the CMPLDW has 133 parameters.

In some more advanced versions of the WECC model, a distributed generator (DG) is also included, which forms a WECC composite load model with DG (CMPLDWG). The DG contains 46 parameters, so the CMPLDWG has 179 parameters in total.

A purpose of this project is to identify the parameters of the WECC composite load model to fit the active and reactive power measurements using event data, and it is a pretty challenging task considering that the WECC model is a highly nonlinear and complex load model with a huge number of parameters. In order to identify the parameters, it is essential to have a convincing representation of the WECC model. It is possible for the researchers/scholars to code the WECC model in Matlab or other programming languages (e.g., python), but considering the great complexity of the WECC model, especially those nonlinear equations and the protection actions, it is very difficult that the WECC model coded in Matlab/python can 100% accurately represent the characteristics of the WECC model. In such cases, some errors may in incurred by the imperfect representation of the WECC load model. An alternative is to use the WECC load module in the PSSE commercial software, which is believed to be the available most accurate representation of the WECC load model. But it is worth noting that the DG is currently unmodeled in the PSSE software.

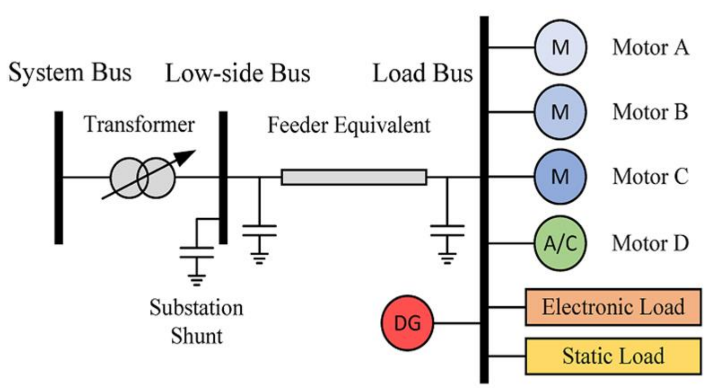

Fig. 0.1 Brief introduction of WECC load model

5.2 Python-PSSE Autonomous Parameter Identification Approach

There are various kinds of optimization methods available, such as conventional methods and heuristic methods. The conventional methods include Lagrangian relaxation, benders decomposition, branch and bound algorithm, linear programing, and mixed-integer programming. The heuristic methods include artificial intelligence methods and bio-inspired methods. The deep Q-learning, asynchronous advantage actor (A3C) algorithm in the category of reinforcement learning are good examples of artificial intelligence methods. And the particle swarm optimization (PSO), genetic algorithm (GA), and salp swarm algorithm (SSA) are good examples of bio-inspired optimization methods.

While the conventional optimization methods are powerful and widely applied, but they could not be applied to solve the parameter identification problem of the WECC load model. This is because the WECC load model is highly nonlinear and could not perform the transformation required during the solution process of the conventional optimization methods. Rather, the heuristic methods have a much less requirement, and they are good candidates for solving the WECC load model parameter identification problem.

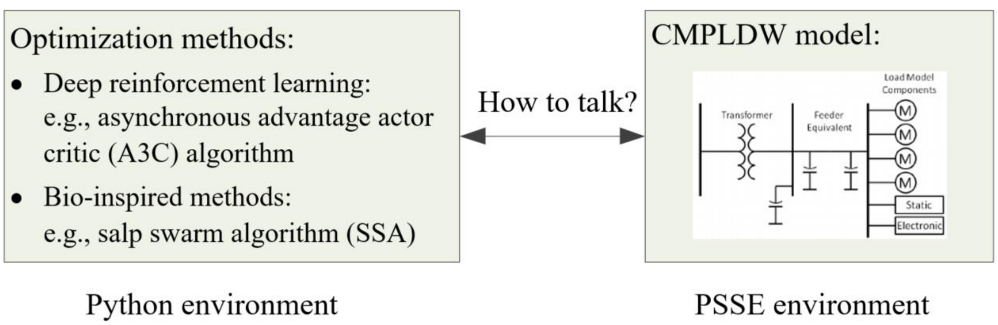

Fig. 0.2 Problem description of Python-PSSE autonomous parameter identification approach

A lot of the heuristic methods can be coded conveniently in the python environment. And the CMPLDW model is sited in the PSSE environment. Thus, a practical problem is that how can we establish a stable connection between the optimization methods sited in the python environment and the CMPLDW model sited in PSSE, and how can we enable them to exchange information efficiently for solving the WECC load model validation problem.

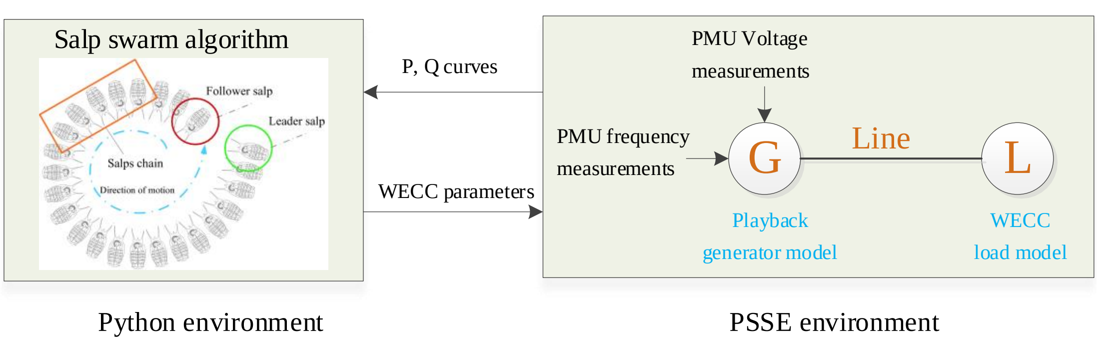

Fig. 0.3 Overview of Python-PSSE autonomous parameter identification approach

An overview of our proposed Python-PSSE autonomous parameter identification approach is shown in Fig. 5.3. We can flexibly select various optimization methods to efficiently optimize the CMPLDW parameters. The salp swarm algorithm [136] is used here as an example due to its high efficiency of searching, and it is coded in python. The salp swarm algorithm mimics the behaviors of a group of salps searching for food. Based on the current best food positions, the leader salp and the following salps update their positions. More details about this algorithm can be found at [136]. In the PSSE environment, a dynamic power system simulation model is built, and it consists of a generator connected to a load via a transmission line. For the generator, the playback generator model is adopted as it allows us to inject disturbance recorded by real PMU data. For the load, the WECC load model is adopted. For the line, the typical parameters of a short transmission line are adopted. The SSA sends the WECC parameters to the PSSE as its inputs. Based on these WECC parameters provided by SSA, a dynamic simulation is conducted in the PSSE using the PMU frequency measurements and voltage measurements. After the simulation is conducted, an active power (P) curve and a reactive power (Q) curve are obtained, and they are provided to the SSA. The SSA then compares the simulated P, Q curves with the real P, Q measurement curves to update the WECC parameters. When the convergence of the SSA is reached, the optimal WECC parameters can be obtained.

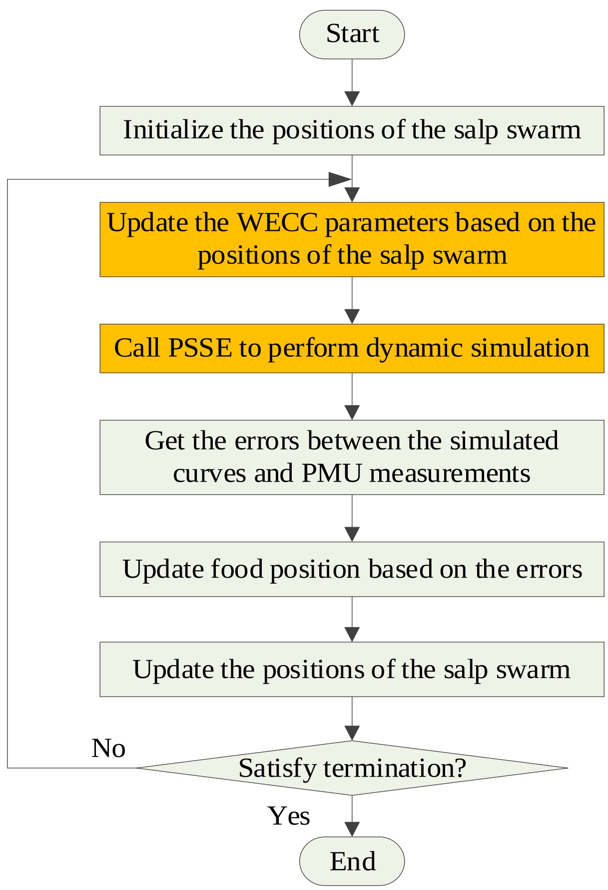

Fig. 0.4 Program flowchart of Python-PSSE autonomous parameter identification approach

The program flowchart of the Python-PSSE autonomous parameter identification approach is depicted in Fig. 5.4 and explained in detail as follows.

- Step 1: Initialize the positions of the salp swarm. Each salp is a candidate solution of the WECC parameter identification problem, and the dimension of a salp equals to the number of WECC parameters to be identified. In order to better explore the searching space, it is better that the values of the salps are randomly distributed within the allowed range.
- Step 2: As each salp is a candidate solution of the WECC parameter identification problem, the WECC parameters are updated based on the positions of the salps.
- Step 3: Call PSSE to perform the dynamic simulation. As mentioned before, the dynamic simulation model has a playback model generator connected to a load modeled by WECC with a short transmission line.
- Step 4: After obtained by simulated P, Q curves, the error between the simulated curves and real PMU measurements can be obtained. It should be noted that the objective function of the SSA is to minimize the root mean square error shown as follows:

  $$\min \sqrt{\frac{1}{2N}\sum_{i=1}^{N}\left[\left(P_i^{sim}-P_i^{PMU}\right)^2+\left(Q_i^{sim}-Q_i^{PMU}\right)^2\right]} \quad (5.1)$$

  where P_i^{sim} is the simulated active power curve; P_i^{PMU} is the active power curve by PMU; Q_i^{sim} is the simulated reactive power curve; Q_i^{PMU} is the reactive power curve by PMU; N is the number of measurements. As can be seen in (5.1), the reactive power and active power are treated equally.
- Step 5: Update food position based on the error, i.e., the position of the salp with the minimal error is the updated food position.
- Step 6: Update the positions of the salp swarm. This step can be conducted based on the principles of the SSA algorithm.
- Step 7: Check if the termination condition is satisfied or not. In this program, the maximum number of iterations is used as the termination criterion. If the termination criterion is not satisfied, the program will go to step 2 and repeat.

5.3 WECC Parameter Identification using AEP Data

Our industrial partner has provided us some real event PMU data. It is about a fault that happened on a 138 kV line. And the fault event was recorded by PMU at a nearby 12.47 kV substation. The recorded voltage curve and frequency deviation curves are shown in Figs. 5-5 and 5-6, respectively. As can be seen in Fig. 5-5, there is a severe frequency drop after the fault, and the voltage quickly recovered to normal after the fault was cleared. The fault has also resulted in some frequency deviations concurrent with the voltage fluctuation, and it is observed in Fig. 5-6 that the frequency deviation is not too severe, but its impact on the load modeling could not be ignored.

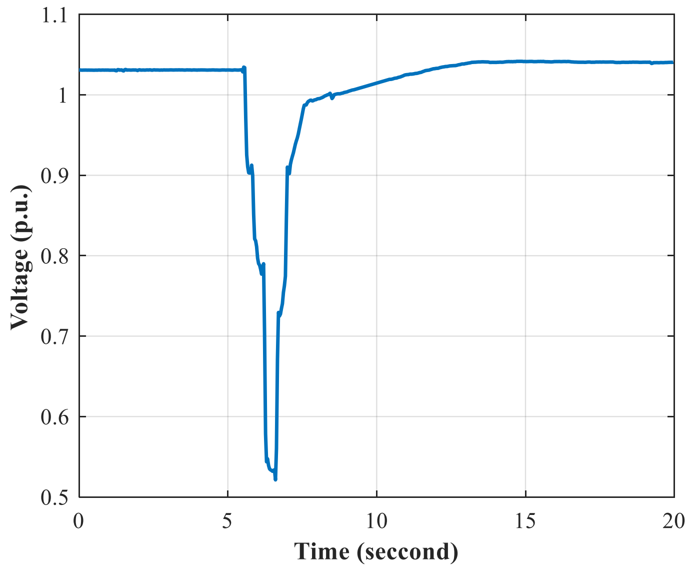

Fig. 0.5 Recorded voltage curve

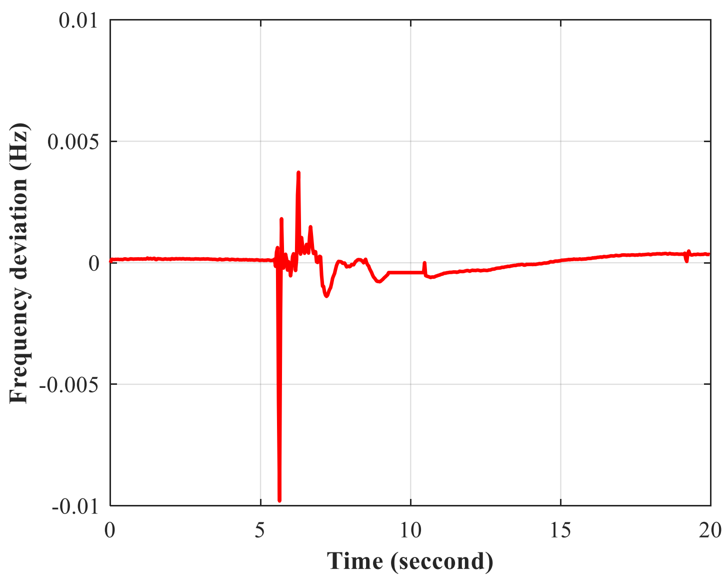

Fig. 0.6 Recorded frequency deviation curve

Each of the 133 CMPLDW parameters has a specific physical meaning; thus, their initial values should be carefully chosen. To the best of our knowledge, there are no well-established upper/lower bounds and typical values of the 133 CMPLDW parameters in the literature. So, we carefully check the industrial report and academic paper, including those reports written by NREL and NERC, and obtain the initial values of the CMPLDW parameters as listed in Table 5-1. All the parameters are within their ranges of physical meanings. These parameters provide a good initial estimation and serve as the basis for further optimization.

Table 0.1 Initial CMPLDW parameters

J+ index	Name	Value	J+ index	Name	Value	J+ index	Name	Value	J+ index	Name	Value	J+ index	Name	Value
0	MVA	-1	27	P1e	2	54	Ftr2A	0.3	81	LpC	0.19	108	Np1	1
1	SubstB	0	28	P1c	0.3	55	Vrc2A	0.1	82	LppC	0.14	109	Kq1	6
2	Rfdr	0.04	29	P2e	1	56	Trc2A	999	83	TpoC	0.2	110	Nq1	2
3	Xfdr	0.04	30	P2c	0.7	57	MtypB	3	84	TppoC	0.0026	111	Kp2	12
4	Fb	0.75	31	Pfrq	0	58	LFmB	0.75	85	HC	0.1	112	Np2	3.2
5	XXf	0.08	32	Q1e	2	59	RaB	0.03	86	EtrqC	2	113	Kq2	11
6	Tfixhs	1	33	Q1c	-0.5	60	LsB	1.8	87	Vtr1C	0	114	Nq2	2.5
7	Tfixls	1	34	Q2e	1	61	LpB	0.19	88	Ttr1C	999	115	Vbrk	0.86
8	LTC	0	35	Q2c	1.5	62	LppB	0.14	89	Ftr1C	0	116	Frst	0.3
9	Tmin	0.9	36	Qfrq	-1	63	TpoB	0.2	90	Vrc1C	999	117	Vrst	0.95
10	Tmax	1.1	37	MtypA	3	64	TppoB	0.0026	91	Trc1C	999	118	CmpKpf	1
11	Step	0.00625	38	LFmA	0.75	65	HB	0.5	92	Vtr2C	0	119	CmpKpf	-3.3
12	Vmin	1.025	39	RsA	0.04	66	EtrqB	2	93	Ttr2C	999	120	Vc1off	0.5
13	Vmax	1.04	40	LsA	1.8	67	Vtr1B	0	94	Ftr2C	0	121	Vc2off	0.4
14	Tdelay	30	41	LpA	0.12	68	Ttr1B	999	95	Vrc2C	999	122	Vc1on	0.65
15	Tstep	5	42	LppA	0.104	69	Ftr1A	0	96	Trc2C	999	123	Vc2on	0.55
16	Rcmp	0	43	TpoA	0.095	70	Vrc1B	999	97	Tstall	0.0333	124	Tth	7
17	Xcmp	0	44	TppoA	0.0021	71	Trc1B	999	98	Trestart	0.3	125	Th1t	0.4
18	FmA	0.237	45	HA	0.1	72	Vtr2B	0	99	Tv	0.025	126	Th2t	3
19	FmB	0.119	46	EtrqA	0	73	Ttr2B	999	100	Tf	0.1	127	Fuvr	0
20	FmC	0.1	47	Vtr1A	0.65	74	Ftr2B	0	101	CompLF	1	128	UVtr1	0
21	FmD	0.24	48	Ttr1A	0.2	75	Vrc2B	999	102	CompPF	0.98	129	Ttr1	999
22	Fel	0.162	49	Ftr1A	0.3	76	Trc2B	999	103	Vstall	0.45	130	UVtr2	0
23	Pfel	1	50	Vrc1A	0.1	77	MtypC	3	104	Rstall	0.124	131	Ttr2	999
24	Vd1	0.7	51	Trc1A	999	78	LFmC	0.75	105	Xstall	0.114	132	FrstPel	1
25	Vd2	0.5	52	Vtr2A	0.65	79	RaC	0.03	106	Lfadj	0			
26	PFs	1	53	Ttr2A	0.33	80	LsC	1.8	107	Kp1	0			

Table 0.2 Selection of parameters for identification

J+ Index	Name	Initial value	Range	J+ Index	Name	Initial value	Range
18	FmA	0.237	[0.0474, 0.711]	35	Q2c	1.5	[-3, 3]
19	FmB	0.119	[0.0238, 0.357]	38	LFmA	0.75	[0.375, 1.125]
20	FmC	0.1	[0.02, 0.3]	39	RaA	0.04	[0.02, 0.06]
21	FmD	0.24	[0.048, 0.72]	58	LFmB	0.75	[0.375, 1.125]
22	Fel	0.162	[0.0324, 0.486]	59	RaB	0.03	[0.015, 0.045]
23	PFel	1	[0.95, 1]	78	LFmC	0.75	[0.375, 1.125]
24	Vd1	0.7	[0.42, 0.77]	79	RaC	0.03	[0.015, 0.045]
25	Vd2	0.5	[0.3, 0.55]	109	Kq1	6	[4.8, 9]
26	PFs	1	[0.85, 1]	110	Nq1	2	[1.6, 3]
28	P1c	0.3	[0.15, 1.5]	124	Tth	5	[4, 10]
30	P2c	0.7	[0.35, 3.5]	125	Th1t	0.4	[0.32, 0.8]
33	Q1c	-0.5	[-1, 1]	126	Th2t	3	[2.4, 6]

Ideally, our approach is able to optimize all the parameters within any range. However, it would be very challenging if we want to identify all the parameters. Also, after some sensitivity analysis, like using the active subspace method described in chapter 3, it is found that not all the parameters have a significant influence on the performance of the WECC load model. So, 24 most critical parameters are selected for identification, as marked in blue in Table 5-1, and their ranges are chosen as shown in Table 5-2. In addition, in practice, we found that the random selection of some parameters (such as LsA, LpA, LppA, TpoA, TppoA, HA, EtrqA, Vtr1A, Ttr1A, Ftr1A, Vrc1A) may collapse the PSSE software during the simuation. Considering all those factors, the parameters and their ranges shown in Table 5-2 are adopted for optimization in the Python-PSSE-combined autonomous parameter identification program. All other 109 parameters are kept unchanged based on their values in Table 5-1. It is worth noting that since it is very convenient to adjust the parameters to be optimized and their ranges, we can quickly update our program and re-run the simulation if needed.

Using the SSA method in python and dynamic simulation in PSSE, simulations are carried out based on the real PMU event data. Specifically, 30 salps are adopted in the simulation, and the optimization is conducted for 50 iterations for each salp, i.e., in total, 1500 dynamic simulations with different WECC parameters are performed. The convergence curve of the SSA is shown in Fig. 5-7. It can be seen that the root mean square error between the simulated curves and real PMU measurement curves drops rapidly with the iterations.

The simulation takes 39 minutes in total. The main computation time is spent on the PSSE dynamic simulation and output data processing, which is inevitable. And the time spent on the SSA itself is negligible. All those demonstrate the efficiency of our proposed Python-PSSE-combined autonomous parameter identification approach.

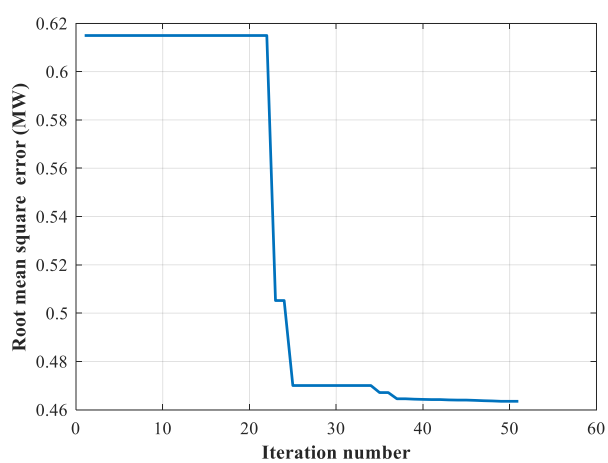

Fig. 0.7 Convergence of SSA

The finally obtained CMPLDW parameters are shown in Table 5-3. It is important to clarify that according to the rules encoded in the WECC load model of PSSE software, if the sum of load fractions FmA, FmB, FmC, FmD, Fel is less than 1, the remainder is static load; if sum of fractions FmA, FmB, FmC, FmD, Fel is greater than 1, fractions are normalized to 1, and there will be no static load.

Table 0.3 Identified CMPLDW parameters

J+ index	Name	Value	J+ index	Name	Value	J+ index	Name	Value	J+ index	Name	Value	J+ index	Name	Value
0	MVA	-1	27	P1e	2	54	Ftr2A	0.3	81	LpC	0.19	108	Np1	1
1	SubstB	0	28	P1c	0.679	55	Vrc2A	0.1	82	LppC	0.14	109	Kq1	6.091
2	Rfdr	0.04	29	P2e	1	56	Trc2A	999	83	TpoC	0.2	110	Nq1	2.965
3	Xfdr	0.04	30	P2c	0.352	57	MtypB	3	84	TppoC	0.0026	111	Kp2	12
4	Fb	0.75	31	Pfrq	0	58	LFmB	0.44	85	HC	0.1	112	Np2	3.2
5	XXf	0.08	32	Q1e	2	59	RaB	0.015	86	EtrqC	2	113	Kq2	11
6	Tfixhs	1	33	Q1c	0.234	60	LsB	1.8	87	Vtr1C	0	114	Nq2	2.5
7	Tfixls	1	34	Q2e	1	61	LpB	0.19	88	Ttr1C	999	115	Vbrk	0.86
8	LTC	0	35	Q2c	-1.841	62	LppB	0.14	89	Ftr1C	0	116	Frst	0.3
9	Tmin	0.9	36	Qfrq	-1	63	TpoB	0.2	90	Vrc1C	999	117	Vrst	0.95
10	Tmax	1.1	37	MtypA	3	64	TppoB	0.0026	91	Trc1C	999	118	CmpKpf	1
11	Step	0.00625	38	LFmA	0.837	65	HB	0.5	92	Vtr2C	0	119	CmpKpf	-3.3
12	Vmin	1.025	39	RsA	0.023	66	EtrqB	2	93	Ttr2C	999	120	Vc1off	0.5
13	Vmax	1.04	40	LsA	1.8	67	Vtr1B	0	94	Ftr2C	0	121	Vc2off	0.4
14	Tdelay	30	41	LpA	0.12	68	Ttr1B	999	95	Vrc2C	999	122	Vc1on	0.65
15	Tstep	5	42	LppA	0.104	69	Ftr1A	0	96	Trc2C	999	123	Vc2on	0.55
16	Rcmp	0	43	TpoA	0.095	70	Vrc1B	999	97	Tstall	0.0333	124	Tth	5.663
17	Xcmp	0	44	TppoA	0.0021	71	Trc1B	999	98	Trestart	0.3	125	Th1t	0.422
18	FmA	0.233	45	HA	0.1	72	Vtr2B	0	99	Tv	0.025	126	Th2t	2.80
19	FmB	0.141	46	EtrqA	0	73	Ttr2B	999	100	Tf	0.1	127	Fuvr	0
20	FmC	0.026	47	Vtr1A	0.65	74	Ftr2B	0	101	CompLF	1	128	UVtr1	0
21	FmD	0.197	48	Ttr1A	0.2	75	Vrc2B	999	102	CompPF	0.98	129	Ttr1	999
22	Fel	0.224	49	Ftr1A	0.3	76	Trc2B	999	103	Vstall	0.45	130	UVtr2	0
23	Pfel	1	50	Vrc1A	0.1	77	MtypC	3	104	Rstall	0.124	131	Ttr2	999
24	Vd1	0.743	51	Trc1A	999	78	LFmC	0.686	105	Xstall	0.114	132	FrstPel	1
25	Vd2	0.314	52	Vtr2A	0.65	79	RaC	0.037	106	Lfadj	0			
26	PFs	1	53	Ttr2A	0.33	80	LsC	1.8	107	Kp1	0			

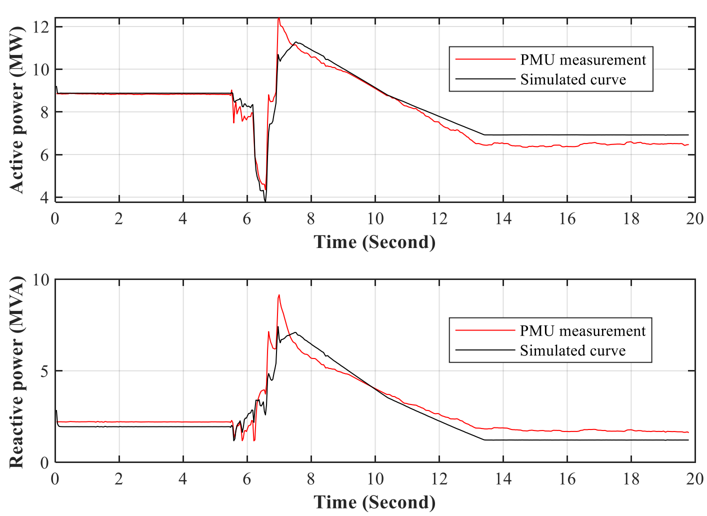

Fig. 0.8 Comparisons of simulated curves and PMU measurements

Using the identified CMPLDW parameters shown in Table 5-3 and the WECC load module in PSSE, the obtained active power and reactive power curves are shown in Fig. 5-8. They are compared with the real PMU measurements, and it can be observed that the simulated curves match pretty well with the PMU measurements, which validates the accuracy of our proposed Python-PSSE-combined autonomous parameter identification approach. Specifically, it is calculated that the root mean square error is 0.46 MW (or 0.46 MAV as we treat active power and reactive equally), which is pretty small and acceptable.

5.4 Summary

This chapter presents a Python-PSSE-combined autonomous parameter identification program. It enables efficient information change between the optimization method sited in Python environment and the WECC load module in PSSE software. As the WECC load module is the available most convincing representation of the WECC load module, this approach can eliminate the possible errors brought by the inaccurate representation of the WECC load modeling. As an example of the heuristic optimization methods, the SSA is adopted to optimize the WECC load parameters using real event data provided by AEP. The obtained results are promising, and they validate the efficiency and accuracy of our proposed Python-PSSE-combined autonomous parameter identification program.

6. Dynamic Large-Signal Order Reduction of Composite Load Model

6.1 Introduction

Load modeling is important to stability analysis, optimization, and controller design [1]. However, due to the diversity of load components and lack of detailed load information and measurements, modeling load is still challenging.

Load models can be classified as static and dynamic models. Static load models such as static constant impedance-current power (ZIP) model and exponential model have simple model structures, nevertheless, they cannot capture the dynamic load behaviors [82],[80]. Motivated by the 1996 blackout of the Western Systems Coordinating Council (WSCC), a widely-used dynamic composite load model was developed [5]. The model consists of a ZIP and a dynamic induction motor (IM). It was designed to represent highly stressed conditions in summer peaks. However, this interim load model was unable to approximate the fault-induced delayed voltage recovery (FIDVR) events [81]. A preliminary WECC composite load model (WECC CLM) was proposed by adding an impedance representing the electrical distance between substation and end users, an electronic load and a single-phase motor [83],[85]. After a series of improvements, the latest WECC composite load model (CMPLDWG) is developed, as shown in Fig. 6.1. The electrical distance between the substation and end-users is represented by a substation transformer, a shunt reactance, and a feeder equivalent. The model consists of three three-phase motors, one AC single-phase motor, one static load, one power electronics component, and a distributed energy resource (DER). The DER in CMPLDWG is currently represented by the PVD1 model [107]. However, PVD1 has 5 modules, 121 parameters and 16 states, which is as complex as the CMPLDW itself. Therefore, the Electric Power Research Institute (EPRI) has developed a simpler yet more comprehensive model to replace PVD1, which is named as DER A model [107].

The above WECC CMPLDW + DER_A model is a complex high-order system, which makes the studies that need numerical solutions time consuming and even computationally infeasible. There are two main reasons for this high computational burden. One is the high-order characteristic increases the computational dimension. The other is the two-time-scale property makes the computation a stiff problem, which requires small time steps to calculate the fast dynamics and results in a long computational time to capture slow dynamics. The fast dynamics are often introduced by the intentionally added inductance and capacitance, moment of inertia, and parasitic elements inherent in the system. However, simply neglecting the fast dynamics does not guarantee stability and accuracy of the model. In order to accelerate computation while maintaining the accuracy and stability of the load model, it is imperative to develop an accurate and easy-to-use reduced-order load model.

The existing model reduction methods usually project the higher dimensional counterpart into a lower dimensional subspace where dynamic features of the original model dominate. The singular perturbation is such kind of method that considers the fast dynamics as boundary layers and includes their solutions into slow dynamics. Singular perturbation method is suitable for analyzing two-time-scale problems and is widely used in power systems analyses. Previous applications of singular perturbation in power systems include reduced-order model of synchronous machines and induction motors, modeling the utility distribution grid-tied systems with wind turbines, and reduced-order microgrid model [84]. This chapter will develop a reduced-order large-signal model of WECC CMPLDW + DER A model using singular perturbation method.

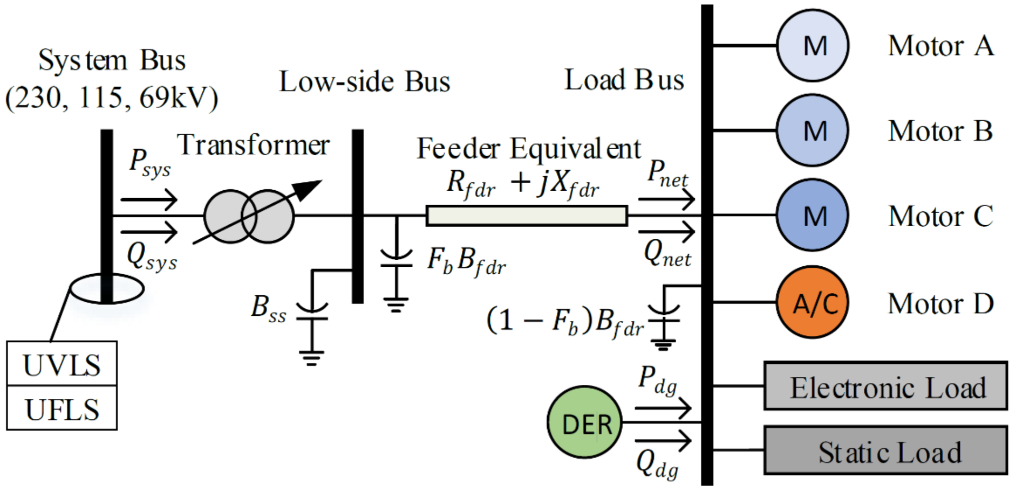

Fig. 0.1 A schematic diagram of the WECC CMPLDWG

6.2 Introduction to Order Reduction Method Based on Singular Perturbation

Singular perturbation method was originally developed to analyze a problem with a small parameter that cannot be approximated by simply setting the parameter value to be zero. It avoids the discontinuity of solution by analyzing the problem in separate time scales. Consider a standard singular perturbation model as follows.

6.2.1 LSOR Based on Singular Perturbation Theory

Consider a standard singular perturbation model as follows,

$$\dot{x} = f\left(t, x, z, \varepsilon\right), \tag{6.1}$$

$$\varepsilon \dot{z} = g\left(t, x, z, \varepsilon\right), \tag{6.2}$$

where $x \in \mathbb{R}^n$, $z \in \mathbb{R}^m$, $t \in [0, t_1]$, and $\varepsilon \in [0, \varepsilon_0]$; f and g are Lipshitz continuous functions.

Selecting the perturbation coefficient ε for real physical systems is challenging. In most cases, we pick it based on our knowledge of the real system. In cases where it is unclear which parameter is small, we can locally linearize the system around the equilibrium point and use modal decomposition to identify the slow and fast dynamics.

When ε is small, the fast transient velocity $\dot{z} = g / \varepsilon$ can be much larger than that of the slow transient $\dot{x}$. To solve this two-time-scale problem, we can set $\varepsilon = 0$, then equation (6.2) degenerates to the following algebraic equation,

$$0 = g\left(t, x, z, 0\right). \tag{6.3}$$

Assuming that equation (6.3) has at least one isolated real root, and satisfies the implicit function theorem, then for each argument, we can obtain the quasi-steady-state (QSS) solution in a local vicinity around the isolated root,

$$z = h\left(t, x\right). \tag{6.4}$$

Substituting equation (6.4) into equation (6.1) and setting $\varepsilon = 0$, we obtain the QSS model,

$$\dot{x} = f\left(t, x, h\left(t, x\right), 0\right). \tag{6.5}$$

We call the QSS system (6.5) the reduced-order model since its order drops from $n + m$ to n. The slow states can be obtained by solving the reduced-order model (6.5), whereas the fast states are represented by equation (6.4). However, (6.4) only gives approximate solution unless ε is zero. To quantify the error between approximate and actual fast states, we denote the error as $y = z - h(x,u)$. Then in the fast-time-scale $\tau = t / \varepsilon$, the dynamics of y are governed as follows,

$$\frac{\mathrm{d}y}{\mathrm{d}\tau} = G(t, x, y, \varepsilon) = g(t, x, h(t, x) + y, \varepsilon) - \varepsilon \frac{\partial h}{\partial t} - \varepsilon \frac{\partial h}{\partial x} f(t, x, h(t, x) + y, \varepsilon). \tag{6.6}$$

Let $\varepsilon = 0$, we obtain the boundary-layer model:

$$\frac{\mathrm{d}y}{\mathrm{d}\tau} = g\left(t, x, y + h\left(t, x\right), 0\right). \tag{6.7}$$

Note that the exact fast states are $z = y + h(t, x)$, but we do not know (x, y). Therefore, if we can guarantee the accuracy of reduced-order model and boundary-layer model, then we can use their solutions $\left(\hat{x}, \hat{y}\right)$ instead of (x, y). However, these models are exact only when ε is exactly zero, which is obviously not the case for the studied system. Thus, we need to quantitatively assess the accuracy of reduced-order model when ε is small yet nonzero. This motivates the next subsection.

6.2.2 Accuracy Assessment

Before deriving the performance guarantee of the proposed high-fidelity order reduction approach, we first introduce a few technical definitions and assumptions:

Assumption 1: On a compact subset of $\Omega_x \times \Omega_y$, the functions f and g are C^1 and has bounded first partial derivative with respect to x, z and ε; g has bounded and continuous first partial derivative with respect to t; h and the Jacobian $\partial g / \partial z$ have bounded first partial derivatives; $\partial f / \partial x$ is Lipschitz in x uniformly in t;

Assumption 2: the origin of the reduced model (6.5) is a uniformly exponentially stable equilibrium and there is a Lyapunov function $V(t, x)$ satisfying

$$W_1(x),, \; V(t,x),, \; W_2(x)$$

$$\frac{\partial V}{\partial t} + \frac{\partial V}{\partial x} f(t,x),, \; -W_3(x) \tag{6.8}$$

where W_i are continuous positive definite functions on Ω_x and $\{x \,|\, W_1(x),, \; c\}$ is a compact subset of Ω_x;

Assumption 3: the origin of the boundary-layer model (6.7) is a uniformly exponentially stable equilibrium;

By Tikhonov's theorem on the infinite time interval [138], there are compact sets Ω_x, Ω_y and positive constant ε^*, and k_i, such that for all $t_0 .. 0$, $x(t_0) \in \Omega_x$, $y(t_0) \in \Omega_y$ and $0 < \varepsilon < \varepsilon^*$, the original system (6.1) and (6.2) has unique solutions $x(t,\varepsilon)$ and $z(t,\varepsilon)$ uniformly satisfying

$$\| x(t,\varepsilon) - \bar{x}(t) \| \;,, \; k_1 \varepsilon \tag{6.9}$$

$$\| z(t,\varepsilon) - h(t,\bar{x}(t)) - \hat{y}(t/\varepsilon) \| \;,, \; k_2 \varepsilon \tag{6.10}$$

where $\bar{x}(t)$ and $\hat{y}(\tau)$ are solutions of the reduced model (6.5) and boundary-layer model (6.7), respectively. Moreover, for any given $T > t_0$, there exists a positive constant $\varepsilon^{**},, \; \varepsilon^*$ such that for $t \in [T, \infty)$ and $\varepsilon < \varepsilon^{**}$, it follows uniformly that

$$\| z(t,\varepsilon) - h(t,\bar{x}(t)) \| \;,, \; k_3 \varepsilon \tag{6.11}$$

We can consider the reduced model as an approximation of the original model. To guarantee its accuracy, the solutions of both slow and fast dynamics of the reduced model should converge to those of the original model exponentially fast and the errors between them should be bounded and small enough (as shown in (6.9) and (6.10)). Note that equation (6.11) means that for small enough ε, the solution of fast transient can be estimated by only quasi-steady-state solution $h(t,\bar{x}(t))$ after $T > t_0$. This plausible result can significantly simplify the original problem.

6.3 Mathematical Representation of WECC Composite Load Model

To apply the singular perturbation theory, we need the mathematical representation of WECC composite load model, which can be found in our previous work [110]. This section will only introduce the dynamic components.

6.3.1 Three-Phase Motor Model

WECC composite load model uses three three-phase motors, A, B and C to represent different types of dynamic components. These three-phase motors have the same structure but different parameter settings. The block diagram of the fifth-order induction motor model is shown in Fig. 6.2. There are four dynamic equations with respect to $E_{q'}$, $E_{d'}$, $E_q"$ and $E_d"$. We can represent the complete fifth-order model as follows,

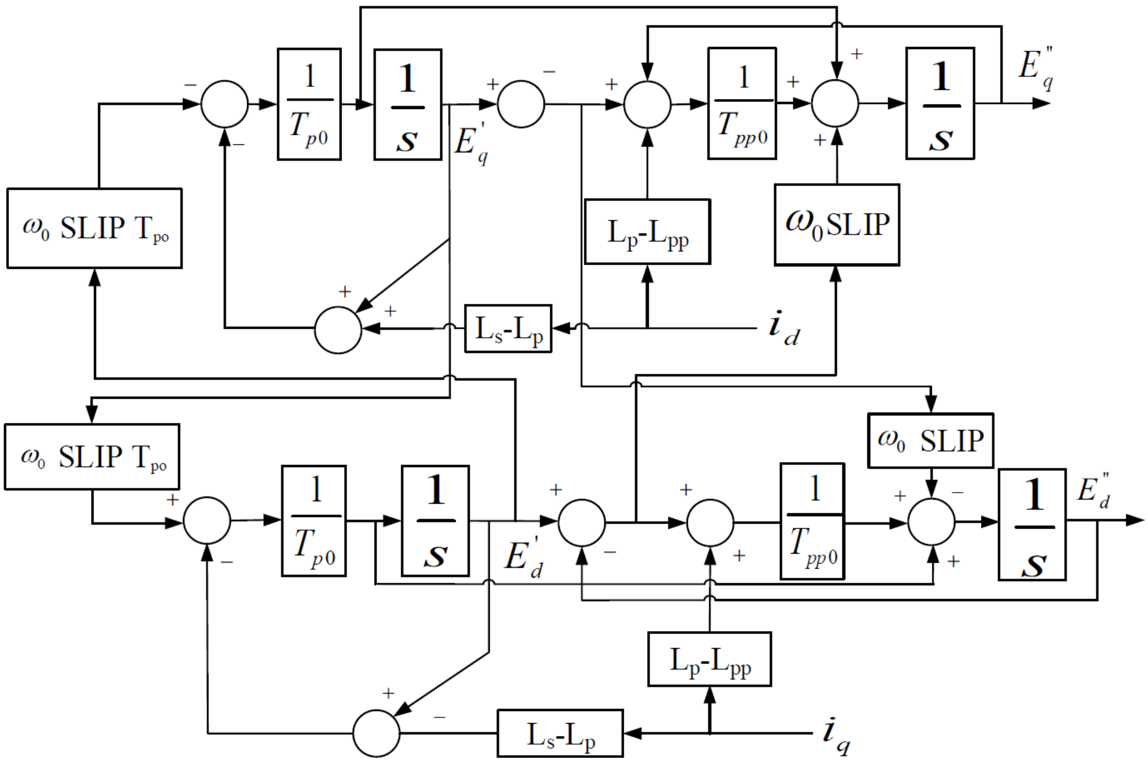

Fig. 0.2 The diagram of three-phase motor

$$\dot{E}_q' = \frac{1}{T_{p0}}\left[-E_q' - i_d\left(L_s - L_p\right) - E_d' \cdot \omega_0 \cdot SLIP \cdot T_{P0}\right] \tag{6.12}$$

$$\dot{E}_d' = \frac{1}{T_{p0}}\left[-E_d' + i_q\left(L_s - L_p\right) + E_q' \cdot \omega_0 \cdot SLIP \cdot T_{P0}\right] \tag{6.13}$$

$$\dot{E}_d'' = \frac{T_{p0} - T_{pp0}}{T_{p0}T_{pp0}} E_d' + \frac{T_{pp0}\left(L_s - L_p\right) + T_{p0}\left(L_p - L_{pp}\right)}{T_{p0}T_{pp0}} i_q - \frac{1}{T_{pp0}} E_d'' + \omega_0 \cdot SLIP \cdot E_q'' \tag{6.14}$$

$$\dot{E}_q'' = \frac{T_{p0} - T_{pp0}}{T_{p0}T_{pp0}} E_q' - \frac{T_{pp0}\left(L_s - L_p\right) + T_{p0}\left(L_p - L_{pp}\right)}{T_{p0}T_{pp0}} i_d - \frac{1}{T_{pp0}} E_q'' - \omega_0 \cdot SLIP \cdot E_d'' \tag{6.15}$$

$$\dot{SLIP} = -\frac{p \cdot E_d'' \cdot i_d + q \cdot E_q'' \cdot i_q - TL}{2Hw} \tag{6.16}$$

$$TL = T_{m0}\left(Aw^2 + Bw + C_0 + Dw^E\right) \tag{6.17}$$

$$T_{m0} = pE_d^{"}i_d + qE_q^{"}i_q \tag{6.18}$$

$$w = 1 - SLIP \tag{6.19}$$

The algebraic equations are:

$$i_d = \frac{r_s}{r_s^2 + L_{pp}^2}(V_d + E_d^{"}) + \frac{L_{pp}}{r_s^2 + L_{pp}^2}(V_q + E_q^{"}) \tag{6.20}$$

$$i_q = \frac{r_s}{r_s^2 + L_{pp}^2}(V_q + E_q^{"}) - \frac{L_{pp}}{r_s^2 + L_{pp}^2}(V_d + E_d^{"}) \tag{6.21}$$

$$P = V_d i_d + V_q i_q, \tag{6.22}$$

$$Q = V_d i_q - V_q i_d, \tag{6.23}$$

where the five state variables are $E_{q'}$, $E_{d'}$, $E_q{}''$, $E_d{}''$ and $SLIP$; L_s, L_p and L_{pp} are synchronous reactance, transient and subtransient reactance, respectively; T_{p0} and T_{pp0} are transient and subtransient rotor time constants, respectively; and ω_0 is the synchronous frequency.

6.3.2 DER_A Model

Recently, EPRI developed a new model to represent aggregate renewable energy resources which is called DER_A. The DER_A model has fewer states and parameters than the previous PVD1 model. Fig. 6.3 shows the diagram of DER_A model. Here we only summarize the dynamic equations that will be used in the order reduction. The complete detailed mathematical model can be found in [149].

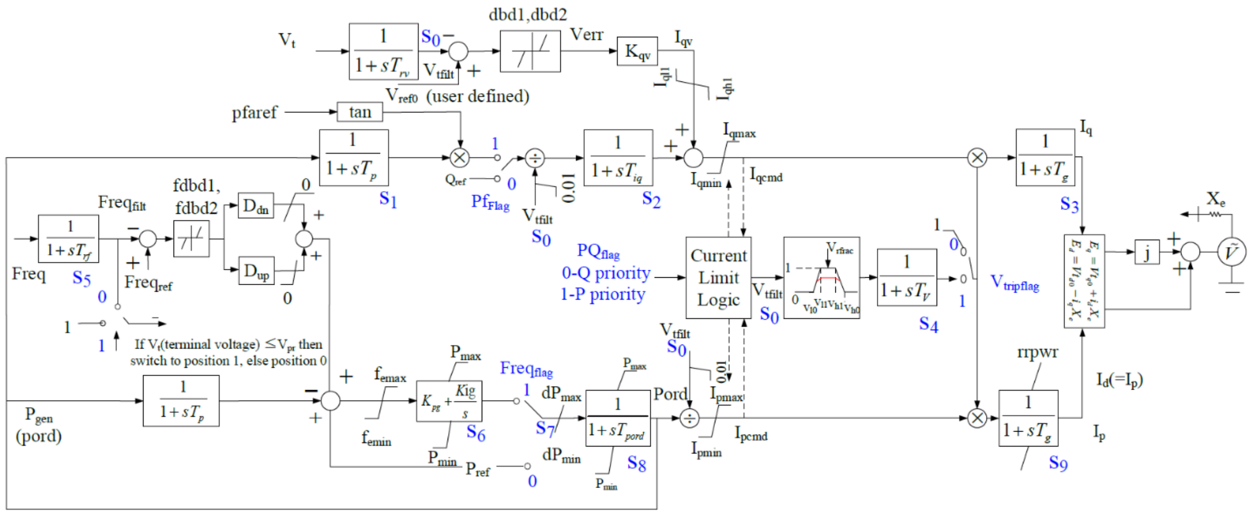

Fig. 0.3 The diagram of DER_A model

$$\dot{S}_0 = \frac{1}{T_{rv}}(V_t - S_0) \tag{6.24}$$

$$\dot{S}_1 = \frac{1}{T_p}(S_8 - S_1) \tag{6.25}$$

$$\dot{S}_2 = \begin{cases} -\dfrac{S_2}{T_{iq}} + \dfrac{Q_{ref}}{T_{iq} sat_1(S_0)} & if\ P_{fFlag} = 0 \\ -\dfrac{S_2}{T_{iq}} + \dfrac{\tan(pfaref) + S_1}{T_{iq} sat_1(S_0)} & if\ P_{fFlag} = 1 \end{cases} \tag{6.26}$$

$$\dot{S}_3 = \begin{cases} -\dfrac{S_3 - sat_2\left(S_2 + sat_2\left(DB_V\left(V_{ref0} - S_0\right) \cdot K_{qv}\right)\right)}{T_g} & if\ V_{tripFlag} = 0 \\ -\dfrac{S_3 - sat_2\left(S_2 + sat_2\left(DB_V\left(V_{ref0} - S_0\right) \cdot K_{qv}\right)\right) \times S_4}{T_g} & if\ V_{tripFlag} = 1 \end{cases} \tag{6.27}$$

$$\dot{S}_4 = \frac{1}{T_v}\left(VoltageTrip(S_0, V_{rfrac}) - S_4\right) \tag{6.28}$$

$$\dot{S}_5 = \frac{1}{T_{rf}}(Freq - S_5) \tag{6.29}$$

$$
\begin{aligned}
\dot{S}_6 = {} & K_{ig} sat_4(P_{ref} - S_1 + sat_5\left[D_{dn} \cdot DB_F(Freq_{ref} - S_5)\right] + sat_6\left[D_{up} \cdot DB_F(Freq_{ref} - S_5)\right]) \\
& + \frac{K_{pg}}{T_p} S_1 + G_{dn}\left(Freq - S_5\right) + G_{up}\left(Freq - S_5\right) - \frac{S_8}{T_p}
\end{aligned} \tag{6.30}
$$

$$
\dot{S}_7 = \begin{cases} 0 & if \;\; Freq_{flag} = 0 \\ sat_8\left(\dot{sat}_7\left(S_6\right)\right) & if \;\; Freq_{flag} = 1 \end{cases} \tag{6.31}
$$

$$
\dot{S}_8 = \frac{1}{T_{pord}}\left(S_7 - S_8\right) \tag{6.32}
$$

$$
\dot{S}_9 = \begin{cases} \dfrac{1}{T_g}\left(sat_9\left(\dfrac{sat_7(S_8)}{sat_1\left(S_0\right)}\right) \times S_4 - S_9 \right) & if \quad V_{tripflag} = 1 \\ \dfrac{1}{T_g}\left(sat_9\left(\dfrac{sat_7(S_8)}{sat_1\left(S_0\right)}\right) - S_9 \right) & if \quad V_{tripflag} = 0 \end{cases} \tag{6.33}
$$

6.4 Order Reduction of WECC Composite Load Model

In this section, we will derive the reduced-order large-signal model of WECC composite load model using singular perturbation method. For the purpose of order-reduction, we only focus on the dynamic components. These components are connected in parallel and we will reduce each individual component's order.

6.4.1 Reduced-Order Three-Phase Motor Model

Each three-phase motor model has five states, $\tilde{x}_M = \left[E_{q'}, E_{d'}, E_{q''}, E_{d''}, SLIP\right]$. When applying the singular perturbation method, the first step is to identify the slow and fast dynamics. Since the fast dynamics are characterized by the small perturbation coefficient ε, we rewrite the left-hand-side of the dynamic equations as

$$
\left[T_{p0}\dot{E}_{q'}, T_{p0}\dot{E}_{d'}, T_{pp0}\dot{E}_{q''}, T_{pp0}\dot{E}_{d''}, H \cdot S\dot{L}IP\right]^T. \tag{6.34}
$$

Given one set of parameters setting in Table 6.1, equation (6.34) becomes

$$
\left[0.1\dot{E}_{q'}, 0.1\dot{E}_{d'}, 0.0026\dot{E}_{q''}, 0.0026\dot{E}_{d''}, 0.1S\dot{L}IP\right]^T. \tag{6.35}
$$

Table 0.1 Parameters of three-phase motor model

Motor A		Motor B		Motor C	
r_{sA}	0.04	r_{sB}	0.03	r_{sC}	0.03
L_{sA}	1.8	L_{sB}	1.8	L_{sC}	1.8
L_{pA}	0.1	L_{pB}	0.16	L_{pC}	0.16
L_{ppA}	0.083	L_{ppB}	0.12	L_{ppC}	0.12
T_{poA}	0.092	T_{poB}	0.1	T_{poC}	0.1
T_{ppoA}	0.002	T_{ppoB}	0.0026	T_{ppoC}	0.0026
H_A	0.05	H_B	1	H_C	0.1
A_A	0	A_B	0	A_C	0
B_A	0	B_B	0	B_C	0
C_A	0	C_B	0	C_C	0
D_A	1	D_B	1	D_C	1
E_{trqA}	0	E_{trqB}	2	E_{trqC}	2
p_A	-1	p_B	-1	p_C	-1
q_A	-1	q_B	-1	q_C	-1
ω_{0A}	120π	ω_{0B}	120π	ω_{0C}	120π

The smaller perturbation coefficients in equation (6.35) suggest that dynamic response velocities of $\left[E_{q'}, E_{d'}, SLIP\right]$ are much slower than the rest of the states. This difference is also an evidence of the two-time-scale property of this model. Then the slow and fast dynamics are divided as follows

$$\dot{x}_M = \begin{bmatrix} x_M \\ z_M \end{bmatrix} \tag{6.36}$$

where $x_M = \left[E_{q'}, E_{d'}, SLIP\right]$, $z_M = \left[E_{q''}, E_{d''}\right]$. For consistence, define the input voltages $\left[V_q, V_d\right]$ as U_M. Following the singular perturbation method (6.1)-(6.5), we can obtain the reduced-order large-signal model of three-phase motor as

$$\dot{x}_{M1} = \frac{1}{T_{p0}}\left[-x_{M1} - i_d\left(L_s - L_p\right) - \omega_0 \cdot T_{P0} \cdot x_{M2} \cdot x_{M3}\right] \tag{6.37}$$

$$\dot{x}_{M2} = \frac{1}{T_{p0}}\left[-x_{M2} + i_q\left(L_s - L_p\right) + \omega_0 \cdot T_{P0} \cdot x_{M1} \cdot x_{M3}\right] \tag{6.38}$$

$$\dot{x}_{M3} = \frac{TL - p \cdot h_2\left(x_M\right) \cdot i_d - q \cdot h_1\left(x_M\right) \cdot i_q}{2H} \tag{6.39}$$

where the quasi-steady-state solutions are

$$h_1\left(x_M\right) = \frac{1}{r_s^2 + L_p^2}\left[\left(L_p L_{pp} + r_s^2\right)x_{M1} - \left(L_p - L_{pp}\right)r_s x_{M2} - \left(L_p - L_{pp}\right)L_p U_1 - \left(L_p - L_{pp}\right)r_s U_2\right] \tag{6.40}$$

$$h_2\left(x_M\right) = \frac{1}{r_s^2 + L_p^2}\left[\left(L_p - L_{pp}\right)r_s x_{M1} - \left(L_p L_{pp} + r_s^2\right)x_{M2} + \left(L_p - L_{pp}\right)r_s U_1 - \left(L_p - L_{pp}\right)L_p U_2\right] \tag{6.41}$$

the other algebraic equations are derived as

$$TL = T_{m0}\left[A\left(1 - x_{M3}\right)^2 + B\left(1 - x_{M3}\right) + C_0 + D\left(1 - x_{M3}\right)^{Etrq}\right] \tag{6.42}$$

$$T_{m0} = p \cdot h_2\left(x_M\right) \cdot i_d + q \cdot h_1\left(x_M\right) \cdot i_q \tag{6.43}$$

$$i_q = \frac{r_s}{r_s^2 + L_p^2}\left(U_{M1} + x_{M1}\right) - \frac{L_p}{r_s^2 + L_p^2}\left(U_{M2} + x_{M2}\right) \tag{6.44}$$

$$i_d = \frac{L_p}{r_s^2 + L_p^2}\left(U_{M1} + x_{M1}\right) + \frac{r_s}{r_s^2 + L_p^2}\left(U_{M2} + x_{M2}\right) \tag{6.45}$$

After obtaining the quasi-steady-state model, we should also derive the boundary-layer model and check whether the Assumptions 1-3 are satisfied. If satisfied, then we can proceed to approximate slow and fast states in terms of the solutions of the reduced model and boundary-layer model. If not, we should make some modification like coordinate transformation or redefining the states, then reselect the slow and fast states. In this case, it can be verified that the assumptions are satisfied under such parameter setting. Moreover, the small perturbation coefficient satisfies the condition of equation (6.11). Therefore, the fast states can be approximated by the quasi-steady state $h_i(x_M)$ only. This approximation significantly simplifies the reduced model.

6.4.2 Reduced-Order DER_A model

The DER_A model has 10 states in total, $\tilde{x}_D = [S_0, S_1, \ldots, S_9]$. Different from the three-phase motor model, due to the existence of switches such as Pf_{Flag} and PQ_{Flag}, the DER_A model is actually a switching system consisting of 2^6 subsystems. Each subsystem is determined when the switches are fixed. Since these switches are preset, we only need to derive the reduced-order model for each subsystem. For brevity, we give the reduced-order model for one of the subsystems to illustrate the reducing procedure. The reduced models for other subsystems can be obtained using the same method.

To find the small perturbation coefficient ε, we rewrite the dynamics a

$$\left[T_{rv}\dot{S}_0, T_p\dot{S}_1, T_{iq}\dot{S}_2, T_g\dot{S}_3, T_v\dot{S}_4, T_{rf}\dot{S}_5, T_p \cdot T_{rf}\dot{S}_6, \dot{S}_7, T_{pord}\dot{S}_8, T_g\dot{S}_9\right]^T. \tag{6.46}$$

Given the parameter setting in Table 6.2, equation (6.46) becomes

$$\left[0.01\dot{S}_0, 0.01\dot{S}_1, 0.005\dot{S}_2, 0.005\dot{S}_3, 0.005\dot{S}_4, 0.01\dot{S}_5, 0.01 \cdot 0.01\dot{S}_6, \dot{S}_7, 0.005\dot{S}_8, 0.005\dot{S}_9\right]^T.$$

The smaller perturbation coefficients in equation (6.47) suggest that dynamic response velocities of $[S_0, S_1, S_5, S_7]$ are much slower than the rest of the states. This difference is also an evidence of the two-time-scale property of this model. Then the slow and fast dynamics are divided as follows

$$\dot{x}_D = \begin{bmatrix} x_D \\ z_D \end{bmatrix}. \tag{6.47}$$

where $x_D = [S_0, S_1, S_5, S_7]$, $z_D = [S_2, S_3, S_4, S_6, S_8, S_9]$. Defining the input voltages $[V_t, Freq]$ as U_D, following the same procedure as above (6.1)-(6.5), we can derive the reduced-order large-signal model of DER_A as

$$\dot{x}_{D1} = \frac{1}{T_{rv}}\left(U_{D1} - x_{D1}\right) \tag{6.48}$$

$$\dot{x}_{D2} = \frac{1}{T_p}\left(x_{D4} - x_{D2}\right) \tag{6.49}$$

$$\dot{x}_{D3} = \frac{1}{T_{rf}}\left(U_{D2} - x_{D3}\right) \tag{6.50}$$

$$\dot{x}_{D4} = 0\,. \tag{6.51}$$

Table 0.2 Parameters of DER_A model

Parameters	Values	Parameters	Values
T_{rv}	0.02 s	T_{pord}	0.02 s
T_p	0.02 s	dP_{min}	-0.5 pu/s
T_{iq}	0.02 s	dP_{max}	0.5 pu/s
V_{ref0}	0 pu	$V_{tripflag}$	1
K_{qv}	5 pu/pu	I_{ql1}	-1 pu
T_g	0.02 s	I_{qh1}	1 pu
Pf_{Flag}	1	X_e	0.25 pu
I_{max}	1.2	$F_{tripflag}$	1
dbd1	-99	PQ_{flag}	0
dbd2	99	typeflag	1
T_v	0.02 s	V_{pr}	0.8 pu
V_{lo}	0.44 pu	D_{up}	0
V_{l1}	0.49 pu	f_{emax}	99 pu
V_{h0}	1.2 pu	f_{emin}	-99 pu
V_{h1}	1.15 pu	f_{dbd1}	-0.0006
t_{vl0}	0.16 s	f_{dbd2}	0.0006

t_{vl1}	0.16 s	$Freq_{flag}$	0
t_{vh0}	0.16 s	P_{min}	0 pu
t_{vh1}	0.16 s	P_{max}	1.1 pu
V_{rfrac}	0.7	K_{pg}	0.1 pu
T_{rf}	0.02 s	K_{ig}	10 pu
D_{dn}	20	c	1 s
a	0.8 pu	d	0.9 pu
b	5	Base: 12.47 kV and 15.0 MVA	

The d - q axis currents i_d and i_q are states S_3 (z_{D2}) and S_9 (z_{D6}), respectively. Their equations are

$$i_q = sat_2\left\{\gamma(x_D)\right\} \times VP\left(x_{D1}, V_{rfrac}\right) + \hat{y}_{D2} \tag{6.52}$$

$$i_d = sat_9\left[\frac{sat_7(x_{D4})}{sat_1(x_{D1})}\right] \times VP\left(x_{D1}, V_{rfrac}\right) + \hat{y}_{D6} \tag{6.53}$$

$$\gamma(x_D) = \frac{\tan(pfaref)\, x_{D2}}{sat_1(x_{D1})} + K_{qv} sat_3\left[DB_V\left(V_{ref0} - x_{D1}\right)\right] \tag{6.54}$$

where $\hat{y}_{D2}$ and $\hat{y}_{D6}$ are the solutions of boundary-layer model:

$$\dot{y}_{D1} = -y_{D1} \tag{6.55}$$

$$\dot{y}_{D2} = y_{D3} - y_{D2} - VP\left(x_{D1}, V_{rfrac}\right) \times \left\{sat_2\left[\gamma(x_D)\right] + sat_2\left[y_{D1} + \gamma(x_D)\right]\right\} \tag{6.56}$$

$$\dot{y}_{D3} = -y_{D3} \tag{6.57}$$

$$\dot{y}_{D4} = -T_{rf}\, y_{D5} \tag{6.58}$$

$$\dot{y}_{D5} = -y_{D5} \tag{6.59}$$

$$\dot{y}_{D6} = -y_{D6} - sat_9\left[\frac{sat_7(x_{D4})}{sat_1(x_{D1})}\right] \times VP\left(x_{D1}, V_{rfrac}\right) + sat_9\left[\frac{sat_7(y_{D5} + x_{D4})}{sat_1(x_{D1})}\right] \times \left[y_{D3} + VP\left(x_{D1}, V_{rfrac}\right)\right] \tag{6.60}$$

As mentioned above, only if the assumptions are satisfied, we can use the reduced model to estimate the original model. It can be verified that the assumptions 1-3 are satisfied in this case. However, the condition of equation (6.11) is not guaranteed. Therefore, we should add a complementary term $\hat{y}(t/\varepsilon)$ which is the solution of boundary-layer model.

The two-time-scale property makes the load model a stiff ordinary differential equation problem. A problem is stiff if the solution being searched varies slowly, however there are nearby solutions varying rapidly. Therefore, the numerical method must take small steps to obtain satisfactory results. The stiffness can increase the computational time. The application of singular perturbation method reduces the order as well as convert the load model from a stiff problem to a non-stiff one, thus reducing the computational time from both sides and allowing the use of non-stiff solver.

6.5 Model Validation via Simulation

In this section, the reduced-order model derived in this chapter is verified through simulation. The reduced-order models of three-phase motor and DER_A are tested on Matlab using different solvers. We compare the performance of the reduced model with the original model to verify the effectiveness of the reduced model. Moreover, we compare the computational time between the two models and different solvers to show the efficiency of reducing computational burden.

6.5.1 Validation of Reduced-Order Three-Phase Motors

To verify the proposed reduced-order model of three-phase motor, we simulated the reduced and original model in Matlab with the same input voltage. Consequently, we can compare their output power and other states. Refer to [107], the bus voltage input is generated by (6.61). The parameters are set as shown in Table 6.2.

$$V(t)=\begin{cases} a & if\ 1,, t<\left(1+b/60\right) \\ \dfrac{(1-d)(c+1-t)}{b/60-c}+1 & if\ \left(1+b/60\right),, t<1+c \\ 1 & otherwise \end{cases} \tag{6.61}$$

Fig. 6.4 shows the generated input voltage. As shown in Fig. 6.5, 6.6 and 6.7 are the state response $E_{q'}$ and $E_{d'}$ of motor A, motor B and motor C, respectively. The blue solid line denotes the $E_{q'}$ and $E_{d'}$ of original model, while the red dashed line represents that of reduced-order model. Fig. 6.8, 6.9 and 6.10 shows the output real and reactive power. The blue solid line denotes the real and reactive power of original model, while the red dashed line represents that of reduced-order model. The mean squared errors of real and reactive power between the original and reduced model are shown in Table. 6.3. The small errors show the accuracy of the proposed reduced-order three-phase model. Moreover, if using ODE45, which is a non-stiff ODE solver, the computational time of the original and reduced model are 8.8120 s and 0.1926 s, respectively. If using ODE15s, which is a stiff ODE solver, the computational time of the original and reduced model are 1.0975 s and 0.1785 s, respectively. This comparison shows that the singular perturbation method converts the original high-order stiff problem to a reduced-order non-stiff problem while reducing the computational time remarkably. This reduction will be more significant in large-scale system with multiple composite loads.

Table 0.3 The mean squared errors between original and reduced-order model of three-phase motor

Motor / Power	Mean square error (MSE)		
	Motor A	Motor B	Motor C
Real power	1.0509×10^{-4}	1.1295×10^{-4}	8.0264×10^{-5}
Reactive power	1.1422×10^{-5}	1.4294×10^{-5}	2.1112×10^{-5}

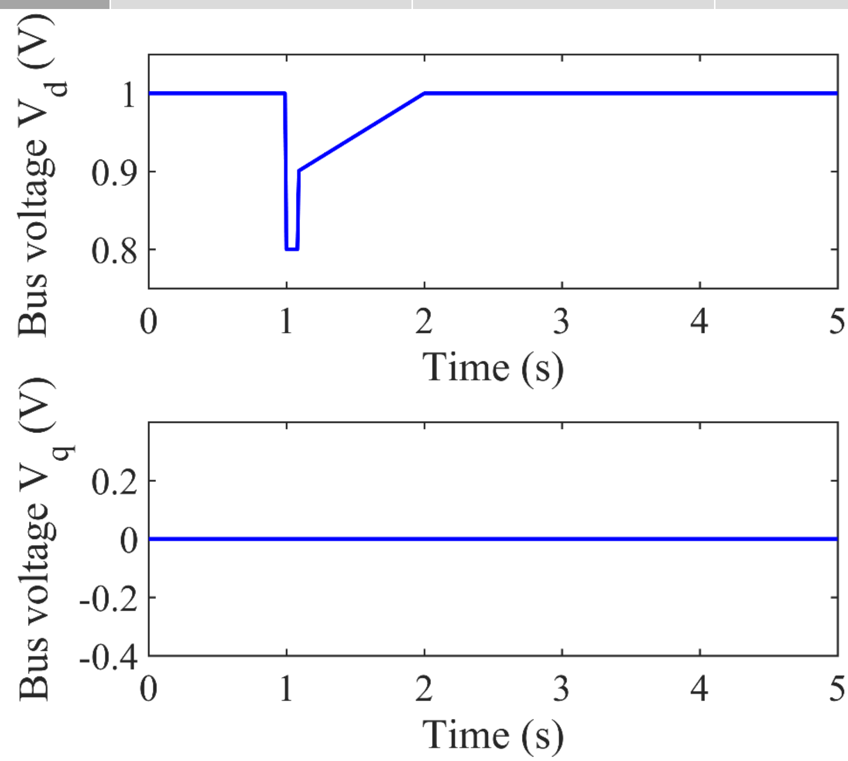

Fig. 0.4 Bus voltages of reduced and original model of three-phase motors

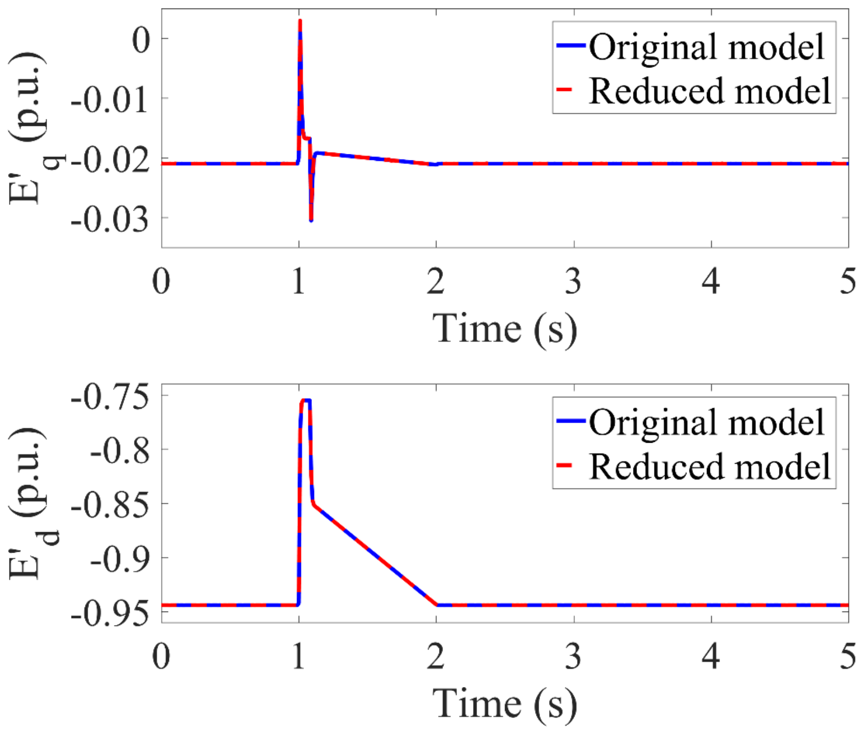

Fig. 0.5 Parameters of reduced and original model of three-phase motor A

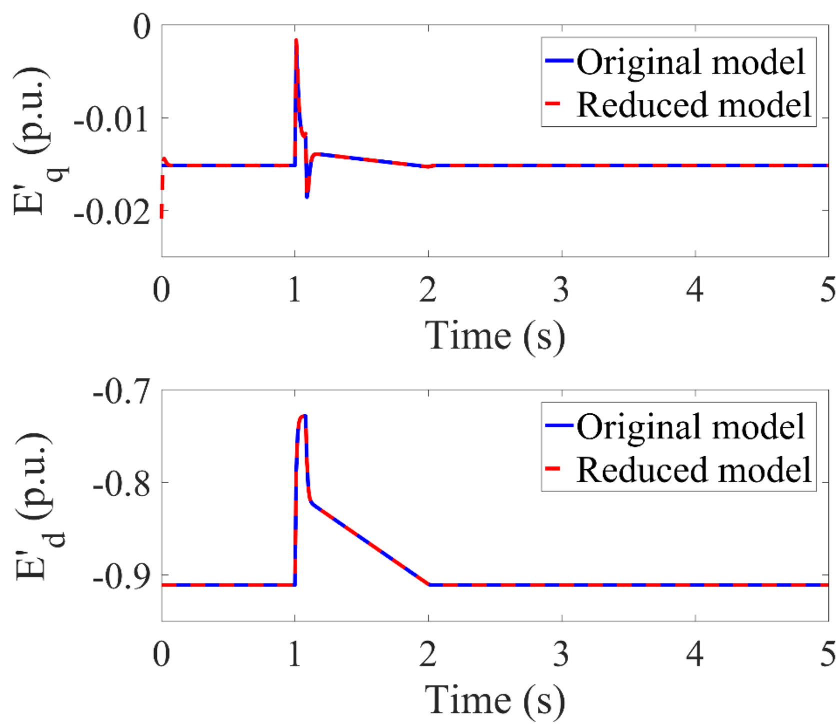

Fig. 0.6 Parameters of reduced and original model of three-phase motor B

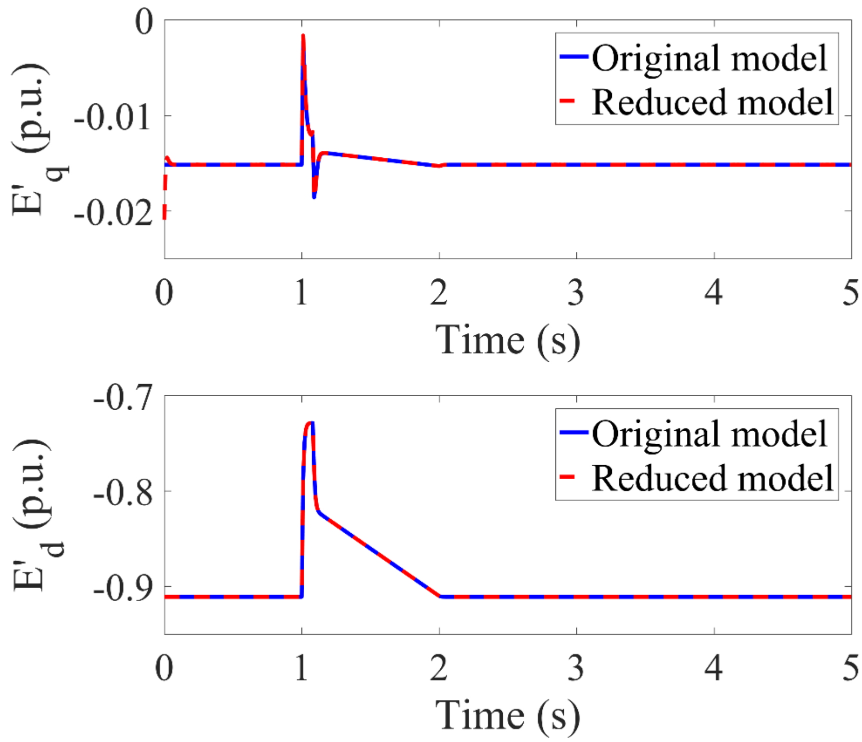

Fig. 0.7 Parameters of reduced and original model of three-phase motor C

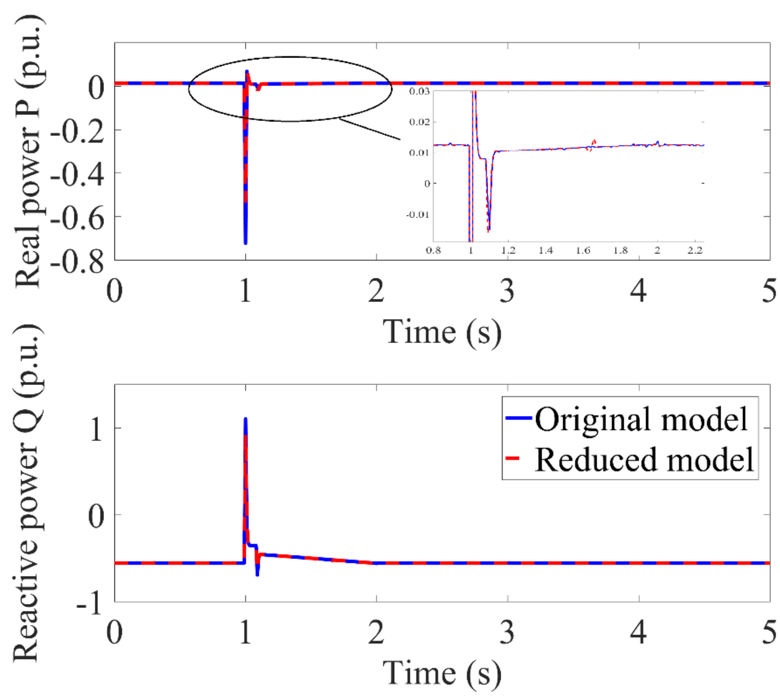

Fig. 0.8 Real and reactive power of reduced and original model of three-phase motor A

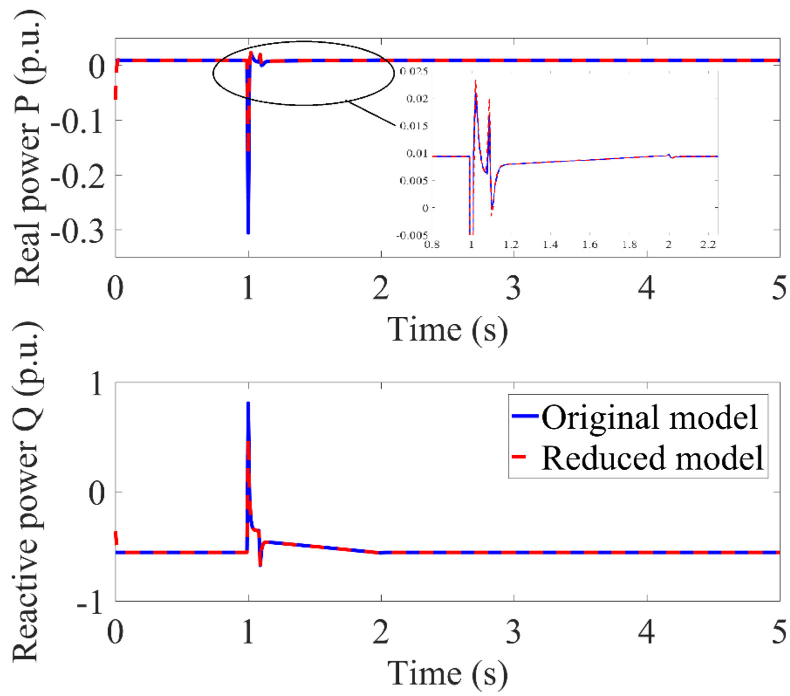

Fig. 0.9 Real and reactive power of reduced and original model of three-phase motor B

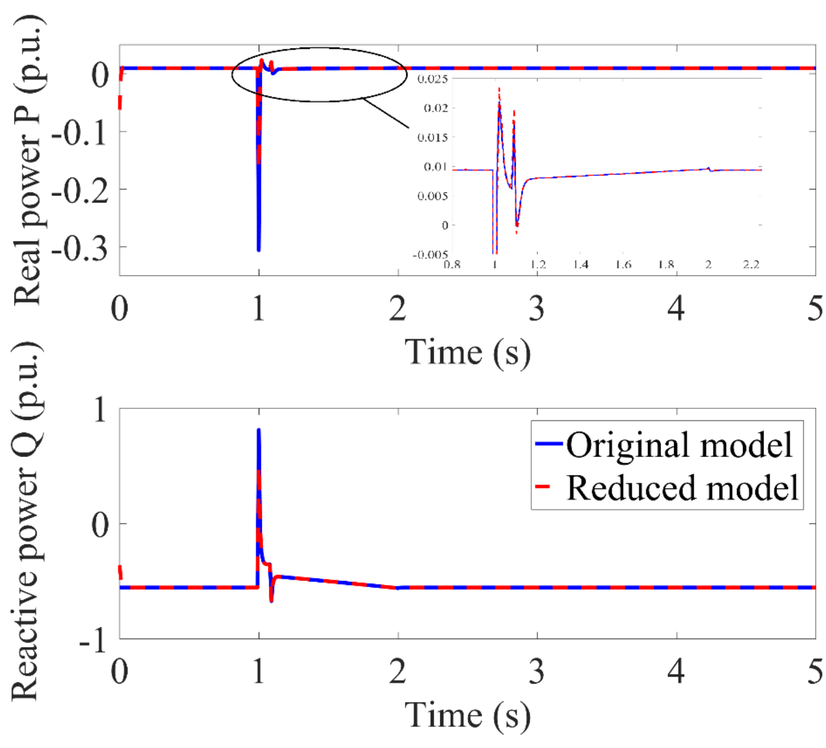

Fig. 0.10 Real and reactive power of reduced and original model of three-phase motor C

6.5.2 Validation of DER_A model

Similar to the verification process of three-phase motor, we simulated the reduced and original model of DER_A in Matlab. The voltage input is the same as (6.61). The frequency input is set to be 60 Hz. The parameters are set as shown in Table 6.2.

Fig. 6.11 shows the filtered voltage and frequency inputs of DER_A. Fig. 6.12 shows the dynamic power responses of DER_A. The blue solid line denotes the power output of original model, while the red dashed line represents that of reduced one. Fig. 6.13 shows filtered voltage V_{tfilt}, filtered generated power $P_{genfilt}$, and filtered current i_q and i_d of reduced and original model of DER_A. The mean square errors (MSE) of real and reactive power are 7.1363×10^{-4} and 1.3045×10^{-5}, respectively. Furthermore, the computational time of the original and reduced model using ODE45 are 11.205 s and 0.2074 s, respectively; the computational time of the original and reduced model using ODE15s are 2.0012 s and 0.1598 s, respectively.

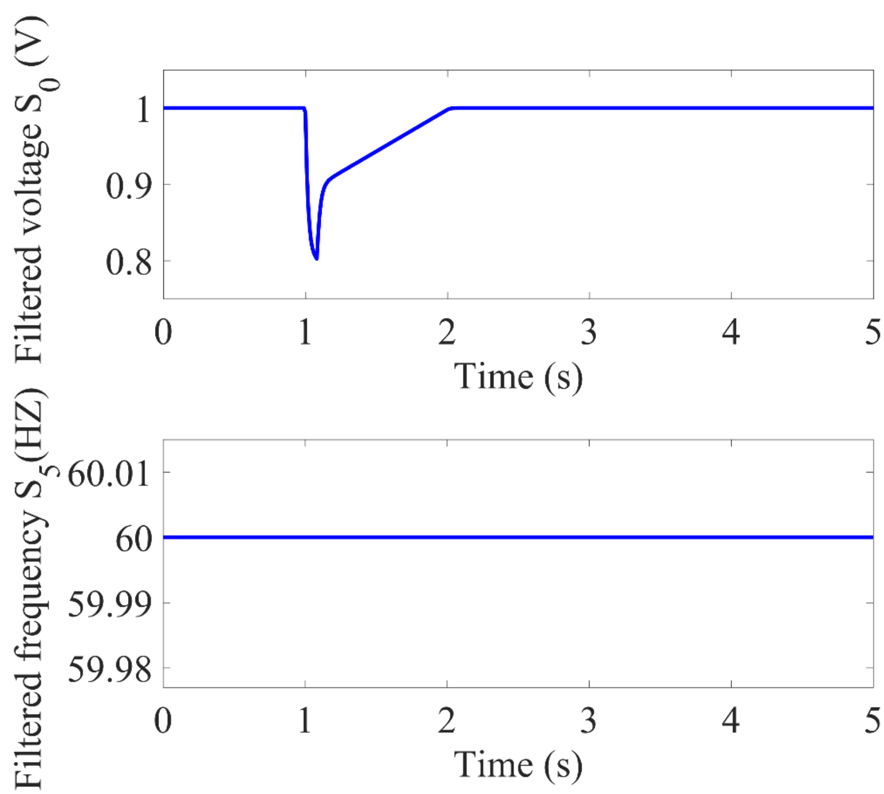

Fig. 0.11 Filtered input voltages and frequency of original and reduced model of DER_A

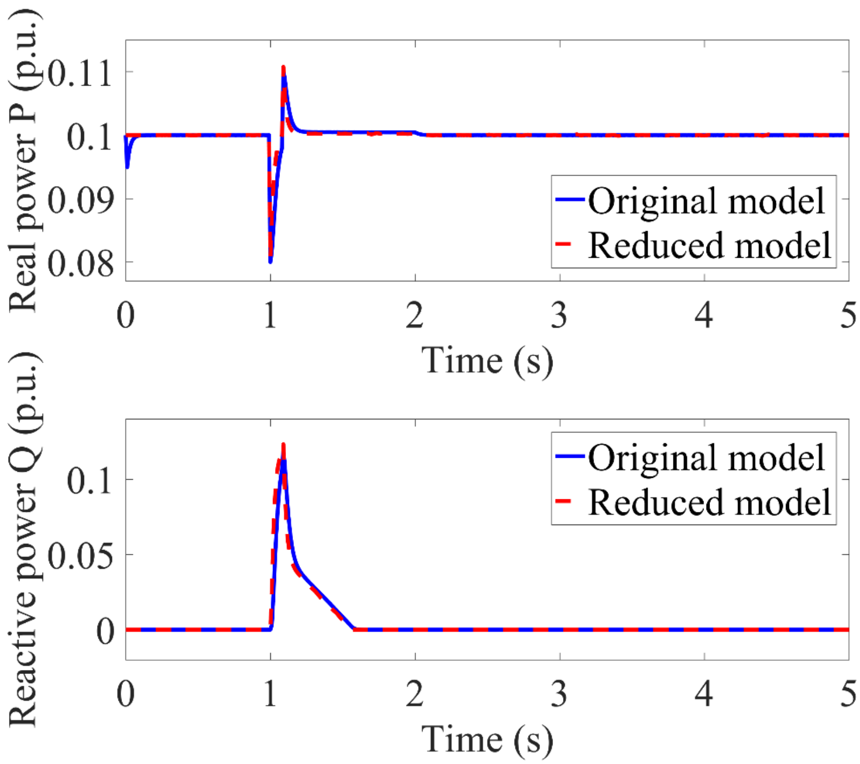

Fig. 0.12 Real and reactive power of reduced and original model of DER_A

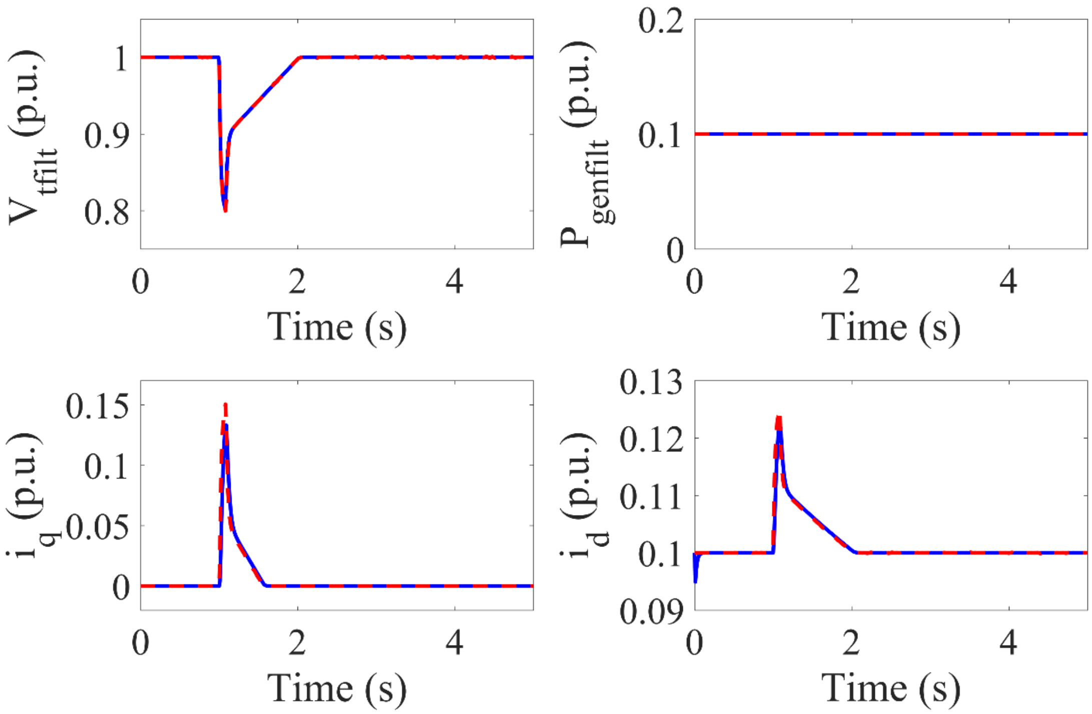

Fig. 0.13 Filtered voltage, filtered generated power, and filtered current of reduced and original model of DER_A

6.6 Summary

This work developed the reduced-order large-signal model of WECC CMPLDW + DER_A model. Several simulations are conducted in Matlab. The comparison analysis shows the accuracy of the proposed reduced model. It also shows that the computational time is reduced significantly using reduced model.

7. Conclusion and Future Work

In this report, we first reviewed the state-of-the-art of load models and parameter identification methods. Second, a cutting-edge parameter reduction approach based on active subspace is proposed to deal with the high dimensional parameter space of the WECC composite load model, which is more comprehensive but with large number of parameters. Third, we proposed a novel deep reinforcement learning based parameter identification for the WECC composite load model. Then, we also test the real PMU data from utility on Python and PSSE using the salp swarm algorithm. Finally, we also proposed the large-signal order reduction method for WECC composite load model which is able to reduce the computational time of each call of the WECC composite load model.

The future research directions are suggested in terms of modeling and identification technologies:

For load model structure development, more sophisticated models that balance flexibility and complexity are needed. Load consumption is time varying due to human behaviors and weather conditions; thus, different load models may be found in different time periods. Conventional load modeling methods using measurement data in a certain period may not be able to capture time-varying load behaviors, and lack generalizability. More research is needed to develop advanced algorithms to perform online load modeling using the real-time data. After developing new load models, they should be integrated in power system analysis programs. How to model and represent seasonal and geographical variations in load models and load composition is also an ongoing research topic. Capturing the time-varying nature of load behaviors is useful to voltage control, state estimation, and energy management. The increasing penetration of DGs and the implementation of demand-side management poses additional challenges to load modeling. WECC identified DGs as one of the main priorities in their further efforts to update CLM. DGs and power electronic loads may have complex control systems, which need to be taken into account in the model development. Customer behavior-driven and DR-enabled load models need to be built to facilitate DR studies. Distribution system models were not well studied in the past. There is a need to develop novel models with reduced complexity and computational requirements to represent ADNs and MGs. Modeling and aggregating DGs, controllable loads, and other technologies in ADNs and MGs is a major research topic. New loads such as electric vehicles and storage devices should be modeled to accurately represent the system. Moreover, modeling the interface and control logics of power electronics and testing their impact on stability and dynamic studies is an important research topic.

Future research on parameter estimation algorithms should be able to process data from existing and emerging measurement devices with different resolutions, such as smart meters, PMUs, and SCADA. Meanwhile, the algorithms should be robust to bad data, missing measurements, changes in the voltage regulation scheme, and noises.

References

[1] C. W. Taylor, Power system voltage stability, McGraw-Hill, 1994.

[2] P. Kundur, Power system stability and control, EPRI series, New York: McGraw-Hill, 1994.

[3] K. E. Wong, M. E. Haque and M. Davies, "Component-based dynamic load modeling of a paper mill," in Proc. 2012 22nd Australasian Universities Power Eng. Conf., Bali, 2012, pp. 1-6.

[4] I. Dzafic, M. Glavic and S. Tesnjak, "A component-based power system model-driven architecture," IEEE Trans. Power Syst., vol. 19, no. 4, pp. 2109-2110, Nov. 2004.

[5] D. Kosterev, A. Meklin, J. Undrill, B. Lesieutre, W. Price, D. Chassin, R. Bravo and S. Yang, "Load modeling in power system studies: WECC progress update," in Proc. IEEE PES General Meeting, Pittsbugh, PA, 2008,pp. 1-8.

[6] WECC MVWG Load Model Report ver. 1.0 (June 2012). [Online] Available:https://www.wecc.biz/Reliability/WECC%20MVWG%20Load%20Model%20Reprt%20ver%201%200.pdf

[7] Electrical Power Research Institute (EPRI), "Advanced load modeling," Tech. Rep. 1007318, Sept. 2002.

[8] A. Gaikwad, P. Markham and P. Pourbeik, "Implementation of the WECC Composite Load Model for utilities using the component-based modeling approach,'' in Proc IEEE/PES Transmission and Distribution Conf. and Expo., Dallas, TX, 2016, pp. 1-5.

[9] L. Zhu, X. Li, H. Ouyang, Y. Wang, W. Liu and K. Shao, "Research on component-based approach load modeling based on energy management system and load control system," in Proc. IEEE PES Innovative Smart Grid Technologies, Tianjin, 2012, pp. 1-6.

[10] S. -H. Lee, S. -E. Son, S. -M. Lee, "Kalman-filter based static load modeling of real power system using K-EMS data," J. Elect. Eng. Technol, vol. 7, no. 3, pp. 304-311, June 2012.

[11] H. Renmu, Ma Jin and D. J. Hill, "Composite load modeling via measurement approach," IEEE Trans. Power Syst., vol. 21, no. 2, pp. 663¬672, May 2006.

[12] Byoung-Kon Choi et al., "Measurement-based dynamic load models: derivation, comparison, and validation," IEEE Trans. Power Syst., vol. 21, no. 3, pp. 1273-1283, Aug. 2006.

[13] Electrical Power Research Institute (EPRI), "Measurement-Based Load Modeling," Tech. Rep. 1014402, Sept. 2006.

[14] J. Ma, D. Han, R. M. He, Z. Y. Dong and D. J. Hill, "Reducing identified parameters of measurement-based composite load model," IEEE Trans. Power Syst., vol. 23, no. 1, pp. 73-83, Feb. 2008.

[15] Ma Jin, H. Renmu and D. J. Hill, "Load modeling by finding support vectors of load data from field measurements," IEEE Trans. Power Syst., vol. 21, no. 2, pp. 723-735, May 2006.

[16] I. F. Visconti, D. A. Lima, J. M. C. d. S. Costa and N. Sobrinho, “Measurement-based load modeling using transfer functions for dynamic simulations,” IEEE Trans. Power Syst., vol. 29, no. 1, pp. 111-120, Jan. 2014.

[17] D. Han, J. Ma, R. m. He and Z. Y. Dong, “A real application of measurement-based load modeling in large-scale power grids and its validation,” IEEE Trans. Power Syst., vol. 24, no. 4, pp. 1753-1764, Nov.2009.

[18] B. K. Choi and H. D. Chiang, “Multiple solutions and plateau phenomenon in measurement-based load model development: issues and suggestions,” IEEE Trans. Power Syst., vol. 24, no. 2, pp. 824-831, May 2009.

[19] F. Hu, K. Sun, A. Del Rosso, E. Farantatos and N. Bhatt, “Measurement based real-time voltage stability monitoring for load areas, ^ IEEE Trans. Power Syst., vol. 31, no. 4, pp. 2787-2798, July 2016.

[20] H. Bai, P. Zhang and V. Ajjarapu, “A novel parameter identification approach via hybrid learning for aggregate load modeling,” IEEE Trans. Power Syst., vol. 24, no. 3, pp. 1145-1154, Aug. 2009.

[21] Y. Ge, A. J. Flueck, D. K. Kim, J. B. Ahn, J. D. Lee and D. Y. Kwon, “An event-oriented method for online load modeling based on synchrophasor data,” IEEE Trans. Smart Grid, vol. 6, no. 4, pp. 2060-2068, July 2015.

[22] P. Regulski, D. S. Vilchis-Rodriguez, S. Djurovic and V. Terzija, “Estimation of composite load model parameters using an improved particle swarm optimization method,” IEEE Trans. Power Del., vol. 30, no. 2, pp. 553-560, April 2015.

[23] J. K. Kim et al., “Fast and reliable estimation of composite load model parameters using analytical similarity of parameter sensitivity,” IEEE Trans. Power Syst., vol. 31, no. 1, pp. 663-671, Jan. 2016.

[24] X. Zhang, S. Grijalva and M. J. Reno, “A time-variant load model based on smart meter data mining,” in Proc. IEEE PES General Meeting Conf. and Expo., National Harbor, MD, 2014, pp. 1-5.

[25] B. Y. Ku, R.J. Thomas, C.-Y. Chiou, C.-J. Lin, “Power system dynamic load modeling using artificial neural networks,” IEEE Trans. Power Syst., vol. 9, no. 4, pp. 1868-1874, Nov. 1994.

[26] A. Keyhani, W. Lu, G.T. Heydt, “Composite neural network load models for power system stability analysis,” in Proc. IEEE PES Power Syst. Conf. and Expo., 2004, pp. 1159-1163.

[27] M. Bostanci, J. Koplowitz, C.W. Taylor, “Identification of power system load dynamics using artificial neural networks, IEEE Trans. Power Syst., vol.12, no.4, pp.1468-1473, Nov. 1997.

[28] G. W. Chang, C. I. Chen and Y. J. Liu, “A neural-network-based method of modeling electric arc furnace load for power engineering study,” IEEE Trans. Power Syst., vol. 25, no. 1, pp. 138-146, Feb. 2010.

[29] Dingguo Chen and R. R. Mohler, “Neural-network-based load modeling and its use in voltage stability analysis,” IEEE Trans. on Control Syst. Tech., vol. 11, no. 4, pp. 460-470, July 2003.

[30] T. Hiyama, M. Tokieda, W. Hubbi and H. Andou, “Artificial neural network based dynamic load modeling,^ IEEE Trans. Power Syst., vol. 12, no. 4, pp. 1573-1583, Nov. 1997.

[31] IEEE Task Force on Load Representation for Dynamic Performance, “Load representation for dynamic performance analysis (of power systems),” IEEE Trans. Power Syst., vol. 8, no. 2, pp. 472-482, May 1993.

[32] IEEE Task Force on Load Representation for Dynamic Performance, “Standard load models for power flow and dynamic performance simulation,” IEEE Trans. Power Syst., vol. 10, pp. 1302-1313, 1995.

[33] IEEE Task Force on Load Representation for Dynamic Performance, “Bibliography on load models for power flow and dynamic performance simulation,” IEEE Trans. Power Syst., vol. 10, no. 1, pp. 523-538, Feb. 1995.

[34] J. V. Milanovic, K. Yamashita, S. Villanueva, S. Djokic and L. M. Korunovic, “International industry practice on power system load for modeling,” IEEE Trans. Power Syst., vol. 28, no. 3, pp. 3038-3046, Aug. 2013.

[35] J. V. Milanovic, et al., “CIGRE WG C4.605: Modelling and aggregation of loads in flexible power networks,” 2014.

[36] A. J. Collin, G. Tsagarakis, A. E. Kiprakis and S. McLaughlin, “Development of low-voltage load models for the residential load sector,” IEEE Trans. Power Syst., vol. 29, no. 5, pp. 2180-2188, Sept. 2014.

[37] S. M. Zali and J. V. Milanovic, “Generic model of active distribution network for large power system stability studies,” IEEE Trans. Power Syst., vol. 28, no. 3, pp. 3123-3133, Aug. 2013.

[38] J. V. Milanovic and S. Mat Zali, “Validation of equivalent dynamic model of active distribution network cell,” IEEE Trans. Power Syst., vol. 28, no.3,pp. 2101-2110, Aug. 2013.

[39] Kuo-Hsiung Tseng, Wen-Shiow Kao and Jia-Renn Lin, “Load model effects on distance relay settings,” IEEE Trans. Po'wer Del., vol. 18, no.4, pp. 1140-1146, Oct. 2003.

[40] W.W. Price, K.A. Wirgau, A. Murdoch, F. Nozari, “Load modeling for power flow and transient stability studies,” EPRI Report EL-5003, Project 849-7, 1987.

[41] EPRI, “Extended transient-midterm stability program package FACTS version user’s manual,” EPRI Project 1208-9, September 1990.

[42] P. Jazayeri, W. Rosehart and D. T. Westwick, “A multistage algorithm for identification of nonlinear aggregate power system loads,” IEEE Trans. Power Syst., vol. 22, no. 3, pp. 1072-1079, Aug. 2007.

[43] D. Hill, “Nonlinear dynamic load models with recovery for voltage stability studies,” IEEE Trans. Power Syst., vol. 8, no. 1, pp. 163-176, Feb.1993.

[44] D. Karlsson, D.J. Hill, “Modeling and identification of nonlinear dynamic loads in power systems,” IEEE Trans. Power Syst., vol.9, no.1, pp.157¬166, Feb 1994.

[45] W. Xu and Y. Mansour, “Voltage stability analysis using generic dynamic load models,” IEEE Trans. Power Syst., vol. 9, no. 1, pp. 479-493, Feb. 1994.

[46] W. S. Kao, C. J. Lin, C. T. Huang, Y. T. Chen, and C. Y. Chiou, “Comparison of simulated power system dynamics applying various load models with actual recorded data,” IEEE Trans. Power Syst., vol. 9, no. 1, pp. 248-254, Feb. 1994.

[47] W. S. Kao, “The effect of load models on unstable low-frequency oscillation damping in Taipower system experience w/wo power system stabilizers,” IEEE Trans. Power Syst., vol. 16, no. 3, pp. 463-472, Aug. 2001.

[48] D. N. Kosterev, C. W. Taylor and W. A. Mittelstadt, “Model validation for the August 10 1996 WSCC system outage,” IEEE Trans. Power Syst., vol. 14, pp. 967-979, Aug. 1999.

[49] L. Pereira, D. Kosterev, P. Mackin, D. Davies, J. Undrill and W. Zhu, “An interim dynamic induction motor model for stability studies in the WSCC,” IEEE Trans. Power Syst., vol. 17, no. 4, pp. 1108-1115, Nov. 2002.

[50] B. Williams, W. Schmus, D. Dawson, “Transmission voltage recovery delayed by stalled air conditioner compressors,” IEEE Trans. Power Syst., vol.7, no.3, pp.1173-1181, Aug. 1992.

[51] J. Shaffer, “Air conditioner response to transmission faults,” IEEE Trans. Power Syst., vol.12, no.2, pp.614-621, May 1997.

[52] A. Bokhari, et al., “Experimental determination of ZIP coefficients for modern residential, commercial and industrial loads,” IEEE Trans. Power Del., vol. 29, no. 3, pp. 1372-1381, Oct. 2013.

[53] L. M. Hajagos and B. Danai, “Laboratory measurements and models of modern loads and their effect on voltage stability studies,” IEEE Trans. Power Syst., vol. 13, no. 2, pp. 584-592, May 1998.

[54] N. Lu, Y. Xie, Z. Huang, F. Puyleart, and S. Yang, “Load component database of household appliances and small office equipment,” in Proc. IEEEPES Gen. Meeting, Pittsburgh, PA, 2008, pp. 1-5.

[55] X. Liang, “A new composite load model structure for industrial facilities,” IEEE Trans. on Ind. Appl., to be published.

[56] X. Liang, and W. Xu, “Aggregation method for motor drive systems,” Electric Power Systems Research (Elsevier), vol. 117, pp. 27 - 35, Dec. 2014.

[57] Q. S. Liu, Y. P. Chen, D. F. Duan, “The load modeling and parameter identification for voltage stability analysis,” in Proc. Int. Conf. Power Syst. Technol., 2002, pp. 2030-2033.

[58] I. Hiskens, “Nonlinear dynamic model evaluation from disturbance measurements,” IEEE Trans. Power Syst., vol. 16, no. 4, pp. 702-710, Nov. 2001.

[59] S. Z. Zhu, J. H. Zheng, S. D. Shen, G. M. Luo, “Effect of load modeling on voltage stability,” in Proc. IEEE Power Eng. Soc. Summer Meeting, Seattle, WA, 2000, pp. 395 - 400.

[60] S. Kamoun and R. P. Malham6, “Convergence characteristics of a maximum likelihood load model identification scheme,” Automatica, vol. 28, no. 5, pp. 885-896, Sept. 1992.

[61] V. Knyazkin, C. Caizares, and L. Sder, “On the parameter estimation and modeling of aggregate power system loads,” IEEE Trans. Power Syst., vol. 19, no. 2, pp. 1023-1031, May 2004.

[62] S.-H. Lee, S.-E. Son, S.-M. Lee, J.-M. Cho, K.-B. Song, and J.-W. Park, “Kalman-filter based static load modeling of real power system using K EMS data,” J. Elect. Eng. Technol., vol. 7, no. 3, pp. 742-750, May 2012.

[63] J. Ma, Z.Y. Dong, P. Zhang, “Using a support vector machine (SVM) to improve generalization ability of load model parameters,” in Proc. IEEE PES Power Syst. Con/ and Expo., Seattle, WA, 2009, pp. 1-8.

[64] L. T. M. Mota, A. A. Mota, “Load modeling at electric power distribution substations using dynamic load parameters estimation,” Int. J. Elect. Power Energy Syst., vol. 26, no. 10, pp. 805-811, 2004.

[65] Z. Wang and J. Wang, "Time-Varying Stochastic Assessment of Conservation Voltage Reduction Based on Load Modeling," IEEE Trans. On Power Syst., vol. 29, no. 5, pp. 2321-2328, Sep. 2014

[66] A. Rouhani and A. Abur, “Real-time dynamic parameter estimation for an exponential dynamic load model,” IEEE Trans. Smart Grid, vol. 7, no. 3, pp. 1530-1536, May 2016.

[67] E. A. Wan and R. Van der Merwe, “The unscented Kalman filter,” Kalman Filtering and Neural Networks, Wiley, 2001.

[68] Z. Wang and J. Wang, "Review on implementation and assessment of conservation voltage reduction," IEEE Trans. Power Syst., vol. 29, no. 3, pp. 1303-1315, May 2014.

[69] J. Zhao, Z. Wang, and J. Wang, "Robust time-varying load modeling for conservation voltage reduction assessment," IEEE Trans. Smart Grid, accepted for publication.

[70] Vignesh V, S. Chakrabarti and S. C. Srivastava, “Classification and modelling of loads in power systems using SVM and optimization approach,” in Proc. IEEE PES General Meeting, Denver, CO, 2015, pp. 1-5.

[71] G. Golub and V. Pereyra, “Separable nonlinear least squares: the variable projection method and its applications,” Inverse Problems, vol. 19, no. 2, Feb. 2003.

[72] A. Patel, K. Wedeward, and M. Smith, “Parameter estimation for inventory of load models in electric power systems,” in Proc. The World Congress on Eng. and Comp. Sci., San Francisco, USA, 2014, pp. 233¬238.

[73] S. Sonet al., “Improvement of composite load modeling based on parameter sensitivity and dependency analyses,” IEEE Trans. Power Syst., vol. 29, no. 1, pp. 242-250, Jan. 2014.

[74] J. K. Kim et al., “Fast and reliable estimation of composite load model parameters using analytical similarity of parameter sensitivity,” IEEE Trans. Power Syst., vol. 31, no. 1, pp. 663-671, Jan. 2016.

[75] Z. Wang and J. Wang, "Analysis of performance and efficiency of conservation voltage optimization considering load model uncertainty," J. of Energy Eng., 10.1061/(ASCE)EY.1943-7897.0000190, 2014.

[76] Z. Wang, J. Wang, B. Chen, M. Begovic, and Y. He, "MPC-based voltage/var optimization for distribution circuits with distributed generators and exponential load models," IEEE Trans. Smart Grid, vol. 5, no. 5, pp. 2412-2420, Sep. 2014.

[77] Z. Wang and Y. He, "Two-stage optimal demand response with battery energy storage systems," IET Generation, Transmission & Distribution, vol. 10, no. 5, pp. 1283-1293, Apr. 2016.

[78] Electrical Power Research Institute (EPRI), “End-use load composition estimation using smart meter data,” Tech. Rep. 1020060, Dec. 2010.

[79] J. Zhao, G. Zhang, M. La Scala, and Z. Wang, “Enhanced robustness of state estimator to bad data processing through multi-innovation analysis,” IEEE Trans. on Ind. Informatics, accepted for publication.

[80] J. Zhao, Z. Wang, C. Chen, and G. Zhang, "Robust voltage instability predictor," IEEE Trans. Power Syst., vol. 11, no. 2, pp. 401-408, Jan. 2017

[81] K. Zhang, H. Zhu, and S. Guo, “Dependency analysis and improved parameter estimation for dynamic composite load modeling,” IEEE Trans. Power Syst., vol. 32, no. 4, pp. 3287–3297, Jul. 2017.

[82] C. Wang, Z. Wang, J. Wang, and D. Zhao, “Robust Time-Varying Parameter Identification for Composite Load Modeling,” IEEE Trans. Smart Grid, vol. 10, no. 1, pp. 967–979, Jan. 2019.

[83] A. Arif, Z. Wang, J. Wang, B. Mather, H. Bashualdo, and D. Zhao, “Load Modeling-A Review,” IEEE Trans. Smart Grid, vol. 9, no. 6, pp. 5986–5999, Nov. 2018.

[84] Z. Ma, Z. Wang, D. Zhao, and B. Cui, “High-fidelity large-signal order reduction approach for composite load model,” IET Gener. Transm. Distrib., vol. 14, no. 21, pp. 4888–4897, Aug. 2020.

[85] Q. Huang, R. Huang, B. J. Palmer, Y. Liu, S. Jin, R. Diao, Y. Chen, and Y. Zhang, “A generic modeling and development approach for WECC composite load model,” Electr. Power Syst. Res., vol. 172, pp. 1–10, Jul. 2019.

[86] A. Saltelli, “Sensitivity analysis for importance assessment,” Risk Anal., vol. 22, no. 3, pp. 579–590, Jun. 2002.

[87] T. Homma and A. Saltelli, “Importance measures in global sensitivity analysis of nonlinear models,” Reliab. Eng. Syst. Saf., vol. 52, no. 1, pp. 1–17, Apr. 1996.

[88] S. Marino, I. B. Hogue, C. J. Ray, and D. E. Kirschner, “A methodology for performing global uncertainty and sensitivity analysis in systems biology,” J. Theor. Biol., vol. 254, no. 1, pp. 178 – 196, Sep. 2008.

[89] M. D. Morris, “Factorial sampling plans for preliminary computational experiments,” Technometrics, vol. 33, no. 2, pp. 161–174, May 1991.

[90] D. K. Lin, “A new class of supersaturated designs,” Technometrics, vol. 35, no. 1, pp. 28–31, Feb. 1993.

[91] A. Dean and S. Lewis, Screening: methods for experimentation in industry, drug discovery, and genetics. Springer Science & Business Media, 2006.

[92] B. Bettonvil and J. P. Kleijnen, “Searching for important factors in simulation models with many factors: Sequential bifurcation,” Eur. J. Oper. Res., vol. 96, no. 1, pp. 180–194, Jan. 1997.

[93] K. Hinkelmann and O. Kempthorne, Design and analysis of experiments. Wiley Online Library, 1994, vol. 1.

[94] B. Iooss and P. Lemaıtre, “A review on global sensitivity analysis methods,” in Uncertainty management in simulation-optimization of complex systems. Springer, 2015, pp. 101–122.

[95] I. M. Sobol, “Global sensitivity indices for nonlinear mathematical models and their monte carlo estimates,” Math. Comput. Simul., vol. 55, no. 1-3, pp. 271–280, Feb. 2001.

[96] A. Saltelli, P. Annoni, I. Azzini, F. Campolongo, M. Ratto, and S. Tarantola, “Variance based sensitivity analysis of model output. design and estimator for the total sensitivity index,” Comput. Phys. Commun., vol. 181, no. 2, pp. 259–270, Feb. 2010.

[97] A. Saltelli, M. Ratto, T. Andres, F. Campolongo, J. Cariboni, D. Gatelli, M. Saisana, and S. Tarantola, Global sensitivity analysis: the primer. John Wiley & Sons, 2008.

[98] A. Saltelli and P. Annoni, “How to avoid a perfunctory sensitivity analysis,” Environ. Model. Softw., vol. 25, no. 12, pp. 1508–1517, Dec. 2010.

[99] H. Scheffe, The analysis of variance. John Wiley & Sons, 1999.

[100] A. Saltelli and R. Bolado, “An alternative way to compute fourier amplitude sensitivity test (FAST),” Compu. Stat. Data An., vol. 26, no. 4, pp. 445 – 460, Feb. 1998.

[101] F. Bu, Z. Ma, Y. Yuan, and Z. Wang, “WECC composite load model parameter identification using evolutionary deep reinforcement learning,” IEEE Trans. Smart Grid, vol. 11, no. 6, pp. 5407–5417, Jul. 2020.

[102] J.-Y. Tissot and C. Prieur, “Bias correction for the estimation of sensitivity indices based on random balance designs,” Reliab. Eng. Syst. Safe., vol. 107, pp. 205 – 213, Nov. 2012.

[103] J. Ma, D. Han, R.-M. He, Z.-Y. Dong, and D. J. Hill, “Reducing identified parameters of measurement-based composite load model,” IEEE Trans. Power Syst., vol. 23, no. 1, pp. 76–83, Jan. 2008.

[104] P. G. Constantine, Active subspaces: Emerging ideas for dimension reduction in parameter studies. SIAM-Society for Industrial and Applied Mathematics, 2015.

[105] T. Loudon and S. Pankavich, “Mathematical analysis and dynamic active subspaces for a long term model of HIV,” Math Biosci Eng, vol. 14, no. 3, pp. 709–733, Jun. 2016.

[106] P. Constantine, M. Emory, J. Larsson, and G. Iaccarino, "Exploiting active subspaces to quantify uncertainty in the numerical simulation of the hyshot ii scramjet," J. Comput. Phys., vol. 302, pp. 1 – 20, Dec. 2015.

[107] "The new aggregated distributed energy resources (DER A) model for transmission planning studies: 2019 update," Electrical Power Research Institute (EPRI), Tech. Rep., 2019.

[108] "Technical reference document: dynamic load modeling," North American Reliability Cooperation, Tech. Rep., 2016.

[109] T. M. Russi, "Uncertainty quantification with experimental data and complex system models," Ph.D. dissertation, UC Berkeley, 2010.

[110] Z. Ma, Z. Wang, Y. Wang, R. Diao, and D. Shi, "Mathematical representation of the WECC composite load model," J. Modern Power Syst. Clean Energy, vol. 8, no. 5, pp. 1015–1023, Aug. 2019.

[111] R. Huang et al., "Calibrating parameters of power system stability models using advanced ensemble Kalman filter," IEEE Trans. Power Syst., vol. 33, no. 3, pp. 2895–2905, Oct. 2017.

[112] Y. Zhang, J. Wang, and Z. Li, "Uncertainty modeling of distributed energy resources: Techniques and challenges," Curr. Sustain. Energy Rep., vol. 6, no. 2, pp. 42–51, Jun. 2019.

[113] M. Cui, J. Wang, and B. Chen, "Flexible machine learning-based cyberattack detection using spatiotemporal patterns for distribution systems," IEEE Trans. Smart Grid, vol. 11, no. 2, pp. 1805–1808, Mar. 2020.

[114] M. Cui, J. Wang, Y. Wang, R. Diao, and D. Shi, "Robust time-varying synthesis load modeling in distribution networks considering voltage disturbances," IEEE Trans. Power Syst., vol. 34, no. 6, pp. 4438–4450, Nov. 2019.

[115] M. Cui, M. Khodayar, C. Chen, X.Wang, Y. Zhang, and M. E. Khodayar, "Deep learning based time varying parameter identification for systemwide load modeling," IEEE Trans. Smart Grid, vol. 10, no. 6, pp. 6102–6114, Nov. 2018.

[116] J.-K. Kim, K. An, and J. Ma, "Fast and reliable estimation of composite load model parameters using analytical similarity of parameter sensitivity," IEEE Trans. Power Syst., vol. 31, no. 1, pp. 663–671, Jan. 2016.

[117] S. Son et al., "Improvement of composite load modeling based on parameter sensitivity and dependency analyses," IEEE Trans. Power Syst., vol. 29, no. 1, pp. 242–250, Jan. 2014.

[118] U.S. Energy Information Administration. (2011). Share of Energy Used by Appliances and Consumer Electronics Increases in U.S. Homes. [Online]. Available: https://www.eia.gov/consumption/residential/reports/2009/electronics.php

[119] U.S. Energy Information Administration. (2018). EIA Electricity Data Now Include Estimated Small-Scale Solar PV Capacity and Generation. [Online]. Available: https://www.eia.gov/todayinenergy/detail.php?id=23972

[120] J. Zhang, M. Cui, and Y. He, “Robustness and adaptability analysis for equivalent model of doubly fed induction generator wind farm using measured data,” Appl. Energy, vol. 261, pp. 1–12, Mar. 2020.

[121] WECC Composite Load Model Specifications. Accessed: Jan. 27, 2015. [Online]. Available: http://home.engineering.iastate.edu/~jdm/ee554/WECC%20Composite%20Load%20Model%20Specifications%2001-27-2015.pdf

[122] X. Wang, Y. Wang, D. Shi, J. Wang, and Z. Wang, “Two-stage WECC composite load modeling: A double deep Q-learning networks approach,” IEEE Trans. Smart Grid, early access, Apr. 15, 2020, doi: 10.1109/TSG.2020.2988171.

[123] E. Conti, V. Madhavan, F. P. Such, J. Lehman, K. Stanley, and J. Clune, “Improving exploration in evolution strategies for deep reinforcement learning via a population of novelty-seeking agents,” in Proc. Adv. Neural Inf. Process. Syst., Dec. 2018, pp. 5032–5043

[124] D. Wierstra, T. Schaul, T. Glasmachers, Y. Sun, J. Peters, and J. Schmidhuber, “Natural evolution strategies,” J. Mach. Learn. Res., vol. 15, no. 1, pp. 949–980, Mar. 2014.

[125] M. Yamada, W. Jitkrittum, L. Sigal, E. P. Xing, and M. Sugiyama. (2019). High-Dimensional Feature Selection by Feature-Wise Kernelized Lasso. [Online]. Available: https://arxiv.org/abs/1202.0515.

[126] S. Wang et al., “A data-driven multi-agent autonomous voltage control framework using deep reinforcement learning,” IEEE Trans. Power Syst., early access, Apr. 23, 2020, doi: 10.1109/TPWRS.2020.2990179.

[127] W. Kersting, Distribution System Modeling and Analysis. New York, NY, USA: CRC Press, 2011.

[128] J. D. Glover, M. S. Sarma, and T. J. Overbye, Power System Analysis and Design, 5th ed. Stamford, CT, USA: Cengage Learn., 2011.

[129] A. Hughes and B. Drury, Electric Motors and Drives, 4th ed. Amsterdam, The Netherlands: Elsevier, 2013.

[130] H. Wu and I. Dobson, “Analysis of induction motor cascading stall in a simple system based on the cascade model,” IEEE Trans. Power Syst., vol. 28, no. 3, pp. 3184–3193, Aug. 2013.

[131] D. C. Yu, H. Liu, H. Sun, S. Lu, and C. Mccarthy, “Protective device coordination enhancement for motor starting programs,” IEEE Trans Power Del., vol. 20, no. 1, pp. 535–537, Jan. 2005.

[132] A. B. Birchfield, T. Xu, K. M. Gegner, K. S. Shetye, and T. J. Overbye, “Grid structural characteristics as validation criteria for synthetic networks,” IEEE Trans. Power Syst., vol. 32, no. 4, pp. 3258–3265, Jul. 2017.

[133] C. M. Bishop, Pattern Recognition and Machine Learning. New York, NY, USA: Springer, 2009.

[134] R. D. Quint. (2015). A Look Into Load Modeling: The Composite Load Model. [Online]. Available: https://gig.lbl.gov/sites/all/files/6bquint-composite-load-model-data.pdf

[135] "Reliability guide: Parameterization of the DER_A model," North Amer. Elect. Rel. Corporat., Atlanta, GA, USA, Rep., 2019.

[136] R. Abbassi, A. Abbassi, A. A. Heidari, and S. Mirjalili, "An efficient SALP swarm-inspired algorithm for parameters identification of photovoltaic cell models," Energy Convers. Manag., vol. 179, pp. 362–372, Jan. 2019.

[137] V. François-Lavet, P. Henderson, R. Islam, M. G. Bellemare, and J. Pineau, "An introduction to deep reinforcement learning," Found. Trends Mach. Learn., vol. 11, nos. 3–4, pp. 219–354, 2018.

[138] H. K. Khalil: 'Nonlinear Systems'. New Jersey: Prentice Hall, 2000